On-Line Optimization for a Batch-Fed Copolymerization Reactor with Partial State Measurement

by

Onyinye Eberechukwu Okorafo

A thesis submitted to the
Department of Chemical Engineering
in conformity with the requirements for
the degree of Master of Applied Science

Queen's University
Kingston, Ontario, Canada
September 2009

Abstract

Polymerization processes require adequate monitoring to ensure that the final product meets specification. Various on-line measuring techniques have been developed and implemented to track polymer properties in reactors. For most processes, however, on-line measurement cannot be implemented. In other situations, certain polymer properties or states might not be measurable and hence have to be estimated.

This work deals with improving an on-line optimization technique and demonstrating its effectiveness by sensitivity analysis. In addition, state estimation is used as a tool to reconstruct states that are unavailable for measurement in a styrene and butyl methacrylate batch-fed solution free-radical copolymerization process subject to on-line optimization.

A hybrid extended Kalman filter is used to observe the nonlinear dynamic system which is subject to real-time dynamic optimization. With very limited measurement information, the states of the system were reconstructed. Additional unobservable quantities were reconstructed using the process model and estimated states.

Acknowledgments

I am very thankful to my supervisors Professor Robin Hutchinson and Professor Martin Guay, for their guidance, patience and continual support during this project. I am also grateful for the consideration they have shown towards my family during difficult times. You both have been incredibly encouraging and dedicated to my work. Thanks for being the best supervisors anyone could ask for!

My gratitude goes to Professors Timothy McKenna, James McLellan and Juliana Ramsay for taking time to be on my thesis committee.

I greatly value all my friends for their unending support and encouragement. I also thank my officemates for creating an interesting and enjoyable study environment. Particularly, I appreciate Ronke for her support and Nick for his patience in answering my Matlab and Latex questions.

Big thanks to my family, Dad, Amby, and Junior for their continual love, encouragement, long distance calls and text messages. Mum, you made me the woman I am today and you are dearly missed.

I acknowledge Third Day Worship Centre (Kingston, Ontario) for helping me grow in my walk with God.

My daddy in heaven, Jesus Christ, I thank you for your unfailing love and for being my rock. To you be all the glory!

Contents

List of Tables

List of Figures

Chapter 1

Introduction

1.1 State Estimation in Polymerization Systems

The polymer industry is continually developing polymer processes to achieve quality products. Polymers are versatile products. They are used to manufacture numerous high demand supplies such as plastics, paints, and paper. Polymers are subject to stringent specifications in end-use products due to safety and quality issues. As a result, there is great demand to develop effective production practices. The only way to achieve optimum performance and quality of the polymer manufacturing process is to incorporate mechanisms to monitor the variables that can affect the polymer properties, and the reaction rates involved in the polymerization process [1].

It is desirable to employ on-line measuring techniques to monitor polymer properties in real-time to facilitate immediate control schemes and regulate the reaction system. A limited number of sensors are available to measure distinct variables that affect the physical and chemical properties of the polymer during the reaction process. Unfortunately, real-time measurements cannot be implemented in a majority of the

processes and in certain situations, some states or polymer properties might not be measurable and hence have to be estimated.

Many observers exist for linear and nonlinear systems and can either be stochastic or deterministic in nature, depending on the existing mathematical structure of the process model and sensor measurement [2]. Linear observers include Kalman filter (stochastic) and Luenberger observer (deterministic). Polymerization reactors are inherently nonlinear in nature and hence require implementation with nonlinear observers. Nonlinear observers include extended Kalman filter (EKF), extended Luenberger observer, high gain observers, and many more listed and discussed in [2], [3].

In general, observers are designed to estimate unmeasured states using the available measurement information, a knowledge of the process dynamics and the noise structure. A schematic of a typical state observer is shown in Figure 1.1.

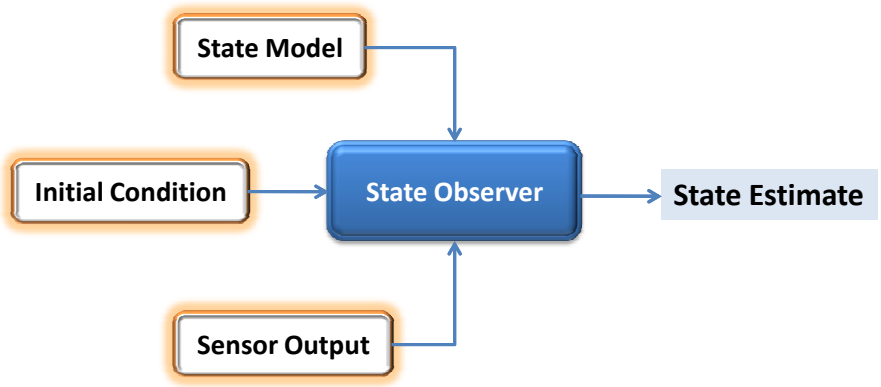

Figure 1.1: State Estimation Procedure.

This research proposes an extended Kalman filtering technique to reconstruct the system states required in the implementation of an on-line optimization routine.

1.2 Motivation of Thesis Project

In practice, acrylic resins for automotive coatings are required to be durable and possess high resistance to physical and chemical wear. These resins are produced at low solvent levels to meet regulations on volatile organic content (VOC) [4]. In addition, the reaction is usually operated under high temperature conditions and at low monomer concentration to improve polymer molecular weight and copolymer composition control [5].

A starved feed feeding policy is utilized to keep the monomer and initiator content at reduced levels. The resulting effect of this feeding strategy is a prolonged batch time. The motivation of this study is to use an on-line optimization scheme to enhance the reactor performance and product quality, while reducing the final batch time of the polymerization reaction. In doing so, a state observer is also designed to reconstruct the unmeasured states of the system from the available measurements.

The challenges of this project include the improvement of the on-line optimization strategy and its robustness to process changes; the development of a robust observer for the process; and the incorporation of the observer into the on-line optimization routine.

1.3 Structure of Thesis

This thesis is organized as follows. Chapter 2 presents theoretical background of Kalman filtering and a review of literature.

Chapter 3 outlines the background of the system studied as well as the theory related to on-line optimization of the semi-batch copolymerization process. The improvements made to the real-time optimization routine are discussed. Simulation results for the optimization scheme are provided. In addition, a sensitivity analysis of the proposed dynamic optimization routine is considered to demonstrate its effectiveness.

In Chapter 4, a hybrid extended Kalman filter is developed for the batch-fed process based on the system dynamic presented in Chapter 3. The hybrid extended Kalman filter is then incorporated in the proposed on-line optimization routine outlined in Chapter 3 to reconstruct the system state variables. The robustness analysis and the simulation results of the integrated algorithm are presented.

Chapter 5 provides conclusions and areas of future work for this research.

Chapter 2

Literature Review

2.1 State Estimation

State estimation is an important tool in control theory that deals with determining the states of a system given the measurement from the sensors of the process. The state variables describe the state of the system. For instance, possible states of a moving vehicle include distance, velocity, and acceleration. In reaction systems, the state variables describe the mass and internal energy of the system. The estimation of a system's state requires a measurement of the state variables. Unfortunately, there are many instances where these variables cannot be measured. Hence, mechanisms to estimate them are required.

State observers have been implemented successfully in numerous research and industrial applications. Ideally, it is desirable that the actual process measurement and model output are in agreement. This is usually not the case due to the presence of noise in the measurement or disturbances in the system. The most common way to reconstruct the imperfectly measured state variable is by designing a state observer

in the form of a Kalman filter or extended Kalman filter. The Kalman filter can be used as both a state estimator and a state observer.

A state estimator estimates the most likely value of the state variables of a dynamical system subject to noise. The Kalman filter is the most widely used state estimator encountered in practice. A state observer, on the other hand, is designed to reconstruct the unmeasured state variables from the sensor measurement of a dynamical system without any considerable process noise or measurement noise [6]. The Kalman filter can also be used as a state observer under the assumption that the dynamical system can be observed [7].

This literature review will highlight different approaches to state estimation, focusing mainly on polymerization processes in the chemical industry.

2.2 State Estimation for Linear and Nonlinear Systems

The choice of state estimation techniques depend on whether the system is linear or nonlinear. It also depends on the noise structure, and the degree of uncertainty in the system dynamics. The Kalman filter (KF), first developed by Kalman [8], assumes linearity of the dynamical system for state estimation from measurements corrupted with noise. The extended Kalman filter (EKF) is a nonlinear variation of the KF that linearizes the nonlinear dynamic model for state estimation purposes. Other variations of KF and EKF exist as shown in Figure 2.1.

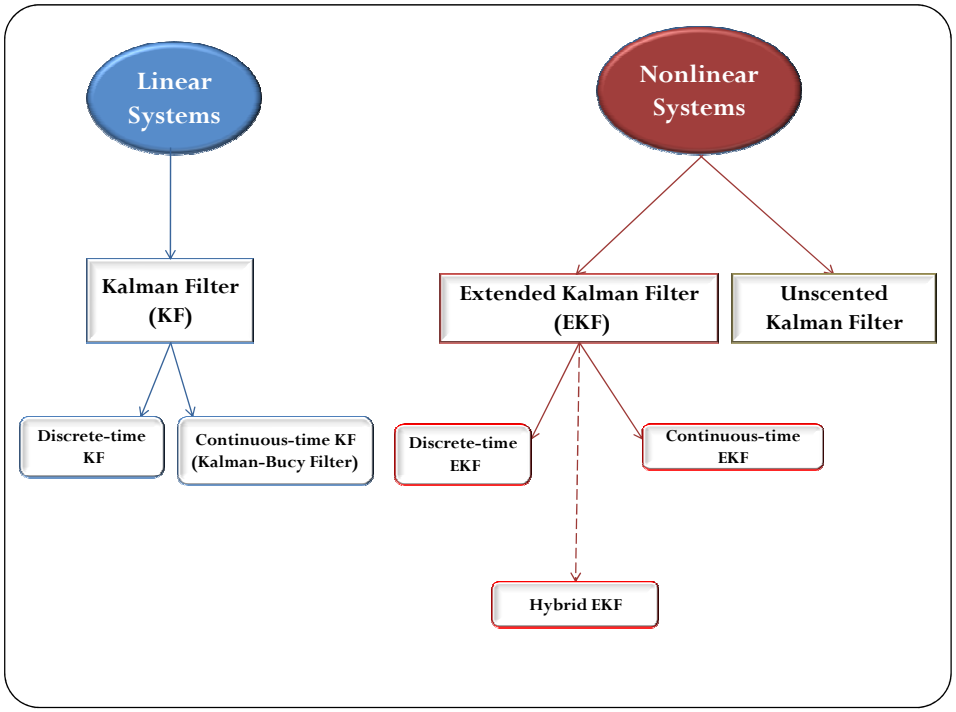

Figure 2.1: Linear and Nonlinear Filter Variations

2.2.1 Kalman Filter Analysis

Following Figure 2.1, the Kalman filter can be implemented in discrete-time or continuous-time. In process control, measurements are obtained from computers which sample in discrete-time. For this reason, the discrete-time KF is more widely used than the continuous-time KF. The discrete-time KF assumes both the linear dynamic system and the model output are in discrete-time. A typical example of a linear discrete-time

system is given by [9]

$$\begin{aligned} x_k &= A_{k-1}x_{k-1} + B_{k-1}u_{k-1} + q_{k-1} \\ z_k &= H_k x_k + r_k \end{aligned} \tag{2.1}$$

where k denotes the time step, x_{k-1} is the discrete-time state at the previous time step $k-1$, u_{k-1} is the input, z_k is the sensor measurement corrupted with noise, which is related to the discrete-time state through the measurement matrix H_k. The state observer seeks to reconstruct the states x_k from the set of **i** sensor measurements $[z_{1k}, z_{2k},...,z_{\mathbf{i}k}]=z_k$, where **i** could be less than the number of states. The plant disturbance and measurement noise q_{k-1} and r_k have noise covariance matrices Q_k and R_k, respectively. The structure of Q_k and R_k should be known to tune the Kalman filter. Matrix A_{k-1} is called the system matrix developed from model equations; B_{k-1} is the input matrix; both matrices are assumed to be independent of any states or input. A more thorough exploration of state estimation theory can be found in [10], [11] and [12].

The Kalman filter algorithm for the system in (2.1) is described by the following procedure.

- Step 1: ***Select the initial conditions***.

$$\hat{x}_0 = E[x_0] \tag{2.2}$$

$$P_0 = E[(x_0 - \hat{x}_0)(x_0 - \hat{x}_0)^T] \tag{2.3}$$

  Assuming all inputs, u_k, are known, the initial values for the state ($\hat{x}_0$) and the uncertainty in that estimate (P_0) are chosen. $E[\cdot]$ denotes the expected value of a random variable or expectation operator. At the first time step, ($\hat{x}_0$) is defined as the expected value of initial state estimate (x_0). The choice of initial

condition for the covariance matrix P_0 depends on the uncertainty associated with the initial state estimates. The more certain the value of the state (x_0) is *a priori*, the closer the covariance matrix is to zero. Otherwise, P_0 gets larger as the confidence in x_0 decreases [7]. The difference between the true state variable and its estimate is called the prediction error ($x_0 - \hat{x}_0$). The Kalman filter is typically derived to achieve optimal state estimates by minimizing the expected value of the squared error in (2.3). More information about expected value minimization can be found in [13], [14], and [15].

- Step 2: ***Estimate ahead***.

$$\hat{x}_k^- = A_{k-1}\hat{x}_{k-1}^+ + B_{k-1}u_{k-1} \tag{2.4}$$

$$P_k^- = A_{k-1}P_{k-1}^+A_{k-1}^T + Q_{k-1} \tag{2.5}$$

In between measurements, the estimated state variables and covariance matrix are predicted to be $\hat{x}_k^-$ and P_k^-, respectively. The superscript $(+)$ represents the *a posteriori* state estimate, given the measurement at time step k is incorporated. The superscript $(-)$, on the other hand, represents the *a priori* state estimate, given prior information of the process before the measurement time step k.

- Step 3: ***Update measurement***.

Updating the measurement is a three step process.

a. ***Compute the gain***.

$$K_k = P_k^-H_k^T(H_kP_k^-H_k^T + R_k)^{-1} \tag{2.6}$$

With knowledge of the predicted *a priori* covariance matrix, the gain is

computed and used to update the estimated state and covariance as shown in Step 3b and 3c.

b. ***Correct the state estimate***

$$\hat{x}_k^+ = \hat{x}_k^- + K_k(z_k - H_k\hat{x}_k^-) \tag{2.7}$$

The state estimate is then corrected with the calculated gain and measurement z_k to obtain a new state estimate, $\hat{x}_k$.

c. ***Correct the error covariance***

$$P_k^+ = P_k^- - K_k H_k P_k^- \tag{2.8}$$

The computed gain is also used to update the error covariance.

Steps 1 through Steps 3 of the Kalman filter algorithm are illustrated in Figure 2.2.

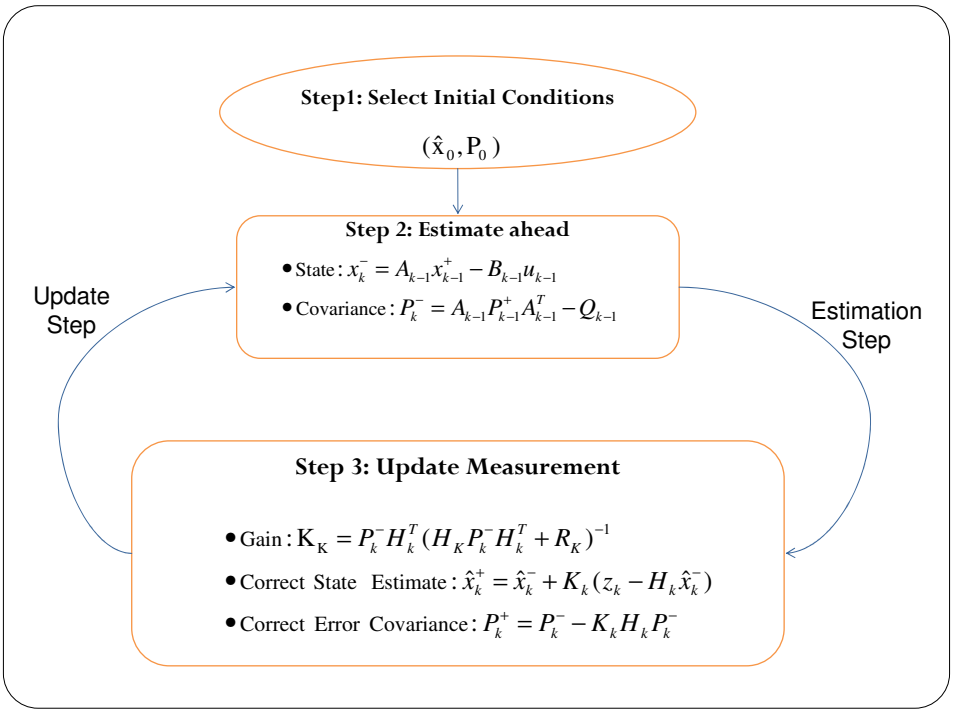

Figure 2.2: Kalman Filter Procedure

An important point to note about the form of the gain K_k and error covariance P_k^+ is that they do not depend on the estimate $\hat{x}_k$. For this reason, the gain matrix K_k does not require computing in real-time; it can be precomputed and accumulated before measurements are acquired [7], [9].

Tuning the Kalman Filter

Knowledge of the structure of the noise covariances (Q_k and R_k) is required to tune the Kalman filter. The dimension of Q_k and R_k have a great impact on the gain K_k in (2.6). This relationship can be seen as follows. The process noise matrix Q_{k-1} affects the predicted covariance P_k^- (2.5), which in turn is used to calculate the gain K_k (2.6). Measurement noise R_k also affects K_k. The value of K_k influences the estimation error $(z_k - H_k\hat{x}_k^-)$ in the predicted state (2.7). For instance, if the value of K_k is large, a small estimation error can yield an aggressive correction to the state estimate, as there is more confidence in the sensor measurement [9], [16]. On the other hand, if K_k is small, then the model dynamics are used to make correction to the state estimate [9], [16]. Kalman filter tuning is quite intuitive and can be found in other sources including [7]. Figure 2.3 illustrates the tuning process for Kalman filtering.

2.2.2 Extended Kalman Filter

The extended Kalman filter is suitable for some nonlinear systems. An EKF is particularly important for conditions that require the current estimate to be linearized about more than one steady-state point. Also, EKFs are applicable to systems with unknown parameters. For instance, if the gain K_k is dependent on previous values of

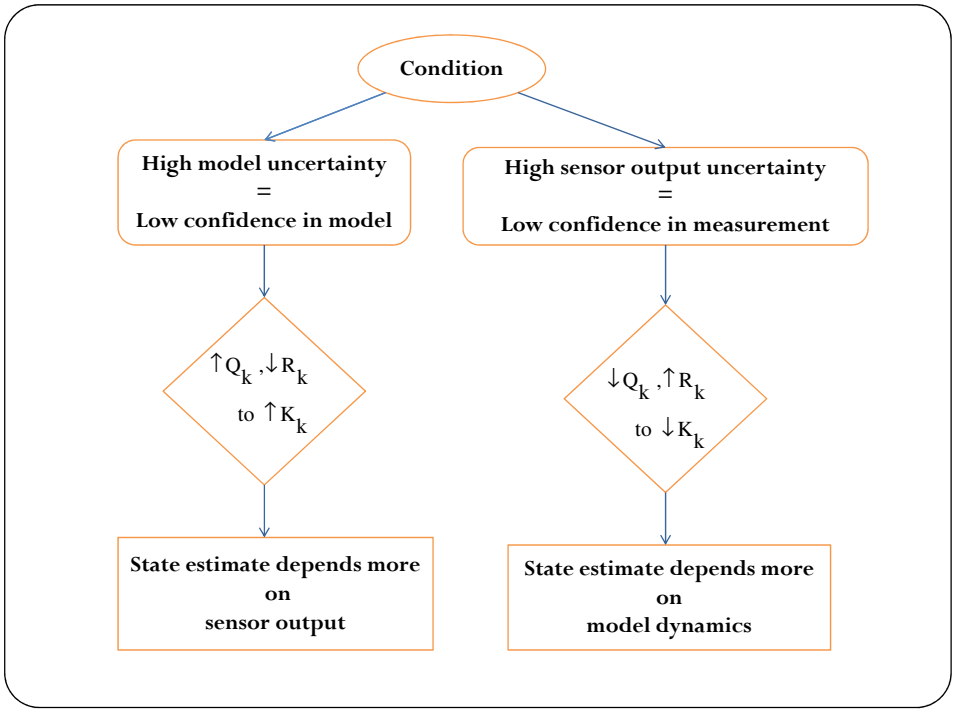

Figure 2.3: Kalman Filter Tuning Process

the state estimate $\hat{x}_k$, this would require the gain to be updated at every time step with knowledge of the state. Hence, systems with parameters that depend on trajectory are better implemented with EKF. This procedure can significantly improve the accuracy of the state estimation problem for systems with parametric uncertainties.

Nonlinear discrete-time systems can be formulated as [7]

$$\begin{aligned} x_k &= f_{k-1}(x_{k-1}, u_{k-1}, q_{k-1}) \\ z_k &= h_k(x_k, r_k) \end{aligned}$$

As in the case of the Kalman filter in (2.1), the noise processes q_{k-1} and r_k, are

both assumed to be zero-mean, independent, white process noise with covariance matrices Q_k and R_k, respectively. The state estimate x_k and sensor measurement z_k require linearization about previous model conditions so that as new measurements become available, x_k and z_k are updated efficiently.

The algorithm for the discrete-time extended Kalman filter in (2.9) is as follows:

- Step 1: ***Select the initial conditions***.

$$\hat{x}_0 = E[x_0] \tag{2.9}$$

$$P_0 = E[(x_0 - \hat{x}_0)(x_0 - \hat{x}_0)^T] \tag{2.10}$$

The same procedure in choosing the initial conditions for the EKF is followed as that of the Kalman filter. The initial state $\hat{x}_0$ and covariance P_0 are starting conditions for the EKF process.

- Step 2: ***Estimate ahead***.

For each time step,

$$\hat{x}_k^- = f_{k-1}(\hat{x}_{k-1}^+, u_{k-1}, 0) \tag{2.11}$$

$$P_k^- = A_{k-1}P_{k-1}^+A_{k-1}^T + G_{k-1}Q_{k-1}G_{k-1}^T \tag{2.12}$$

where the EKF system matrix linearized about the *a posteriori* state estimate for each time step is given as $A_{k-1} = \frac{\partial f_{k-1}}{\partial x}|_{\hat{x}_{k-1}^+}$ and $G_{k-1} = \frac{\partial f_{k-1}}{\partial q}|_{\hat{x}_{k-1}^+}$. The predictions from the state and covariance here in Step 2 is used to correct the gain, error covariance, and state estimate as shown in Step 3.

- Step 3: ***Update Measurement***.

Updating the measurement for each time step is performed for three step:

a. ***Compute the Gain***

$$K_k = P_k^- H_k^T (H_k P_k^- H_k^T + V_k R_k V_k^T)^{-1} \tag{2.13}$$

b. ***Correct the State Estimate***

$$\hat{x}_k^+ = \hat{x}_k^- + K_k[z_k - h_k(\hat{x}_k^-, 0)] \tag{2.14}$$

c. ***Correct the Error Covariance***

$$P_k^+ = P_k^- - K_k H_k P_k^- \tag{2.15}$$

where the matrices evaluated at the state estimate *a priori* is given as $H_k = \frac{\partial h_k}{\partial x}|_{\hat{x}_k^-}$ and $V_k = \frac{\partial h_k}{\partial r}|_{\hat{x}_k^-}$.

2.2.3 Limitations of Kalman Filtering Techniques

For Kalman filtering technique to be implemented, the process and measurement noise structure that affects the system should be known. This requirement is a major shortcoming of Kalman filtering methods since the noise processes are usually unidentified.

Some of the early methods to estimate noise covariance include Output Correlation Method and Innovation Correction Method developed by Mehra [17] via least squares algorithms. The Innovation Correction Method was improved upon by Belanger [18]. More recent noise covariance estimation procedures include autocovariance least squares method developed by Odelson et al. [19], which Rajamani and Rawlings [20] improved upon by introducing optimal weighting and semidefinite programming.

2.3 Application of Kalman Filtering to Polymerization Systems

Numerous applications of state estimation have been cited in literature in various fields of chemical engineering such as polymer processes, biotechnology, and process control. This literature review will be restricted to applications in fields of polymerization processes.

There have been numerous studies of on-line techniques to monitor polymerization processes. On-line densitometry and viscometry was considered by Na and Rhee [21] to conduct an experimental study on the solution polymerization of styrene which was assumed to follow the free radical polymerization reaction kinetics including transfer to monomer and solvent. In their study, a multivariable polynomial autoregressive moving-average (ARMA) model identification for a continuous styrene polymerization reactor was performed by simulation and experimentation. Cherfi and Fevotte [22] assessed the robustness of fiber-optic Near-Infrared (NIR) spectroscopy in their on-line measurement of conversion for both batch and semi-continuous systems, where solution polymerization of methyl methacrylate (MMA) in toluene was monitored at different operating conditions.

However, many challenges and difficulties are encountered when using on-line measuring techniques exclusively. For this reason, on-line methods are implemented with state estimation to improve the performance.

The major issues with reactor application for polymer processes include

- ***Calibration of On-line Monitoring Equipment.***

  To effectively control polymerization processes, the system requires measurement in real-time so that it can be adjusted in a timely manner to achieve the desired response. On-line monitoring can be quite a challenging task. Most polymerization reactor measuring equipment such as Raman spectroscopy for on-line measurement of monomer concentration require extensive calibration which makes it less convenient for the user [23]. Cherfi et al. [1] elaborate on the lack of robustness due to complex modeling, sensitive and prolonged calibration required by most on-line measuring techniques.

- ***Model Equations for On-line Measurement Equipment.***

  On-line measurement equipment such as calorimetry, viscometry, and densitometry have considerable limitations as they require sufficient model equations to provide monomer concentration information from given data [23]. State estimation techniques such as EKF that handle nonlinearities in models, when used in conjunction with model dependent methods such as calorimetry, reduce model discrepancies and performance error, thereby improving on-line measurement procedure [23].

- ***Inability to Measure Certain Properties.***

  Thus far, it is very difficult to measure molecular weight on-line. In fact, there are limited studies in which on-line techniques are used to estimate molecular weight. One case was reported by Kreft and Reed [24] where monomer and polymer concentration measurement was combined with viscosity and light scattering signals to compute molecular weight. Scarcity of on-line measurement

for molecular weight can be problematic in the polymerization industry. It normally requires the estimation of molecular weight information from irregular or delayed experimental analysis which can affect performance of the reactor [25]. Hence, a superior estimation technique is commonly used to calculate molecular weight accurately.

The preferred way to achieve optimal performance in polymer manufacturing process is to monitor the variables that affect the end-product of the polymer properties, and the reaction rates involved in the polymerization process [1]. For the aforementioned shortcomings of on-line monitoring, state estimation techniques are economically inevitable to enable effective control and safe operation of the polymerization reactor.

Literature Review

One of the earliest application of Kalman filtering to polymerization processes was performed by Jo and Bankoff [26]. Free-radical polymerization of vinyl acetate was studied and simulations with various Kalman filter algorithms were tested to provide estimates of weight-average molecular weight and conversion [26]. After developing the kinetic equations, they selected parameters to be adjusted to evaluate the effect of 1) the initial estimate of state variables, 2) process noise covariance, 3) measurement noise covariance, and 4) parameter augmentation. For their study, parameters were adjusted to monitor the effect on the tuning of the filter. They concluded that having poor initial estimates of the state covariance matrix or of the state variables is acceptable but that small estimates of the process noise covariance may cause divergence of the filter. The point was also observed by Park et al. [27]. Fitzgerald [28] and

Schlee et al. [29] elaborate on divergence issues of the Kalman filter by investigating the mechanisms by which error sources affect performance of the filter.

Semino et al. [30] investigated the effect of parameter estimation in the extended Kalman filter for polymerization reactors. From their study on methyl methacrylate polymerization, parameter estimates are incorporated with estimation algorithms to effectively handle analytical error in the model [30]. Kozub and MacGregor [31], and Liotta et al. [32] also address the need for parameters that can be estimated. Liotta et al. [32] suggest adapting the parameter by extending the state of the system to include parameters to be estimated.

Berber et al. [33] performed batch styrene polymerization defined by kinetics of initiator decomposition, initiation, propagation and termination. They were able to integrate an extended Kalman filter in their control algorithm to extract information about the states of the system from noisy measurement. Their algorithm was employed in an on-line control and monitoring software package [33]. They designed two filters to estimate monomer concentration and initiator concentration from available measurement corrupted with noise.

Valappil and Georgakis [34] studied model predictive control of end-use properties in batch reactors. Part of their research was on state estimation of a styrene polymerization process. From their study, conclusions made include 1) the chosen estimated parameters do impact the operation of the EKF, 2) states and parameters with the most uncertainties are typically chosen for estimation, and 3) adapted parameters should be chosen so that the system is observable with existing measurement [34]. Their adaptive parameters were selected randomly. They implemented a two-time scale filter such that their states were updated based on frequent measurements as

well as delayed measurements, depending on availability of measurement information at certain points in the system.

Park et al. [27] monitored a semi-batch methyl methacrylate (MMA) and methyl acrylate (MA) copolymerization reactor using on-line densitometry and viscometry. With an extended Kalman filter (EKF) as the state estimator, Park et al. [27] were able to monitor copolymer properties on-line under both isothermal and non-isothermal conditions. The reactants were assumed to follow free radical copolymerization kinetics including chain transfer to solvent and monomer. Mass balance equations for each reacting component were formulated as well as mass balances for moments of polymer concentration. Park et al. [27] also determined an expression for average molecular weight based on intrinsic viscosity. Their result of on-line measurements for both the isothermal and non-isothermal conditions demonstrated that the on-line viscometry and densitometry can be used to monitor polymer variables in copolymerization reactions. The estimated result using an EKF traced the on-line measurements successfully. Hence, they were able to design a model predictive control algorithm to implement with the copolymerization reactor to improve the performance of the reactor and control polymer qualities.

Kramer et al. [35] performed re-optimization on a semi-continuous emulsion copolymerization (SCEP) system. As mentioned earlier, limitations of on-line technique include inability to measure some polymer properties on-line. Knowledge of co-monomer composition, which is usually not available from on-line measurement, is required to calculate reaction rates [35]. To reach their optimization goal of minimizing batch time, the reaction rates are to be maximized, while maintaining a reaction rate ratio for the co-monomer and thus control copolymer composition [35]. Kramer

et al. [35] stated that models have to be reduced before they can be used for on-line optimization and state estimation. The re-optimization technique employed similar physical model used in Kramer and Gesthuisen [36], which was also reduced by Gesthuisen et al. [37] to develop a simple "pseudo-bulk" kinetic model [35]. The same simultaneous optimization approach as in Cuthrell and Biegler [38], [39], omitting finite elements, was implemented [35]. Successful optimization results were obtained with the reduced model.

Rantow et al. [40] also incorporated a reduced-order model for a semi-batch n-butyl acrylate solution polymerization system. The model was able to predict spectroscopic and chromatographic polymer properties. The nonlinear state estimator formulated based on the reduced model was successful in providing enhanced estimates as proven by the real-time simulation results [40]. Abel et al. [41] used a reduced model, as well, to optimize an industrial semi-batch reactor with the objective to meet polymer quality constraints while reducing the batch time.

Work in Literature Review Compared to Work in Thesis

The on-line optimization techniques presented in this literature review is different from that of this thesis project. For this research, a new technique is incorporated where the observer is connected to an on-line optimization scheme. The feedback measurements of the process are included directly in the optimization procedure as opposed to a control scheme for tracking the calculated trajectories.

Thus far, other researchers have not implemented a true on-line optimization technique as they required former knowledge of the profile structure to generate continuous optimal profiles for batch processes [42]. For instance, Kramer et al. [35] started with

a pre-calculated optimal feed trajectory for their re-optimization strategy. However, the on-line optimization routine with feedback measurements selected for this work is easier to implement. The proposed approach is accomplished by splitting the optimization problem into two, the elapsed cost and future cost, so that the optimization will only be implemented on the remaining portion of the batch instead of the whole profile. Hence, the optimization is based on present conditions rather than the initial conditions of the process.

Alternative State Observers

As mentioned in the Introduction, a variety of observers exist for state estimation. Biagiola and Figueroa [3] provide an extensive review of nonlinear observers. In their work, a high-gain observer was formulated to estimate the entire state vector and time varying parameters of an open-loop unstable continuous stirred tank reactor (CSTR). Their observer design was used in a control scheme to track the temperature profile in the reactor. Kravaris et al. [43] designed a nonlinear observer to estimate the process state variables, together with unknown process or sensor disturbances. They tested their observer design on a biological reactor through simulation studies. Soroush [2] proposed a reduced-order nonlinear observer technique with an adaptive rate of decay of the observer error. The proposed observer was tested on free-radical polymerization reactors, classical chemical reactors and bio-reactors. Astorga et al. [44] considered a continuous-discrete observer and tested it on different copolymerization processes. Chen et al. [45] devised a particle filter for on-line state and parameter estimation in a highly non-linear batch process.

In choosing an observer design, there often is a trade-off between computation and performance. As shown for the alternative state observers, most of them are not

implemented in a true on-line fashion. For instance, Biagiola and Figueroa [3] required a controller to track the temperature profile of the reactor. These observers also have disadvantages. High gain observers are known to be very sensitive to noise. Particle filters require high computation and are not always feasible to implement on-line. In this work, however, a hybrid extended Kalman filter is designed and implemented directly with an on-line optimization routine without the need for controller design for tracking computed profiles. More of the reasons for choosing the Kalman filtering technique is discussed in Chapter 4.

Chapter 3

Real-Time Optimization Scheme

This chapter introduces the polymer reactor system treated in this study. Some new contributions in the development to the initial model derived by Li and Hutchinson [5] are also presented. The on-line optimization scheme and the improvements made to the optimization codes since Perea's [46] addition to the preliminary work are discussed. In addition, a sensitivity analysis is performed on the optimization scheme with updated parameters.

3.1 System Under Study

3.1.1 Initial Work

The motivation for this research originated from an experimental study performed by Li and Hutchinson [5], where solution free-radical copolymerization of butyl methacrylate (BMA) and styrene (STY) was studied under starved-feed conditions. They performed the starved-feed semi-batch BMA/ STY experimentation at 138^0C. Monomer

was added at varying feed compositions at a fixed rate over a period of 6 hours; with respect to monomer, *tert*-butyl peroxyacetate (TBPA) initiator was fed at a constant feed composition of 2.0 wt%. A schematic of the process is shown in Figure 3.1.

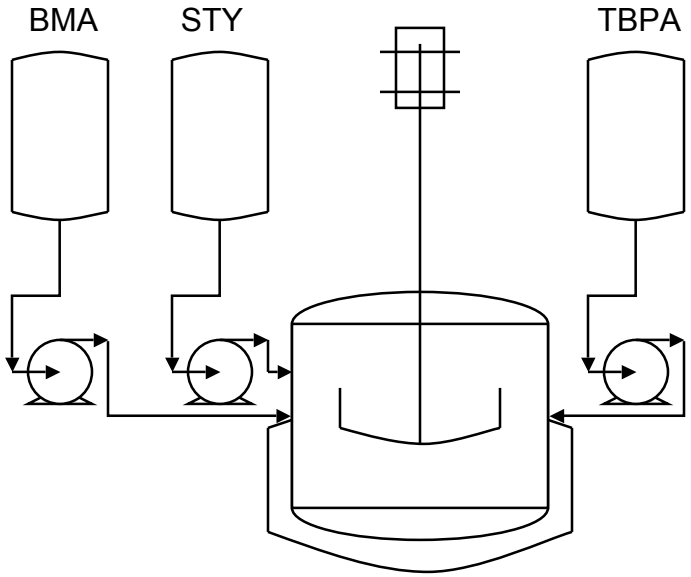

Figure 3.1: Semi-batch reactor setup. Styrene (STY), butyl methacrylate (BMA), and *tert*-butyl peroxyacetate (TBPA) initiator flow rates can be changed separately [46]

.

The model developed for the BMA/ STY study included very detailed mechanisms including depropagation and penultimate propagation kinetics. The results (Figure 3.2) from their study demonstrated success in maintaining low monomer levels throughout the experimentation as the monomer and polymer compositions remained fairly steady.

As Figure 3.2 shows, considerable consistency in polymer composition is achieved when starved-feed operation is implemented. However, adequate monitoring and

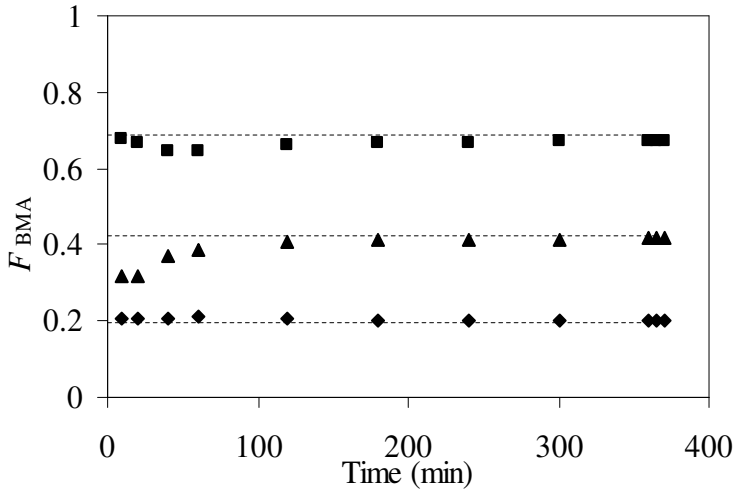

Figure 3.2: Cumulative copolymer composition as calculated from gas chromatography measurement of residual monomer for the feed ratios (wt%) of 75/25 BMA/STY (■); 50/50 BMA/STY (▲); 25/75 BMA/STY (♦) [5]

.

control is needed to attain adequate product quality, in light of possible disturbances that may affect the polymerization process. In addition, there is an incentive to reduce batch time to improve the productivity of the fed-batch process.. For these reasons, further research has been conducted to devise an on-line monitoring process to optimize the system. The main benefit of the optimized system is the reduction of batch time with no deviation from the nominal product specifications.

3.1.2 Contributions of this study

The same BMA/ STY copolymerization system was studied by Perea [46]. Within the scope of this study, Perea's [46] main contributions were revisited. The objectives

of this research are to reformulate the simplified reduced order dynamic model developed in [46] and to investigate the robustness properties of the real-time optimization control scheme.

Reduced Model

Neglecting methacrylate depropagation, styrene thermal initiation and penultimate chain growth kinetics, a reduced order model can be formulated to describe the dynamics of the BMA/STY fed-batch system. Since the full mechanistic model requires further reduction to be used for on-line optimization or state estimation, many authors ([35], [37], [40], and [41]) have derived simplified models to formulate and implement optimization procedures.

In this study, a simplified process model is considered. The derivation of the model relies on several simplifying assumptions such as constant physical properties, perfect mixing, long chain hypothesis (LCH) and radical stationarity/ quasi steady-state assumption (QSSA). Moment balances are performed on live (radical) and dead polymer chains. Mass balances are performed on monomer, solvent and initiator. The kinetic mechanism scheme for the copolymerization process is shown in Table 3.1.

In the free radical copolymerization kinetic mechanism presented in Table 3.1, the initiator I decomposes with efficiency f and rate coefficient k_d to form two primary radicals I^*. For growing polymer radicals P_n and dead polymer chains D_n, subscript n is the number of monomeric units. Primary radicals combine with monomer M_j to initiate polymer radical P_1^j. Monomer M_j adds to radical P_n^i in a chain propagation step with rate coefficient $k_{p_{ij}}$. Chain termination by combination with rate coefficient

Table 3.1: Free radical copolymerization kinetic mechanism for BMA/ STY system

Initiator Decomposition	$I \xrightarrow{k_d} 2fI^*$
Chain Initiation	$I^* + M_j \xrightarrow{k_{i_j}} P_1^j$
Chain Propagation	$P_n^i + M_j \xrightarrow{k_{p_{ij}}} P_{n+1}^j$
Chain Termination	
By Combination	$P_n^i + P_m^j \xrightarrow{k_{tc_{ij}}} D_{n+m}$
By Disproportionation	$P_n^i + P_m^j \xrightarrow{k_{td_{ij}}} D_n + D_m$
Chain Transfer	
To Monomer	$P_n^i + M_j \xrightarrow{k_{tr_{ij}}^{mon}} D_n + P_1^j$
To Solvent	$P_n^i + S \xrightarrow{k_{tr_i}^{sol}} D_n + S^*$ $S^* + M_j \xrightarrow{k_{i_j}^{sol}} D_n + P_1^j$

$k_{tc_{ij}}$ or disproportionation with rate coefficient $k_{td_{ij}}$ happens when two chains unite. Chain transfer occurs when hydrogen is abstracted from monomer M_j or solvent S by radical i, with rate coefficient $k_{tr_{ij}}^{mon}$ and $k_{tr_i}^{sol}$. Chain termination and chain transfer form dead chains.

The model parameters and kinetic rate coefficient for the optimization work presented in Table 3.1 are the same as that used in the original experimentation in [5]. These parameters and coefficients are shown in Table 3.2. The basis for deriving the rate constants and choosing the parameters are explained in [5].

Dynamic Mathematical Model

After the derivation of the reduced model, a dynamic mathematical model is developed based on the reduced kinetic mechanisms. These mechanisms are incorporated into the semi-batch material balances to account for process changes and to maintain polymer quality with a real-time measurement-based optimization control method.

Table 3.2: Model parameters and kinetic rate coefficients for butyl methacrylate (A)/ styrene (B) system [5]

Kinetic Mechanism	**Rate Term**	**Value at 138^{0}C**
Initiation [s^{-1}]	$k_d(s^{-1}) = 6.78 \times 10^{-15}\exp(-17714T^{-1})$ $f = 0.515$	1.32×10^{-3}
Propagation [$L.mol^{-1}.s^{-1}$]	$k_{p_{AA}} = 3.80 \times 10^6\exp(-2754.2T^{-1})$ $k_{p_{BB}} = 4.266 \times 10^7\exp(-3910T^{-1})$ $r_A = \frac{k_{p_{AA}}}{k_{p_{AB}}} = 0.42$, $r_B = \frac{k_{p_{BB}}}{k_{p_{BA}}} = 0.61$	4.69×10^3 3.16×10^3
Termination [$L.mol^{-1}.s^{-1}$]	$k_t^{cop} = 4.5 \times 10^8$ $\alpha = 0.65$, $\beta = 0.01$, $\gamma = 0.33$	
Chain Transfer [$L.mol^{-1}.s^{-1}$]		
To monomer	$k_{tr_{AA}}^{mon} = 1.56 \times 10^2\exp(-2621T^{-1})$ $k_{tr_{BB}}^{mon} = 2.31 \times 10^6\exp(-6377T^{-1})$ $k_{tr_{ij}}^{mon} = k_{tr_{jj}}^{mon} \frac{k_{p_{ij}}}{k_{p_{jj}}}$	0.27 0.427
To solvent	$k_{tr_{AA}}^{sol} = C_A^{sol} k_{p_{AA}}$ $k_{tr_{BB}}^{sol} = C_B^{sol} k_{p_{BB}}$ $C_A^{sol} = 5.0 \times 10^{-4}$, $C_B^{sol} = 8.0 \times 10^{-4}$	2.345 2.528
Physical Properties		
Density [$kg.L^{-1}$]	$\rho_{BMA} = 0.915 - 9.64 \times 10^{-4}T(^0C)$ $\rho_{ST} = 0.919 - 6.65 \times 10^{-4}T(^0C)$ $\rho_{pol} = 1.19 - 8.07 \times 10^{-4}T(^0C)$ $\rho_{sol} = 0.892 - 1.3 \times 10^{-3}T(^0C)$	0.782 0.827 1.079 0.713
Molecular Weight [$kg.mol^{-1}$]	$\bar{M}_A = 142.2 \times 10^{-3}$ $\bar{M}_B = 104.15 \times 10^{-3}$ $\bar{M}_I = 132.16 \times 10^{-3}$ $\bar{M}_{sol} = 106.17 \times 10^{-3}$	

The BMA/ STY copolymerization reaction is expressed by (3.1):

$$\frac{dx_1}{dt} = u_1(t) - x_1\left(k_{p_{AA}}\lambda_o^A(t) + k_{p_{BA}}\lambda_o^B(t)\right) \tag{3.1a}$$
$$\frac{dx_2}{dt} = u_2(t) - x_2\left(k_{p_{BB}}\lambda_o^B(t) + k_{p_{AB}}\lambda_o^A(t)\right) \tag{3.1b}$$
$$\frac{dx_3}{dt} = u_3(t) - k_d x_3(t) \tag{3.1c}$$
$$\frac{dx_4}{dt} = x_1\left(k_{p_{AA}}\lambda_o^A(t) + k_{p_{BA}}\lambda_o^B(t)\right) \tag{3.1d}$$
$$\frac{dx_5}{dt} = x_2\left(k_{p_{BB}}\lambda_o^B(t) + k_{p_{AB}}\lambda_o^A(t)\right) \tag{3.1e}$$
$$\frac{dx_6}{dt} = V(t)R_{\mu_0}(t) \tag{3.1f}$$

where x_1, x_2 and x_3 denote the total mass of unreacted BMA, STY and initiator, respectively; x_4 and x_5 denote the mass of BMA and STY in the polymer chains; x_6 is the moles of polymer in the system (needed to compute the number-averaged molecular weight); u_1, u_2 and u_3 are the input mass flow rates of BMA, STY and initiator; $\lambda_o^A(t)$ and $\lambda_o^B(t)$ are given by (3.5) below.

Based on a quasi steady-state assumption, the total moles of radicals is given by

$$\lambda_o^{tot} = \left(\frac{2k_D f}{\bar{M}_I}\right)^{1/2}\left(\frac{\rho_{tot}(t)}{k_t^{cop}(t)}\right)^{1/2}\left(\frac{x_3}{M_r(t)}\right)^{1/2} \tag{3.2}$$

Assuming the volume in the reactor is additive, the total density of the system $\rho_{tot}(t)$ is derived; $\bar{M}_I$ is the molar mass of initiator; and the cumulative mass is formulated as

$$M_r(t) = x_1 + x_2 + x_3 + x_4 + x_5 + m_{sol} \tag{3.3}$$

where m_{sol} represents the amount of solvent in the reactor at the beginning of the reaction; and $k_t^{cop}(t)$ is the copolymerization termination rate coefficient that is estimated by fitting model predictions to experimental data.

The mole fraction of unreacted monomer is given as

$$f_1(t) = \frac{x_1(t)\bar{M}_B}{x_1(t)\bar{M}_B + x_2(t)\bar{M}_A}; f_2(t) = 1 - f_1(t) \tag{3.4}$$

where $\bar{M}_A$ and $\bar{M}_B$ are monomer molar masses.

The radical concentration of BMA(^{A}) and STY(^{B}) is

$$\lambda_o^A(t) = \lambda_o^{tot}(t) f_R^A(t); \quad \lambda_o^B(t) = \lambda_o^{tot}(t) f_R^B(t) \tag{3.5}$$

where the long-chain hypothesis is used to calculate each radical fraction:

$$f_R^A(t) = \frac{k_{p_{BA}}\bar{M}_B x_1}{k_{p_{BA}}\bar{M}_B x_1 + k_{p_{AB}}\bar{M}_A x_2}; f_R^B(t) = 1 - f_R^A(t) \tag{3.6}$$

The rate of chain generation, used to calculate the polymer molecular weight, is as follows:

$$R_{\mu_0}(t) = R_{init}(t) + R_{tr}^{sol}(t) + R_{tr}^{mon}(t) - R_{tc}(t)^{1/2} \tag{3.7}$$

where the rate of radical production from initiation, transfer to solvent, transfer to monomer, and termination by combination is given as:

$$
\begin{aligned}
R_{init}(t) &= \frac{1}{M_r(t)}\left(\frac{2k_d f}{\bar{M}_I}\rho_{tot}(t)x_3\right) \\
R_{tr}^{sol}(t) &= \frac{s(t)}{M_r(t)}\lambda_o^{tot}(t)\rho_{tot}(t) \\
R_{tf}^{mon}(t) &= \left[m_1(t)\frac{x_1}{M_r(t)} + m_2(t)\frac{x_2}{M_r(t)}\right]\lambda_o^{tot}\rho_{tot}(t) \\
R_{tc}(t) &= k_t^{cop}\Bigg((1-\alpha)\left(\lambda_o^A(t)\right)^2 + (1-\beta)\left(\lambda_o^B(t)\right)^2 \\
&\qquad +2(1-\gamma)\lambda_o^A(t)\lambda_o^B(t)\Bigg)
\end{aligned}
\tag{3.8}
$$

where

$$
\begin{aligned}
m_1(t) &= \frac{1}{\bar{M}_A}\left(k_{tr_{AA}}^{mon} f_R^A(t) + k_{tr_{BA}}^{mon} f_R^B(t)\right) \\
m_2(t) &= \frac{1}{\bar{M}_B}\left(k_{tr_{BB}}^{mon} f_R^B(t) + k_{tr_{AB}}^{mon} f_R^A(t)\right) \\
s(t) &= \frac{m_{sol}}{\bar{M}_{sol}}\left(k_{tr_{AA}}^{sol} f_R^A(t) + k_{tr_{BA}}^{sol} f_R^B(t)\right)
\end{aligned}
$$

The parameters α, β and γ represent the fraction of termination occurring by disproportionation for A, BB and AB, respectively.

The monomer conversion formulated in terms of the states of the system is

$$\chi_m(t) = \frac{x_4 + x_5}{x_1 + x_2 + x_4 + x_5}$$

The number-average molecular weight and copolymer composition, both important quantities for the determination of polymer quality, are calculated as

$$M_n(t) = \frac{x_4 + x_5}{x_6}, \quad F(t) = \left(\frac{x_4}{\bar{M}_A}\right)\left(\frac{x_4}{\bar{M}_A} + \frac{x_5}{\bar{M}_B}\right)^{-1}$$

It is imperative that $M_n(t)$ and $F(t)$ remain relatively constant throughout the reaction period to ensure that high conversion is achieved. The optimization problem formulated below is designed to keep $M_n(t)$ and $F(t)$ at their setpoints while meeting the constraints of the system. The real-time optimization scheme employed in this study is described below.

Real-Time Optimization Scheme

A real-time optimization scheme is formulated to effectively monitor and control the BMA/ STY polymerization process. As explained in the last section of Chapter 2, a real-time optimization scheme is proposed in which on-line measurements of process variables are used to update optimal trajectories in real-time. This technique contrasts with existing techniques in which a tracking controller is used to track an optimal trajectory computed off-line. Using a suitable model of the process, the procedure employs a real-time dynamic optimization routine similar to model predictive control that guarantees continuous improvement of the user defined cost subject to state and input constraints.

The real-time optimization scheme is based on a nominal dynamic optimization problem of interest. A generic dynamic optimization problem can be represented mathematically as follows:

$$\min_{\theta \ldots \theta_p, T} J = \int_0^T q(x(t), u(t))dt \tag{3.9}$$

subject to the dynamics in (3.1) and the following constraints

$$w(x(t), u(t)) \geq 0 \tag{3.10}$$

$$x(0) = x_o \tag{3.11}$$

$$x(T) = x_f \tag{3.12}$$

$$u_j(t) = \sum_{i=1}^{N} \theta_{ij} \Xi_j(t), 1 \leq j \leq p \tag{3.13}$$

where x are the state variables of the system, u represents the input variables. It is assumed that the input trajectories $u_j(t)$ are parameterized as described in (3.13), where θ are parameters to be found and Ξ are basic functions. The objective is to minimize the cost function (3.9) subject to the process dynamics (3.1) and the constraints on the path (3.10) and the end-point variable (3.12).

It is assumed that there exists a continuous control u that can steer the system from the states at the initial point to the states of the system at the final time. The optimal control problem is then solved with respect to the parameter values. The parameters are assumed to be contained in a compact convex subset of the constrained set (3.9) in $\mathbb{R}^N$. The cost function and the constraints of the optimization problem are assumed to be sufficiently smooth. The constrained set is assumed to be convex with respect to the parameters. In addition, the cost J is also assumed to be convex with respect to the parameters. Following the necessary conditions of optimization, these assumptions guarantee the existence of a local optimizer for the constrained problem.

For the purpose of this study, the cost function is designed to maintain the number-average molecular weight $M_n(t)$ and copolymer composition $F(t)$ at their respective setpoints. A suitable cost function for this purpose is the following quadratic functional:

$$J = \int_0^{t_f} \left(\omega_1 \left(\frac{M_n(t)}{M_{sp}} - 1 \right)^2 + \omega_2 \left(\frac{F(t)}{F_{sp}} - 1 \right)^2 \right) dt \tag{3.14}$$

where the setpoints for molecular weight and copolymer composition are M_{sp} and F_{sp}, respectively; ω_1 and ω_2 are weights used to scale the cost function. The batch time t_f, assumed to be a positive nonzero number, is considered as a decision variable along with the parameters θ.

The constraints of the system are designed to handle important performance objectives for the fed-batch system. The most important constraints of the system are used to ensure safety of the system. They restrict the amount of heat discharge, the unreacted monomer and initiator as follows:

$$0 \leq x_k \leq x_k^{max},\ x_{k+3} \geq 0 \quad k \in \{1,\ 2,\ 3\} \tag{3.15}$$

Additional constraints on the input variables ensure that flow rates are positive. They are stated as:

$$0 \leq u_k(t) \leq u_k^{max}, \quad k \in \{1,\ 2,\ 3\} \tag{3.16}$$

The end-point constraint guarantees that a desired mass of polymer is reached at the end of the batch. It is given by:

$$x_4(t_f) + x_5(t_f) = m_{pol}(t_f) \tag{3.17}$$

Having defined the cost function and the state and input constraints, one must assign a specific choice for the input parameterization (3.13). In this study, the input variables are chosen to be the flow rates. For the duration of the batch, the input or

control functions were parameterized as

$$\begin{aligned} u_1(t) &= \theta_1 \\ u_2(t) &= \theta_2\theta_1 \\ u_3(t) &= \theta_3\theta_1 \end{aligned} \tag{3.18}$$

where θ_1, θ_2 and θ_3 are the parameters to be assigned in the solution of the optimization problem. This parameterization mirrors the constant flow rate conditions employed in the experimental study of [5]. The conditions outlined in [5] provide some valuable initial estimates for the parameters that are considered in numerical implementation of the proposed real-time optimization scheme and the simulation study described below.

The challenge associated with the design of a real-time optimization scheme is to devise an algorithm that can solve the optimization problem (3.9) as efficiently as possible to permit real-time updates of the parameters of the input trajectories. To achieve this, the real-time optimization scheme implements a transformed version of the nominal optimization problem that can take into account new process measurements and constraints.

The optimization procedure aims to regulate the plant process by adapting to disturbances in real-time while directing the system towards the local optimum of the objective function in (3.14) with respect to the parameterization in (3.18). The optimization searches for the optimum within a restricted set of parameters to reach a local optimum.

The incorporation of the constraints is a vital part of the proposed algorithm. A standard mechanism used to incorporate constraints is to define barrier functions. Logarithmic barrier functions are used to penalize all parameter values which violate

the constraints. By construction, this implies that a known feasible set of parameters is known that is in the interior of the constraint set. Barrier functions form the basis of so-called interior point methods.

In the context of real-time optimization, interior point methods are used to transform the constrained optimization problem into an unconstrained one subject to the strict feasibility of the initial estimate of solution to the optimizer [42]. Barrier functions are defined to handle all path constraints in the optimization problem.

The m **path constraints** are defined as

$$w_k = -x_k + x_k^{max} + \epsilon,\ w_{k+3} = x_k + \epsilon,\ k = 1,\ 2,\ 3.$$

The **input constraints** are defined as

$$w_{k+6} = -u_k + u_k^{max} + \epsilon,\ w_{k+9} = u_k + \epsilon,\ k = 1,\ 2,\ 3.$$

A typical logarithmic barrier function to handle the path constraints is of the general form

$$-\mu_1 \sum_{j=1}^{m} \log\left(w_j + \epsilon\right)$$

where μ_1 and ϵ are constant strictly positive tuning parameters. This time-varying quantity can be added to the integrand of the cost functional J to penalize any parameter value that violates the path constraints.

End-point constraints are typically not handled using interior point methods as knowledge of parameters that meet such constraints is typically much more difficult. To handle these constraints, a terminal penalty function is used.

Let the **end-point constraints** be defined as

$$w_f = x_4 + x_5 - m_{pol}(t_f),$$

then a terminal penalty function is included by adding a term of the form Mw_f^2 to

the cost function J where M is a potentially large positive number.

Having defined the barrier functions and terminal penalty function, the cost functional for the nominal optimization problem can be transformed to

$$J_{ip}(\theta) = \int_0^{t_f} \left(\omega_1 \left(\frac{M_n(\tau)}{M_{sp}} - 1 \right)^2 + \omega_2 \left(\frac{F(\tau)}{F_{sp}} - 1 \right)^2 - \mu_1 \sum_{j=1}^{m} \log\left(w_j + \epsilon\right) \right) d\tau + M(w_f)^2 \tag{3.19}$$

where the integration variable is $\tau \in [0, t_f]$. The algorithm parameter $M > 0$ is the penalty function; the barrier function parameter $\mu_1 > 0$ is for the logarithm expression; and the constraint relaxation factor $\epsilon > 0$ avoids singularity of the barrier term. Typically, small values of μ and ϵ are chosen to avoid breach in constraint and a large value of M is used to ensure the endpoint constraints are met [42].

This transformation of the cost functional is such that the optimization of J_{ip} can be solved using unconstrained optimization techniques such as gradient based searches.

The following assumptions ensure that there exists a local optimum of the constrained optimization problem:

- The parameters are within a compact subset Ω_p of $\mathbb{R}^N$,
  where convex subset of $\mathbb{R}^N$ is given by the constrained parameter set
  $\Omega = \left\{ \theta_n \in \mathbb{R}^N \,|w(x(t), \phi(\theta, t) \geq 0, \ \forall t \in [0, t_f] \right\}$

- The cost functional J is convex and continuously differentiable on Ω_p,
  $J : \mathbb{R}^N \to \mathbb{R}$

Having defined a transformed optimization encoding the path and end-point constraints, a measurement-based real-time optimization scheme can be designed.

Assume that a new measurement, $x(t)$, is available at a given time t. Up to time t, an input trajectory $u(\tau)$ has already been applied over the interval $\tau \in [0, t)$, accounting for a certain portion of the cost. Clearly, this incurred cost can no longer be affected by changes in the control policy. However, one can still have an impact on the total batch cost if one can predict the remaining cost from the current time to the end of the batch. That is, the cost incurred at time t can be estimated as follows

$$\begin{aligned} J_{ip}(\theta(t)) \quad = \quad & \int_0^t (L(x(\tau), u(\tau))d\tau + \int_t^T L(x_p(\tau), \hat{u}(\theta(t), \tau))d\tau \\ & + M||x_p(T) - x_f||^2 \end{aligned} \tag{3.20}$$

where $L(x, u) = q(x, u) - \mu_1 \sum_{j=1}^{m} \log(w_j(x, u) + \epsilon)$. The cost in (3.19) is split in two. The first integral represents the elapsed cost which is calculated from the measured states up to time t. The second integral represents the predicted cost remaining and is calculated using the current parameter values. Using this estimate of the current cost, one can determine the future outcome of the batch. More importantly, one can compute the gradient of the cost with respect to the parameters and, hence, update the remaining profile of the batch. The simplest update is to update the parameters in the direction of the gradient of $J_{ip}(t)$ with respect to θ as follows,

$$\dot{\theta} = -k\nabla_\theta J_{ip} \tag{3.21}$$

where $k > 0$ is an adaptive gain or positive definite scaling matrix.

Following standard adaptive control techniques, a projection algorithm is used to prevent the update law from leaving the set ω_W. The modified update law can be written as

$$\dot{\theta} = \text{Proj}\left(-k\nabla_\theta J_{ip}, \Omega_w\right) \tag{3.22}$$

where the projection algorithm Proj$(\cdot)$ is such that:

- The parameters stay within the convex set $\Omega_w = \{\theta \in \Omega_p \,|\|\theta\| \leq \eta\}$ for some $\eta > 0$
- The cost is strictly decreasing except when the gradient is zero, which occurs at the local minima (at the end of the batch).

Exact expressions for the projection algorithm depends on the shape of the convex set Ω_w. The most common sets used in adaptive control include hypercubes and spherical sets.

The update law (3.22) is implemented as follows. At each time t, the gradient estimate is computed using the updated measurements and model predictions. The parameters are then updated in the direction of the gradient. This strategy ensures that the cost functional J_{ip} decreases at each subsequent step. A simple Lyapunov-based argument can be used to demonstrate the continuous decrease of the cost. To show this, one only needs to differentiate the cost functional with respect to time and substitute the value for the update law and confirm that $\dot{J}_{ip} \leq 0 \; \forall t \geq 0$.

3.1.3 Additional Contribution of this Study

Within the scope of this study, many additional modifications have been made to enhance Perea's [46] research contributions. These changes have been tabulated in Table 3.3 to outline the distinction between the former and current model parameters and rate coefficients. The basis of contrast is for the BMA/ STY optimization

comparative to the typical starved feed strategy for BMA/ STY 50:50 feed rate ratio.

Table 3.3: Updated model parameters and kinetic rate coefficients (A=BMA, B=STY, j=1,2,3,4)

Symbol	Previous Value	Current Value
Algorithm Parameters		
M	2 x 10^{4}	1 x 10^{8}
μ	1 x 10^{-11}	1 x 10^{-1}
k_j	(1 x 10^{-12}, 1 x 10^{-5}, 1 x 10^{-5},1 x 10^{-4})	5 x 10^{-3}
Weighting Factors		
ω_1	1 x 10^{4}	1000
ω_2	1 x 10^{4}	1000
Rate Coefficients		
Termination [L.mol^{-1}.s^{-1}]		
k_t^{cop}	$10^{(f_{1(t)}log(k_t^{AA})+f_{2(t)}log(k_t^{BB}))}$	4.5 x 10^{8}
Transfer to solvent ratio		
C_A^{sol}	5.55exp(-4590T^{-1})	5 x 10^{-4}
C_B^{sol}	1 x 10^{-4}	8 x 10^{-4}

As can be seen in Table 3.3, a major difference from the previous work is the algorithm parameters. In (3.22), the gradient of J_{ip} is obtained with respect to the parameter θ. For the former research, the adaptive gain k is given by $k_j I$, where I represents the identity matrix. Hence, four adaptive gains (k_1, k_2, k_3, k_4) are needed for the update law (3.22). In the current study, the adaptive gain is given by

$$k = k_0 \Gamma^{-1}$$

where Γ is the Hessian of J_{ip} with respect to the parameters. That is,

$$\Gamma = \frac{\partial^2 J_{ip}}{\partial \theta \partial \theta^T}.$$

The resulting update is a Newton like update law. The Hessian matrix is used to remove any scaling issue that can arise in gradient-based descent. In contrast to Perea's work, the use of the Newton-like update allows one to use a single gain

parameter $k_0 = 0.005$ for all simulations. The major drawback is the increase in computation required for the calculation of the Hessian.

Further distinction from the previous study is the value of the copolymerization termination rate coefficient $k_t^{cop}(t)$, which was formerly computed with respect to the monomer molar composition $k_{t_{AA}}$ and the homo-termination rate coefficient $k_{t_{BB}}$ as $\log(k_t^{cop}(t)) = f_1(t)\log(k_{t_{AA}}) + f_2(t)\log(k_{t_{BB}})$. The updated parameter value $k_t^{cop}(t)$ is estimated using experimental data to obtain the best representation of the monomer concentrations in Figure 3.3. The updated reduced model showed reasonable accuracy when compared with the experimental data reported in [5], as shown in Figure 3.3.

The chain transfer to solvent ratios (C_A^{sol} and C_B^{sol}) were updated based upon more recent experimental work over a wider range of operating conditions, as described in Wei and Hutchinson [47].

In this study, various alternative parameterization of the input trajectories are considered. Three distinct parameterizations are studied. The three different cases are given as follows:

- Case 1: Single Constant (3.18)

$$u_1(t) = \theta_1,\ u_2(t) = \theta_2\theta_1,\ u_3(t) = \theta_3\theta_1$$

- Case 2: Exponential starved-feed strategy

$$u_1(t) = \theta_1 \exp^{\theta_2 t},\ u_2(t) = \theta_3 u_1(t),\ u_3(t) = \theta_4 u_1(t) \tag{3.23}$$

- Case 3: Independent exponential starved-feed operation

$$u_1(t) = \theta_1 \exp^{\theta_2 t},\ u_2(t) = \theta_3 \exp^{\theta_4 t},\ u_3(t) = \theta_5 \exp^{\theta_6 t} \tag{3.24}$$

The results from the optimization of the updated model for Case 1, Case 2, and Case 3 are presented in the next section of this thesis.

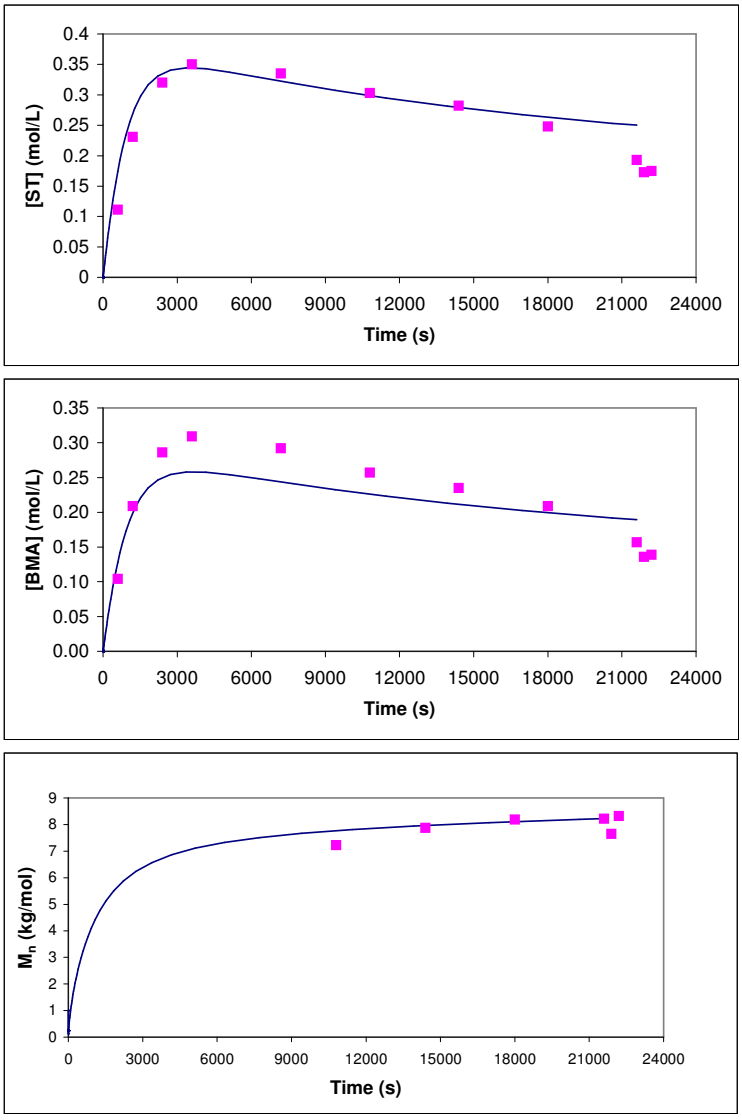

Figure 3.3: Reduced model predictions (lines) compared to experimental data (dots) in [5] for BMA concentration (top), STY concentration (middle), and number-averaged molecular weight M_n (bottom)

3.2 Optimization Results

The case studies set the initial conditions for monomer and initiator mass feed rates as used in the experimental study in [5] and shown in Table 3.4.

Table 3.4: Starved feed policy used in Li and Hutchinson [5]

Results	**50 : 50 BMA : STY (wtratio)**	**Description**
m_{BMA}^{fed} (kg)	2.46×10^{-1}	Total mass of BMA feed
m_{STY}^{fed} (kg)	2.46×10^{-1}	Total mass of STY feed
m_{TBPA}^{fed} (kg)	9.7×10^{-3}	Total mass of initiator feed
t_f (min)	360	Final batch time

For Case 1 to 3,

- The initial conditions are

$$x_i(0) = 0,\ i = 1, \ldots, 6$$

- The setpoints are

$$\begin{aligned} M_n(kg/mol) &= 8 \\ F(BMA\ mole\ fraction) &= 0.43 \end{aligned}$$

- The input and state constraints are

$$\begin{aligned} u_i(t) &\in [0, 0.03], i = 1, 2, 3 \\ x_1(t) &\in [0, 0.03] \\ x_2(t) &\in [0, 0.03] \\ x_3(t) &\in [0, 5.0 \times 10^{-3}] \end{aligned}$$

- The end-point constraint (final mass of polymer) is

$$m_{pol}(t_f)(kg) = 0.474$$

- Algorithm parameter are

$$\begin{aligned} k &= 5 \times 10^{-3} \\ \epsilon &= 1 \times 10^{-12} \\ M &= 1 \times 10^{8} \\ \mu &= 1 \times 10^{-1} \end{aligned}$$

Simulation Results

The simulation results for Case 2 is shown in Figures 3.4, 3.5, 3.6, and 3.7 for total number of steps $n = 30,000$. These optimization results are obtained starting from the initial trajectory with constant feeds that match the experimental conditions in Table 3.4. In other words, the on-line optimization software starts with the initial inputs for the experiment and improves the profile of the batch in real-time as it minimizes the time. The simulation time for the 360 minutes (21600 seconds) batch experiment is 2.59 minutes using a 1.86Ghz Intel Core 2 processor, showing that on-line implementation of this algorithm is indeed feasible.

The outputs of the system, $M_n(kg/mol)$, F, mass of polymer generated, and total

mass of reactor content, are presented in Figure 3.4. The subsequent input profiles, u_1, u_2, u_3, are shown in Figure 3.5. The state trajectories, x_1, x_2, x_3, are displayed in Figure 3.6. The profiles for x_1 and x_2 approach their upper bound. Trajectories for x_4, x_5, x_6 are shown in Figure 3.7. Implementation of the optimization scheme reduced the batch time by 31%, while maintaining product quality ($M_n(kg/mol)$ and F) on target.

M_n and F for Case 1, 2, and 3 are compared in Figures 3.8 and 3.9, respectively. The trajectories are seen to improve for all three cases. Case 3 has the best profile with the fastest approach to the M_n setpoint and the greatest reduction in batch time from 21600 sec to 12600 sec (42% reduction in t_f). This result is expected since the parameterization in Case 3 contains the most degrees of freedom and flexibility, especially by the decoupling of initiator and monomer feed rates. The next best result was for Case 1 at 14600 sec (32% reduction in t_f), followed by Case 2 at 14900 sec. Case 1 had a slightly lower final batch time which was unexpected as Case 2 has more flexibility in the input parameterizations.

From the results in this section, the proposed on-line optimization scheme is proven to be effective, and to reach the objective of meeting the specification for the polymer while satisfying the constraints and reducing the batch time. The effectiveness of the optimization scheme is justified as all the setpoints are met for the molecular weight, copolymer composition, states, input, endpoint constraint for final polymer produced and mass of reactor content. Further details are given in the recent publication describing this work [48].

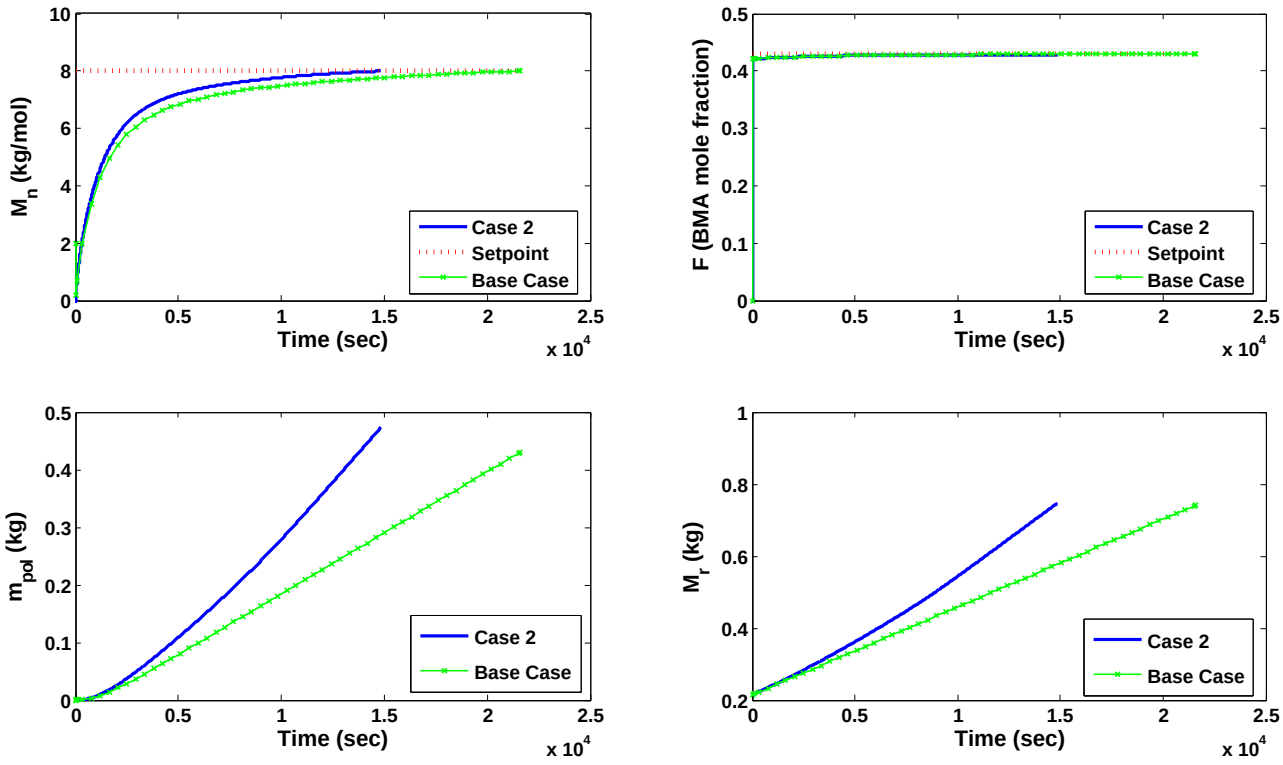

Figure 3.4: Profiles for M_n (kg/mol), F (BMA mole fraction), mass of polymer generated (kg) and total mass of reactor content (kg) with Case 2 dynamic optimization for $u_i(t) \in [0, 0.03], i = 1, 2, 3, x_1(t) = x_2(t) \in [0, 0.03], x_3(t) \in [0, 5.0 \times 10^{-3}], k = 5 \times 10^{-3}$; base case model represents experimental setup with constant input

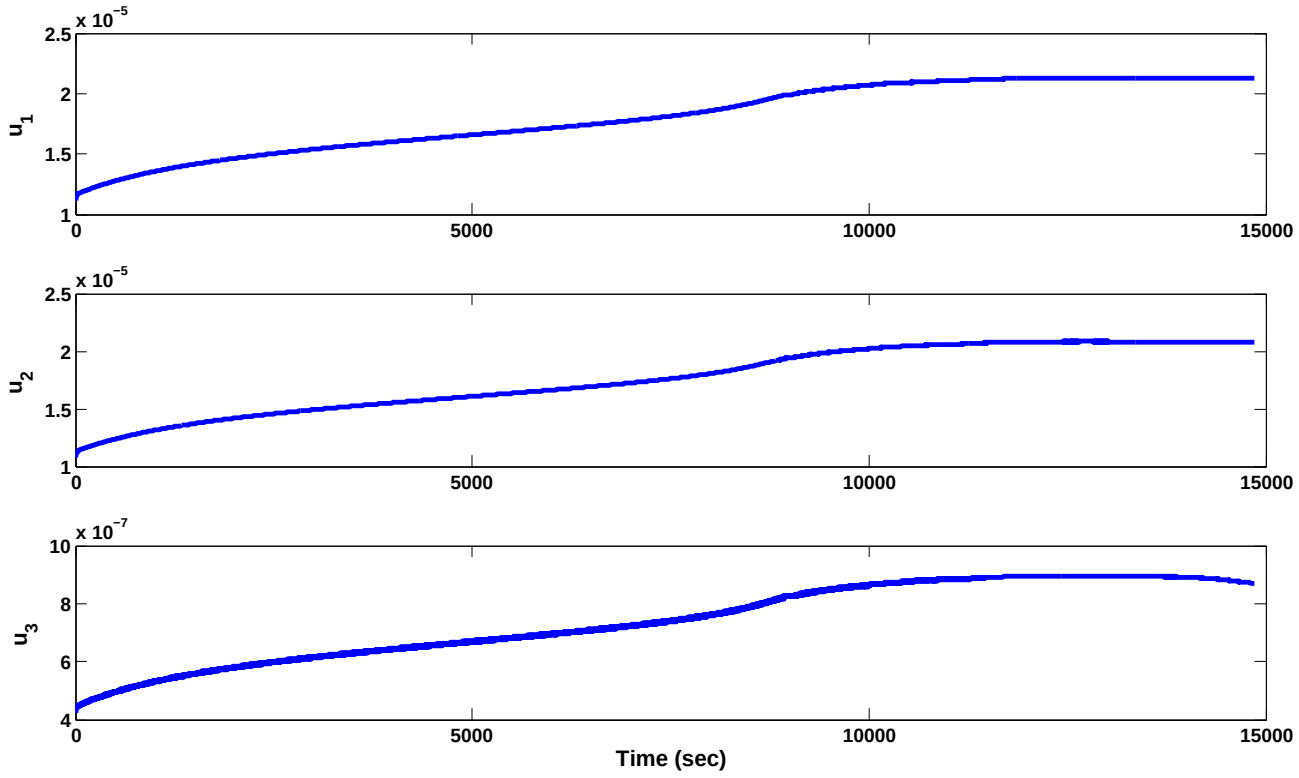

Figure 3.5: Profiles for u_1, u_2, u_3 with Case 2 dynamic optimization for $u_i(t) \in [0, 0.03], i = 1, 2, 3, x_1(t) = x_2(t) \in [0, 0.03], x_3(t) \in [0, 5.0 \times 10^{-3}], k = 5 \times 10^{-3}$

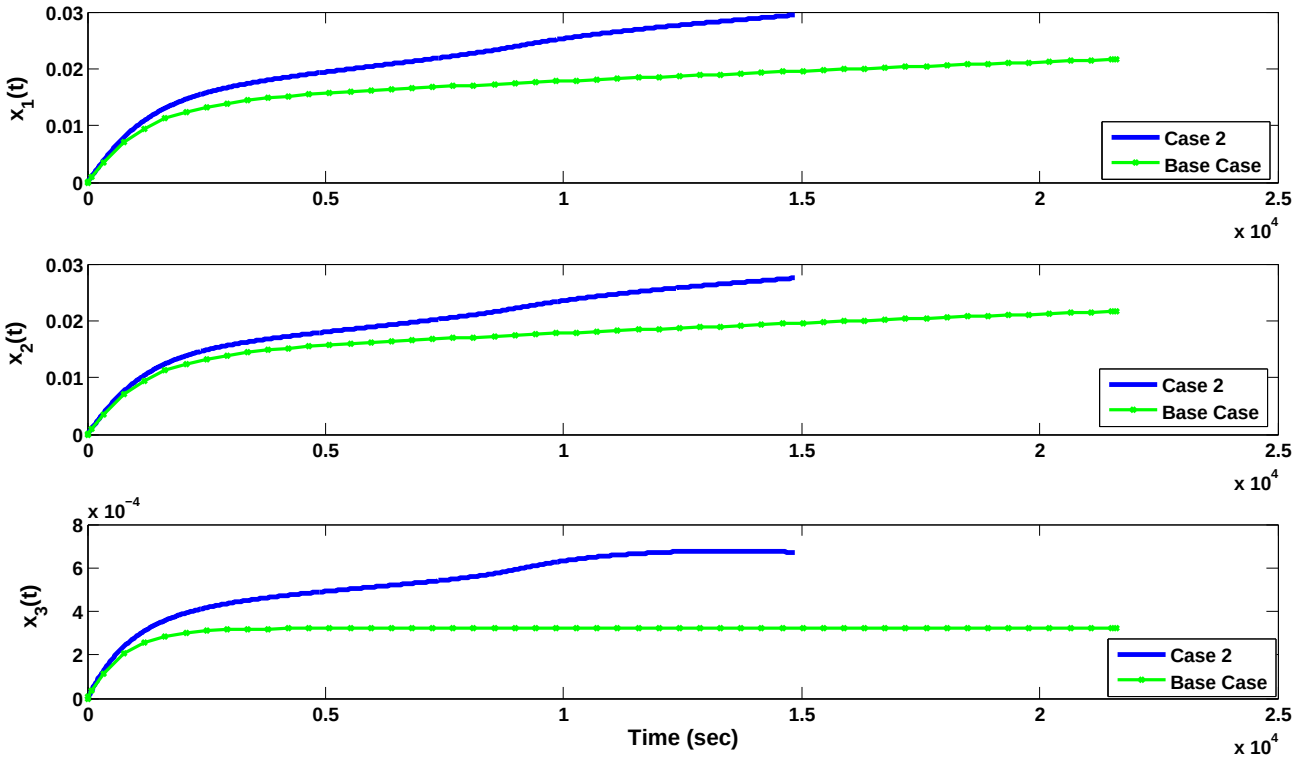

Figure 3.6: Profiles for x_1, x_2, x_3 with Case 2 dynamic optimization for $u_i(t) \in [0, 0.03], i = 1, 2, 3, x_1(t) = x_2(t) \in [0, 0.03], x_3(t) \in [0, 5.0 \times 10^{-3}], k = 5 \times 10^{-3}$; base case model represents experimental setup with constant input

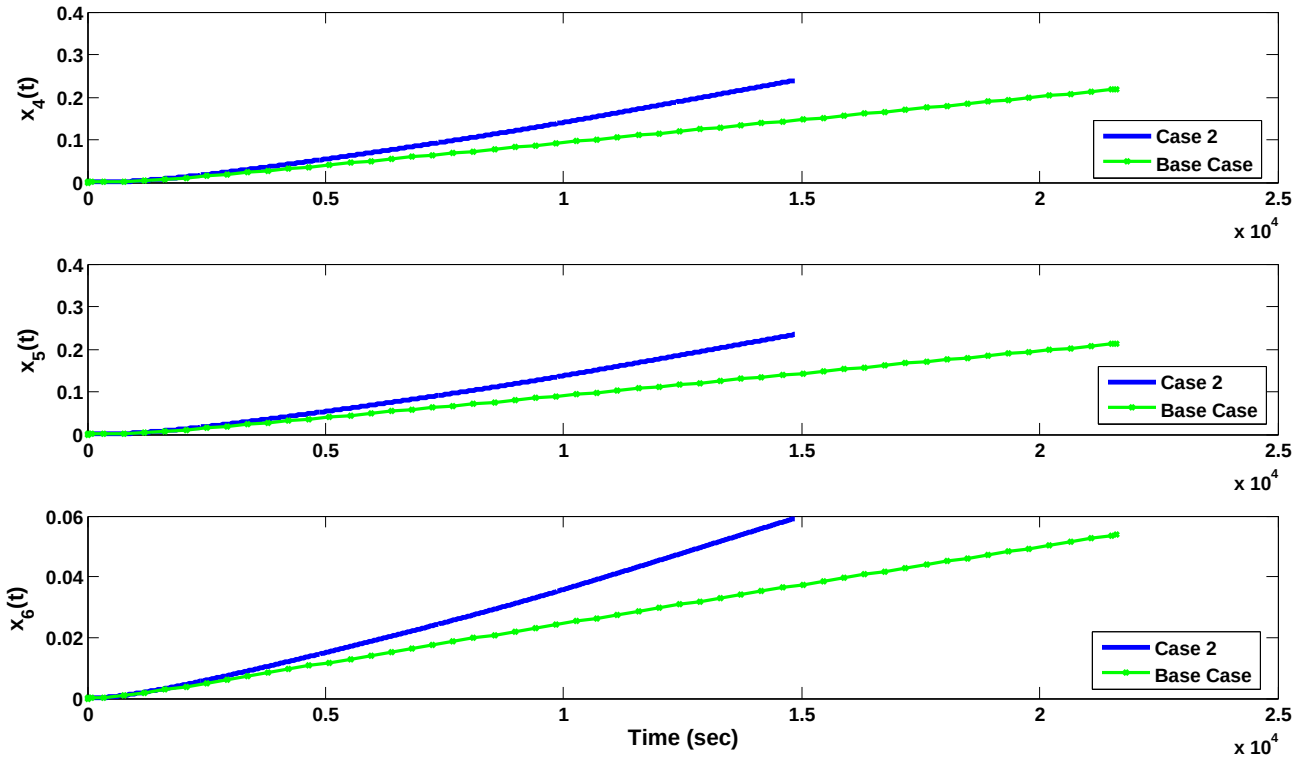

Figure 3.7: Profiles for x_4, x_5, x_6 with Case 2 dynamic optimization with $u_i(t) \in [0, 0.03], i = 1, 2, 3, x_1(t) = x_2(t) \in [0, 0.03], x_3(t) \in [0, 5.0 \times 10^{-3}], k = 5 \times 10^{-3}$; base case model represents experimental setup with constant input

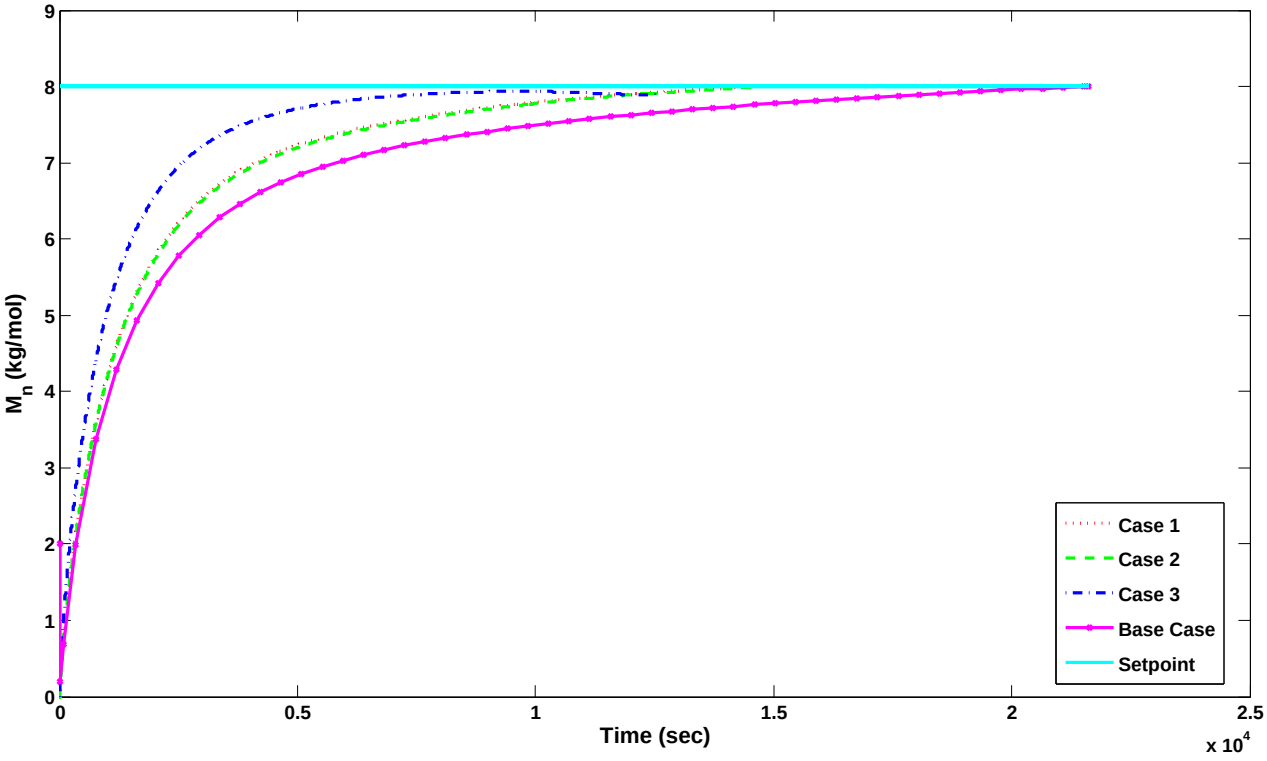

Figure 3.8: M_n real-time optimization for Case 1, 2 and 3 with $u_i(t) \in [0, 0.03], i = 1, 2, 3, x_1(t) = x_2(t) \in [0, 0.03], x_3(t) \in [0, 5.0 \times 10^{-3}], k = 5 \times 10^{-3}$; base case model represents experimental setup with constant input

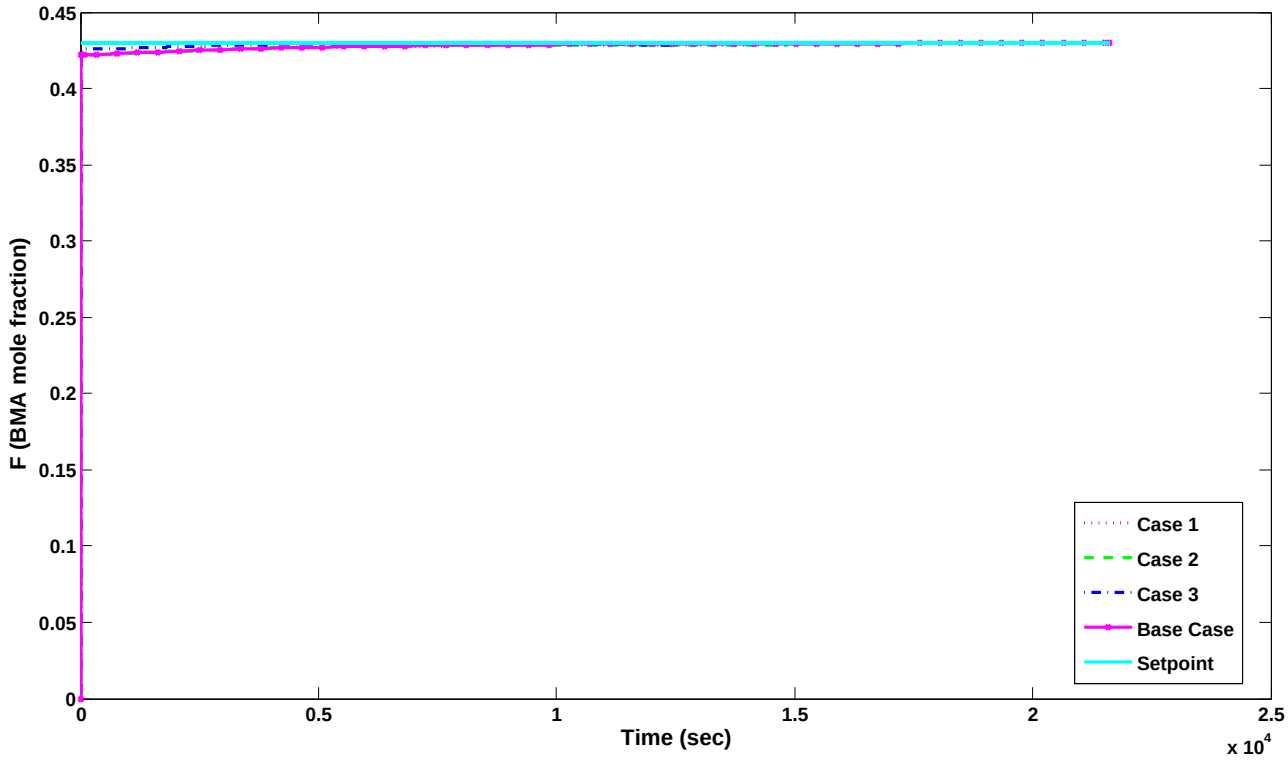

Figure 3.9: F real-time optimization for Case 1, 2 and 3 with $u_i(t) \in [0, 0.03], i = 1, 2, 3, x_1(t) = x_2(t) \in [0, 0.03], x_3(t) \in [0, 5.0 \times 10^{-3}], k = 5 \times 10^{-3}$; base case model represents experimental setup with constant input

3.3 Sensitivity Analysis

It is important to know the extent of robustness of an optimization routine used in a process. Before incorporating the extended Kalman filter (see Chapter 4), a set of simulations was performed to test the outcome of varying the parameters and boundaries of the optimization scheme.

Simulations in this section were done using Case 2. Case 2 allows for exponential feeding in starved-feed strategy which means flexibility in the input and monomer feed rates so that the optimization profiles can be improved. This improvement translates to enhanced product quality, better reactor efficiency, and also shorter reaction time. The same initial conditions, setpoints, constraints and algorithm parameters as in the previous section were used, unless otherwise specified.

The effect of the number of time interval, adaptive gain, BMA and STY constraint relaxation, and initiator constraint tightening on the optimization scheme were analyzed. A summary of the entire sensitivity analysis is presented at the end of this chapter.

1. **Effect of number of time intervals,** n: For a higher value $n = 40000$, $n = 30000$ and a lower value $n = 20000$, the simulations in Figure 3.10 show that increasing the number of iterations for a fixed time leads to faster approach to the setpoint and reduction in the batch time. The greater the number of steps, the shorter the time interval for updating the profile, resulting in a faster convergence of the optimization routine as shown in the result in Table 3.5. However, this improvement in batch time came at the cost of increased computation time. For $n = 40000$, $n = 30000$ and $n = 20000$, the 360 minutes simulation took 4.07 minutes, 2.59 minutes and 2.02 minutes, respectively, using

a 1.86Ghz Intel Core 2 processor.

Table 3.5: The effect of varying the number of intervals n on final batch time for Case 2

n	$\mathbf{t_f}$**(sec)**
40000	14000
30000	14900
20000	16200

2. **Effect of adaptive gain,** k: For a 50% increase in the adaptive gain $k = 0.0075$, $k = 0.005$ and for a 50% decrease in the adaptive gain $k = 0.0025$, the simulations in Figure 3.11 show that there is a limit to which the batch can be improved by increasing the gain. The projection algorithm in (3.22) ensures that the cost decreases until the gradient is zero; so at some point, increasing the adaptive gain k will no longer have an effect on the rate of change of the parameters. Hence, the slight variation in the state profiles found with changing the gains lead to approximately the same molecular weight and copolymer composition trajectories. Consequently, all of the simulations for the higher two gains ($k = 0.0075$ and $k = 0.005$) resulted in equivalent batch times as summarized in Table 3.6, and $k = 0.0025$ produced only a slightly longer batch time.

Table 3.6: The effect of varying the adaptive gain k on final batch time for Case 2

k	$\mathbf{t_f}$**(sec)**
0.0075	14900
0.005	14900
0.0025	15200

3. **Effect of relaxing the constraint on x_1 and x_2**: For relaxing the constraints on x_1 and x_2 from 0.03 to 0.06, the simulations in Figure 3.12 illustrate similar profiles for both tests in the state profiles which led to similar molecular weight and copolymer composition trajectories. Table 3.7 shows approximately the same final batch time results, despite relaxation of the constraints. This result was unexpected, as allowing monomer in the batch should permit the batch to be completed faster. However, since the states (x_1 and x_2) did not exceed their upper bound limits at 0.03 to begin with, increasing the x_1 and x_2 limit to 0.06 resulted in only a very slight improvement to the batch time.

Table 3.7: The effect of relaxing x_1 and x_2 constraint

$\mathbf{x_1 = x_2}$	$\mathbf{t_f}$**(sec)**
0.03	14900
0.06	14700

4. **Effect of tightening the constraint on x_3**: Restraining initiator level x_3 further from 5×10^{-3} to 5×10^{-4}, the simulations in Figure 3.13 and Table 3.8 show that the more relaxed the constraint is on the initiator, the faster the batch can be completed. This is expected, as the greater the amount of initiator permitted in a reactor, the greater the amount of free radicals that

can be produced in the system. As a result, the rate of propagation increases which leads to a quicker reaction as shown in the state trajectories in Figure 3.13, where the states for x_3 =5×10^{-3} approach their limit much faster. Also, more flexibility in controlling M_n is achieved.

Table 3.8: The effect of stiffening the x_3 constraint

$\mathbf{x_3}$	$\mathbf{t_f}$(sec)
5×10^{-3}	14900
5×10^{-4}	17100

3.4 Summary

In this chapter, the polymer reactor system used in this project was introduced. The major updates to the initial model parameters and rate coefficients were presented. Improvements to the on-line optimization scheme were discussed. Finally, sensitivity analysis of the on-line optimization routine for the BMA/ STY copolymerization system was performed to determine robustness of the system.

The objectives of the real-time optimization scheme is to reach the setpoint of the molecular weight and copolymer composition, while minimizing the batch time. For all the cases with different parameterizations, the improved optimization scheme with updated parameters proved successful in achieving these objectives as shown in the results (Figures 3.4 to Figures 3.9). Case 3 demonstrated the greatest reduction in the final batch time (42%) since it contained the most flexibility in monomer and initiator feed rates. This flexibility in feed rates allowed the optimization routine to adjust the process freely to achieve the desired response.

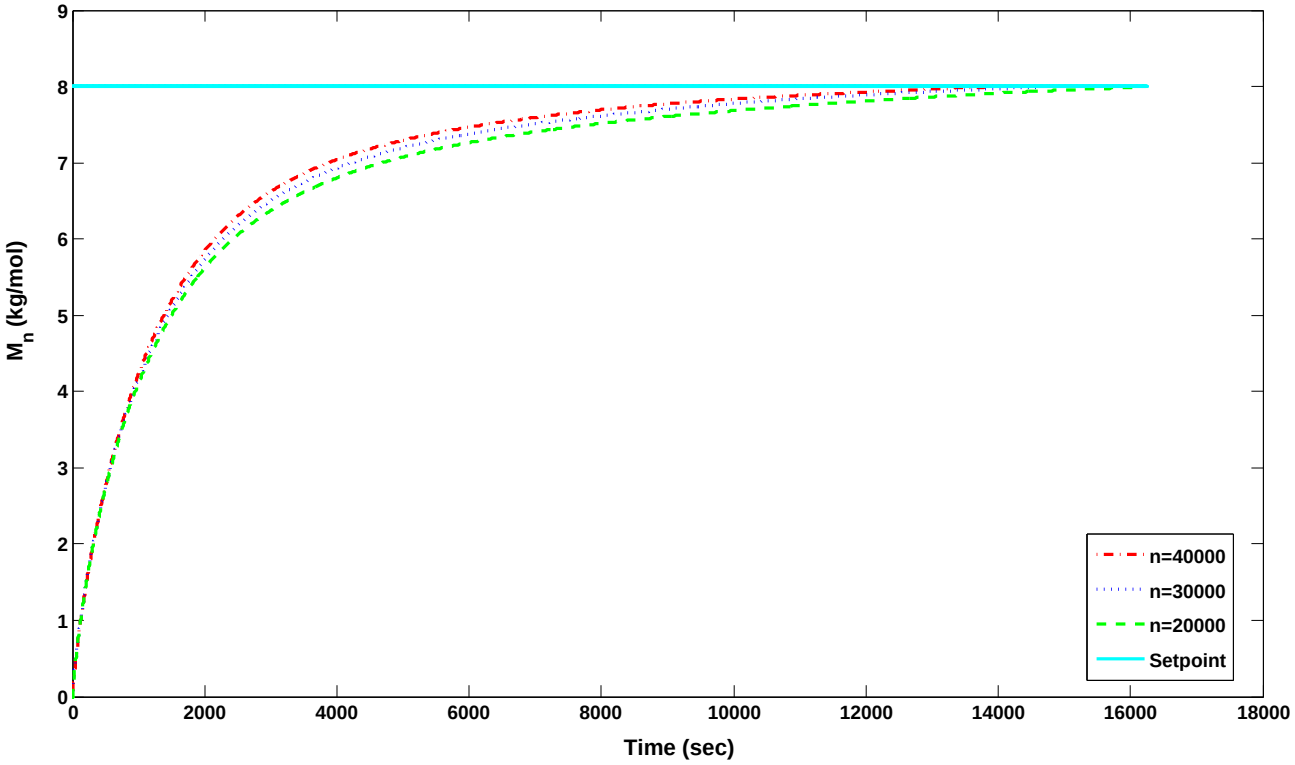

Figure 3.10: M_n for $n = 40000$, $n = 30000$ and $n = 20000$ with Case 2 dynamic optimization for $u_i(t) \in [0, 0.03], i = 1, 2, 3, x_1(t) = x_2(t) \in [0, 0.03], x_3(t) \in [0, 5.0 \times 10^{-3}], k = 5 \times 10^{-3}$

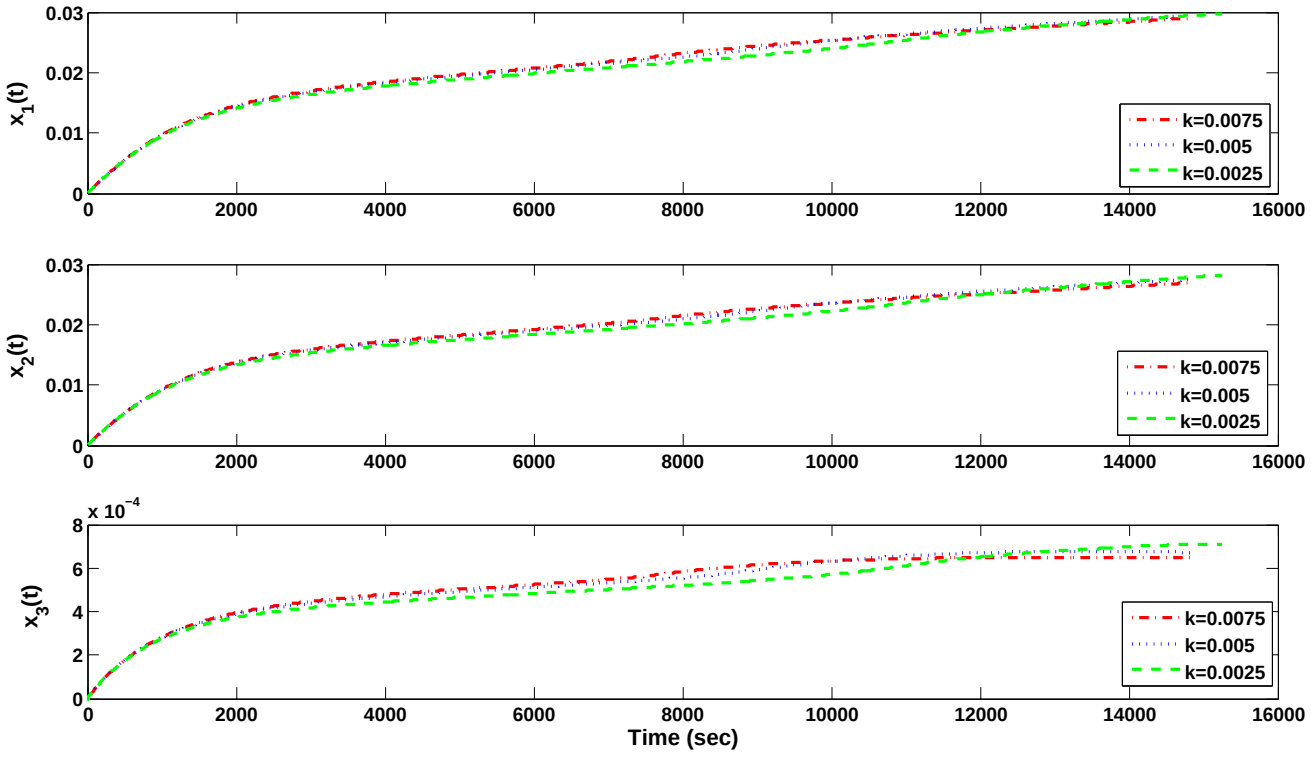

Figure 3.11: x_1, x_2, and x_3 profiles with Case 2 dynamic optimization for $u_i(t) \in [0, 0.03], i = 1, 2, 3, x_1(t) = x_2(t) \in [0, 0.03], x_3(t) \in [0, 5.0 \times 10^{-3}], k = 0.0075, k = 0.005$ and $k = 0.0025$

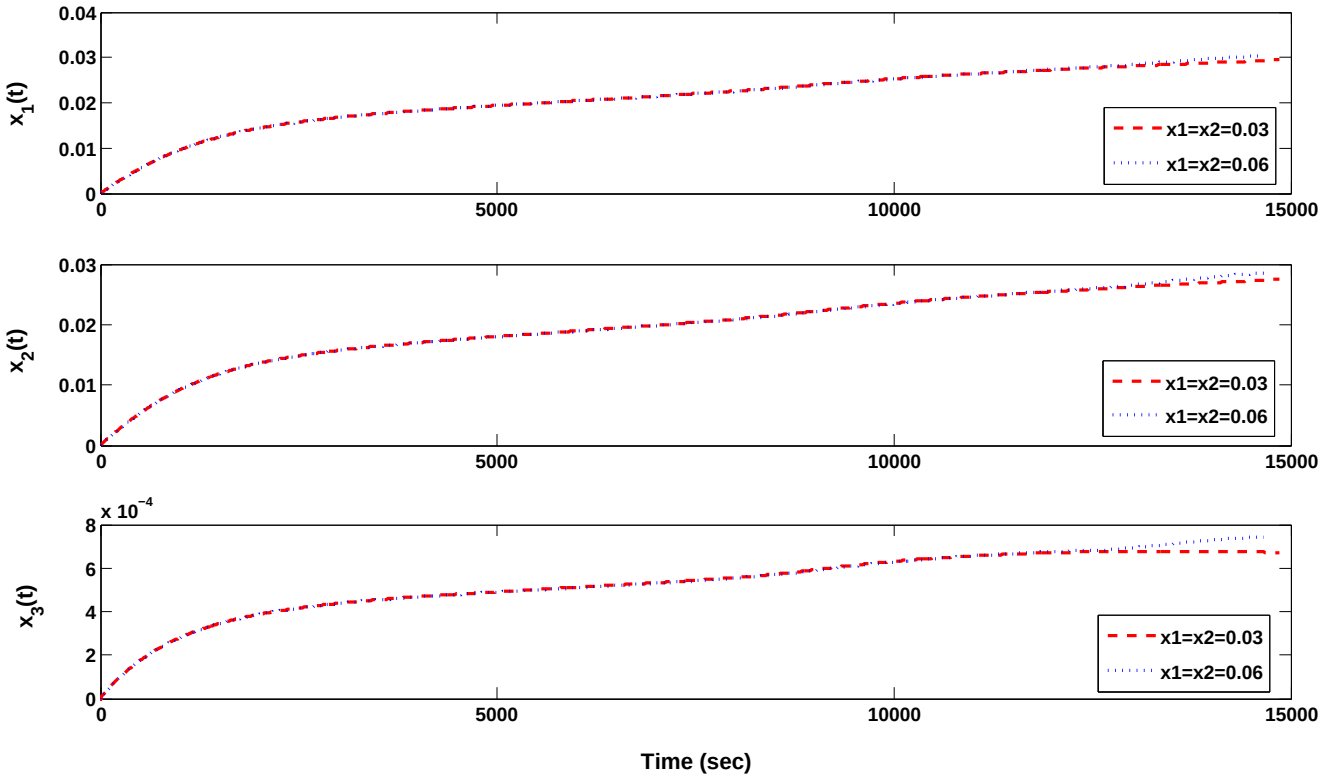

Figure 3.12: x_1, x_2, and x_3 profiles with Case 2 dynamic optimization for $u_i(t) \in [0, 0.03], i = 1, 2, 3, x_1(t) = x_2(t) \in [0, 0.06], x_3(t) \in [0, 5.0 \times 10^{-3}], k = 5 \times 10^{-3}$

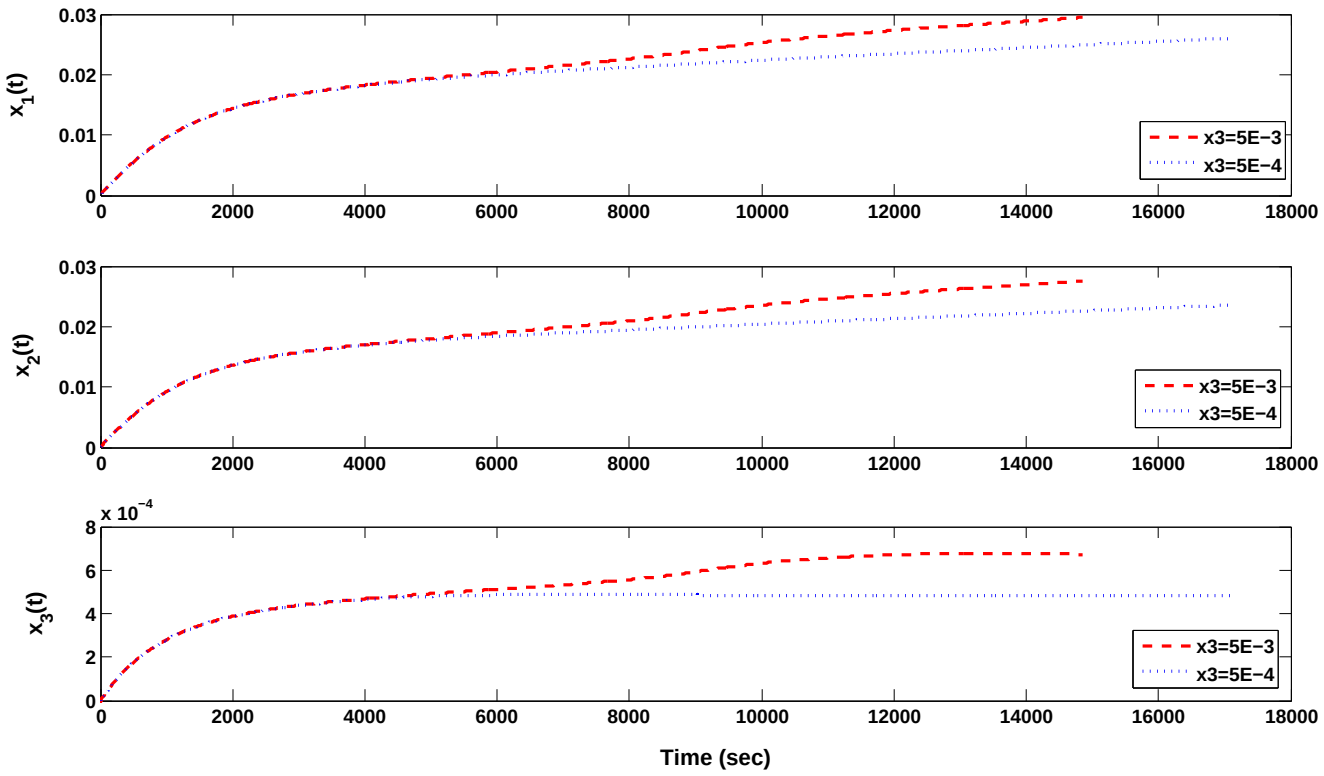

Figure 3.13: x_1, x_2, and x_3 profiles with Case 2 dynamic optimization for $u_i(t) \in [0, 0.03], i = 1, 2, 3, x_1(t) = x_2(t) \in [0, 0.03], x_3(t) \in [0, 5.0 \times 10^{-4}], k = 5 \times 10^{-3}$

From the sensitivity analysis, the on-line optimization scheme also met its objectives despite the large alteration of the process parameters. The system showed little improvement to the final batch time for changes to the adaptive gain k and monomer (x_1 and x_2) constraint relaxation. However, a reduction in the final batch time was seen for increasing the number of time intervals n and also for relaxing the constraint for initiator x_3. n has an impact on the speed of convergence of the optimization routine, while x_3 affects the rate of polymer propagation.

From all the results in this chapter, the real-time optimization routine was shown to be successful in minimizing the batch time and reaching the molecular weight and copolymer composition targets. It was also robust to process changes. The input, state, total mass of reactor content constraints were satisfied and the final mass of polymer was reached.

Chapter 4

State Estimation with On-Line Optimization

4.1 Observer Selection

As discussed in the introduction of this thesis, a wide variety of observers exist for state estimation. However, more indepth research would be required to look at different observers. The extended Kalman filter was chosen for state estimation for the following reasons:

- The process initial conditions are known for this problem. Although it is generally recognized that EKF does not provide good estimates if the estimated initial conditions are far from the actual ones, this is not the case in this work.
- Nonlinearity of the process.
- Ease of implementation.

- Possibility to include unknown parameters.
- The EKF has been proven to be appropriate for on-line implementation (see Chapter 2 for further elaboration).

The extended Kalman filter is a suitable observer for the process presented in this thesis. As elaborated in Chapter 2, the most prevalent Kalman filtering technique in Advanced Process Control is the discrete-time filter due to required implementation in a digital computer. Continuous-time system dynamics are often discretized and implemented with discrete-time extended Kalman filter due to possible lack of adequate computational power needed to integrate the system dynamics with other EKFs [7]. This work, however, uses a hybrid EKF which is also known as a continuous-discrete EKF.

The hybrid EKF is designed for systems with continuous-time dynamics and discrete-time measurements [7]. In reality, processes are generally continuous so the hybrid EKF is beneficial as errors that arise from assumptions and approximations from converting continuous-time models to discrete-time equivalents are avoided. Another advantage of the hybrid EKF is that the measurements are discrete in nature, which is crucial as digital computers sample in discrete-time.

4.2 Hybrid Extended Kalman Filter

The nonlinear dynamic system with continuous-time dynamics and discrete-time measurements is modeled as [7]

$$\begin{aligned} \dot{x} &= f(x, u, q, t) \\ z_k &= h_k(x_k, r_k) \end{aligned} \tag{4.1}$$

As presented in the case of the Kalman filter in (2.1), the noise processes $q(t)$ and r_k for the hybrid EKF, are both assumed to be zero-mean, independent, white process noise with covariance matrices Q and R_k, respectively. The state observer seeks to reconstruct the states $\dot{x}$ from the sensor measurements z_k .

Hybrid EKF Algorithm

For the process in (4.1), the same procedure followed for the KF and EKF (2.3) is used in choosing initial conditions for the hybrid EKF. The initial conditions for the hybrid EKF process are initial state $\hat{x}_0^+$ and covariance P_0^+:

$$\hat{x}_0^+ = 0 \tag{4.2}$$

$$P_0^+ = \mathbf{diag}[1e^{-7}, 1e^{-7}, 1e^{-8}, 1e^{-7}, 1e^{-7}] \tag{4.3}$$

The next two steps are crucial in the filter construction.

Estimation Step

The estimation stage where the state and covariance are propagated between observations from time $(k-1)^+$ to k^-, with the corresponding equation as

$$\dot{\hat{x}} = f(\hat{x}, u, 0, t) \tag{4.4}$$

$$\dot{P} = AP + PA^T + GQG^T \tag{4.5}$$

with A and G evaluated at the state estimate as $A = \frac{\partial f}{\partial x}|_{\hat{x}}$ and $G = \frac{\partial f}{\partial q}|_{\hat{x}}$. The integration starts with $\hat{x} = \hat{x}_{k-1}^+$ and $P = P_{k-1}^+$ and ends with $\hat{x} = \hat{x}_k^-$ and $P = P_k^-$. The R term is not included in the equation for $\dot{P}$ since the integration of P is between measurements, at the time when no measurement is available.

Update Step

The correction step occurs when measurement is available at time k. The measurement z_k is then incorporated into the state estimate:

1) ***Update Gain Matrix***

$$K_k = P_k^- H_k^T (H_k P_k^- H_k^T + V_k R_k V_k^T)^{-1} \tag{4.6}$$

2) ***Update State Estimate***

$$\hat{x}_k^+ = \hat{x}_k^- + K_k[z_k - h_k(\hat{x}_k^-, r_0, t_k)] \tag{4.7}$$

3) ***Update Error Covariance***

$$P_k^+ = (I - K_k H_k) P_k^- (I - K_k H_k)^T + K_k H_k R_k V_k^T K_k^T \tag{4.8}$$

with $H_k = \frac{\partial h_k}{\partial x_k}|_{\hat{x}^-}$ and $V_k = \frac{\partial h_k}{\partial r_k}|_{\hat{x}^-}$. The nominal measurement noise r_0 is zero initially.

4.2.1 System Dynamics with Hybrid EKF

For the butyl methacrylate and styrene (BMA/ STY) solution free-radical copolymerization system, all six states (x_1-x_6) of the system are to be estimated. In the problem presented in Chapter 3, it was assumed that all the states were available for measurement. Hence, state variable measurements x_1 to x_6 were sent to the optimizer to update the control action. However, this is not the case for the actual process. The sixth state (x_6) must be estimated for the calculation of the number-averaged molecular weight M_n, and is dependent on x_1 through x_5 which are assumed to be observed. Therefore, only the first five states are reconstructed using the hybrid EKF. Figure 4.1 compares the former problem description in Chapter 3 to the current one.

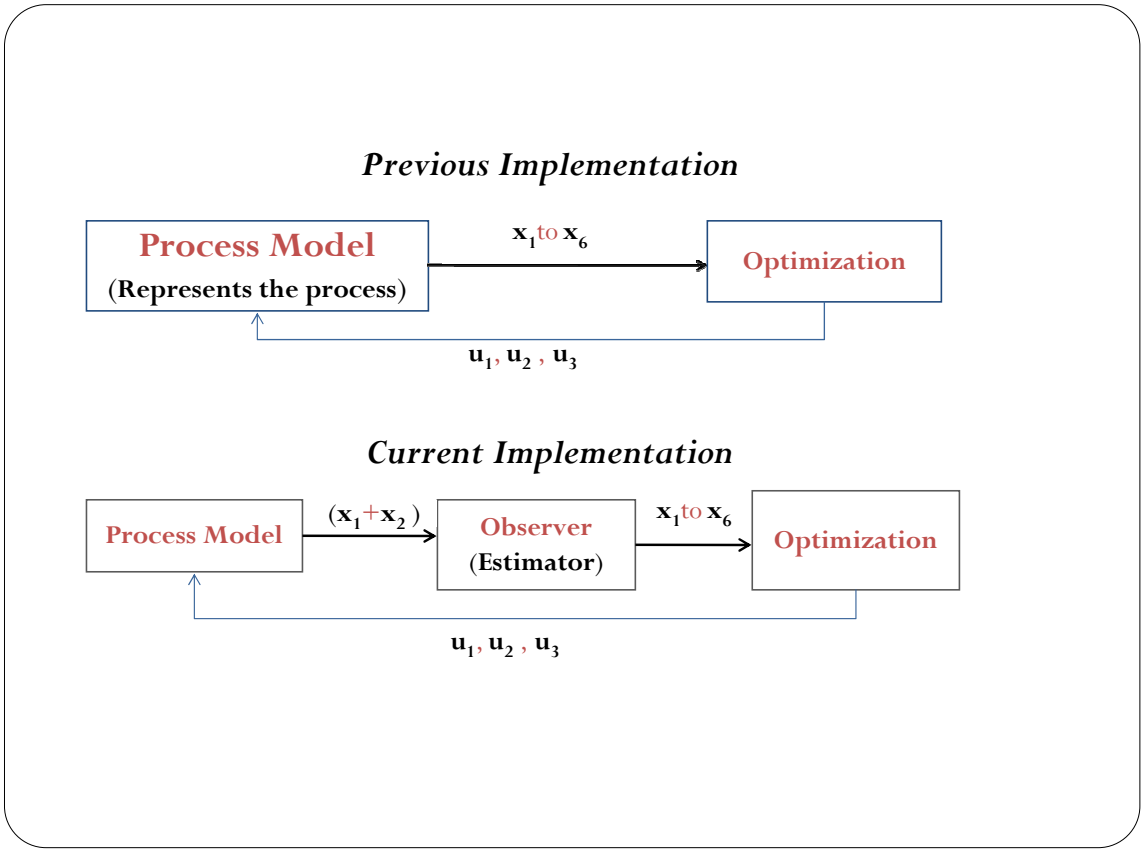

Figure 4.1: Distinction between the former problem description in Chapter 3 and the present one

Following (4.1), the nonlinear system equations to be reconstructed using the hybrid EKF are

$$\frac{dx_1}{dt} = u_1(t) - x_1\left(k_{p_{AA}}\lambda_o^A(t) + k_{p_{BA}}\lambda_o^B(t)\right) + q_1 \tag{4.9a}$$
$$\frac{dx_2}{dt} = u_2(t) - x_2\left(k_{p_{BB}}\lambda_o^B(t) + k_{p_{AB}}\lambda_o^A(t)\right) + q_2 \tag{4.9b}$$
$$\frac{dx_3}{dt} = u_3(t) - k_d x_3(t) + q_3 \tag{4.9c}$$
$$\frac{dx_4}{dt} = x_1\left(k_{p_{AA}}\lambda_o^A(t) + k_{p_{BA}}\lambda_o^B(t)\right) + q_4 \tag{4.9d}$$
$$\frac{dx_5}{dt} = x_2\left(k_{p_{BB}}\lambda_o^B(t) + k_{p_{AB}}\lambda_o^A(t)\right) + q_5 \tag{4.9e}$$

The definitions for (3.1) are also applicable for (4.9).

It is assumed that two measurements are available, z_1 and z_2. The observation equations that relate to the states are

$$z_1 = (x_1 + x_2) + r_1 \tag{4.10a}$$
$$z_2 = (x_4 + x_5) + r_2 \tag{4.10b}$$

z_1 is assumed to be inferred by infra-red (IR) spectroscopy and z_2 is deduced from the equation

$$z_2 = \int_0^T (u_1 + u_2)dt - (x_1 + x_2) \tag{4.11}$$
$$= (x_4 + x_5) \tag{4.12}$$

To estimate the state x_3, two assumptions were made 1) the initiation coefficient k_d is known perfectly, and 2) there is no uncertainty or noise associated with the measurement of u_3. With these assumptions, the hybrid EKF reconstructs x_3 from

the system dynamic equation in (4.1):

$$\frac{dx_3}{dt} = u_3(t) - k_d x_3(t) + q_3$$

The output of the process equations (4.9 - 4.10) were used to estimate x_6, with the system equations as

$$\frac{dx_6}{dt} = V(t)R_{\mu_0}(t) \tag{4.13}$$

4.2.2 Filter Design Parameters and Analysis

Design parameters were chosen for the hybrid EKF following theoretical and practical consideration as outlined in this section. Values for the measurement noise covariance R, initial error covariance P_0, sensor measurement z_k are given by

$$\begin{aligned} P_0 &= \mathbf{diag}[1e^{-7}, 1e^{-7}, 1e^{-8}, 1e^{-7}, 1e^{-7}] \\ R &= 0.01^2\mathbf{I}_{4x4} \\ z_k &= H_k + \sqrt{R}(\delta_{2x1}) \end{aligned}$$

where I is the identity matrix and δ is the random noise matrix generated by Matlab. As discussed in Chapter 2, the choice of P_0 depends on how well the initial states (x_0) are known. The greater the confidence in the initial state values, the closer the covariance matrix would be to zero. And as mentioned in Chapter 3, the initial states are all zero $x_i(0) = 0,\ i = 1, \ldots, 6$. For this reason, P_0 was selected to be very close to zero . The system dynamics (4.9) were left in the continuous state for implementation with the hybrid EKF; thus, errors that arise from discretization were avoided. Following the Kalman Filter Tuning Process in Figure 2.3, it is assumed that the uncertainty in the system is introduced by noise in the measurement; thus a

large noise covariance R was chosen so that the state estimate depends more on the system dynamics. The measurements are assumed to be corrupted with random noise of zero-mean structure, which is usually the case for the noise pattern of most systems.

Hybrid EKF Analysis

The parameter values were incorporated into the hybrid EKF algorithm. The system was simulated for all six states (x_1 - x_6) using the same condition as in section 3.2 of Chapter 3. The results with their error analysis as well as the molecular weight M_n and copolymer composition F plots were generated.

The hybrid EKF reconstructs the states successfully as shown in Figures 4.2 through 4.8 with all estimation errors less than 4×10^{-4}, which also results in precise estimates of molecular weight and copolymer composition.

4.3 Filter Implementation with Optimization

As mentioned earlier in this chapter, the results shown in Chapter 3 assumed that all six states are available for measurement through simulation of the closed-loop system of the process model. Only two measurements exist in reality and these two measurements (4.10) are now extracted from the process model and sent to the optimization software. As each measurement becomes available, it is sent to the hybrid EKF for reconstruction of the first five states from which the sixth state is calculated. An ordinary differential-equation solver package in Fortran, ODESSA [49], was used to compute the first-order sensitivities. The new estimates from the observer were used as initial conditions for the gradient estimator. The steepest descent approach (**??**) was used for the update law and the computed inputs at that point are applied to

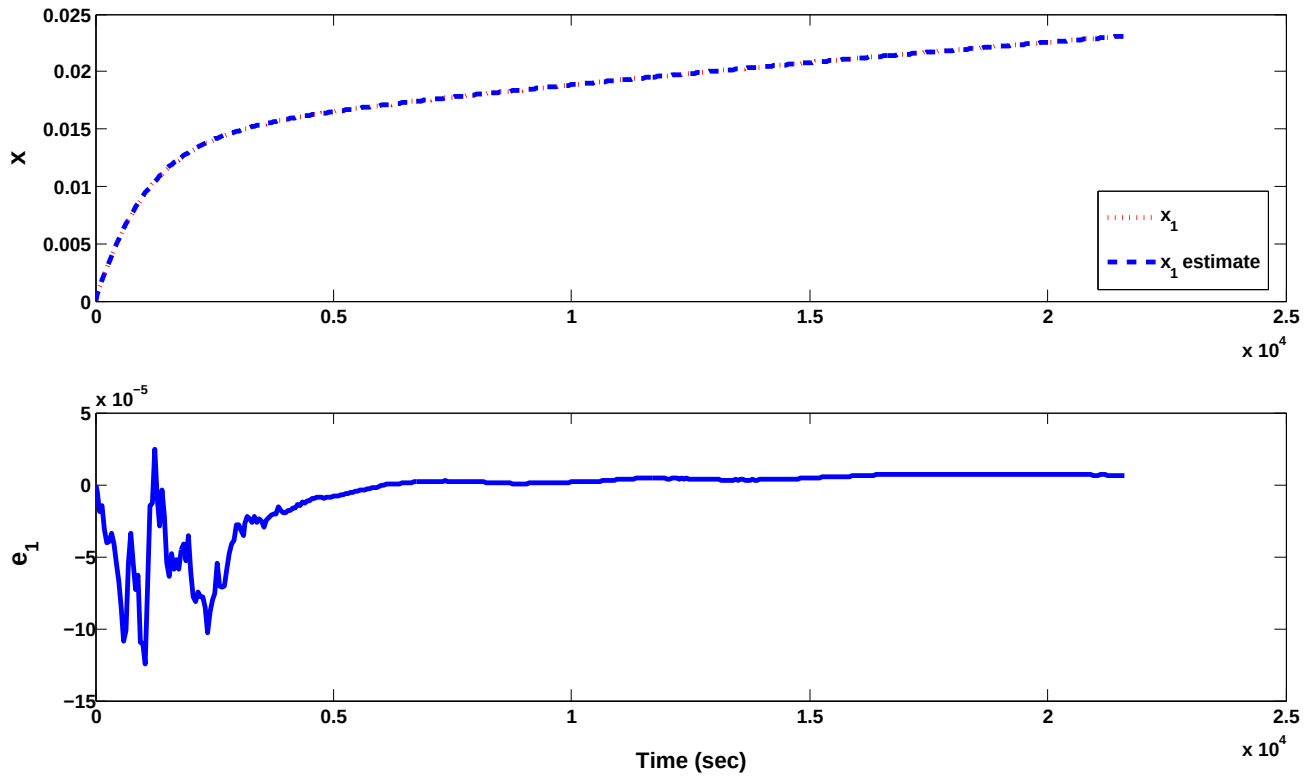

Figure 4.2: Open-loop trajectory for true state x_1, x_1 estimate from hybrid EKF and prediction error e_1 with measurement noise covariance $\mathrm{R} = 0.01^2\mathbf{I}_{4x4}$. $e_1 = x_1 - \hat{x}_1$

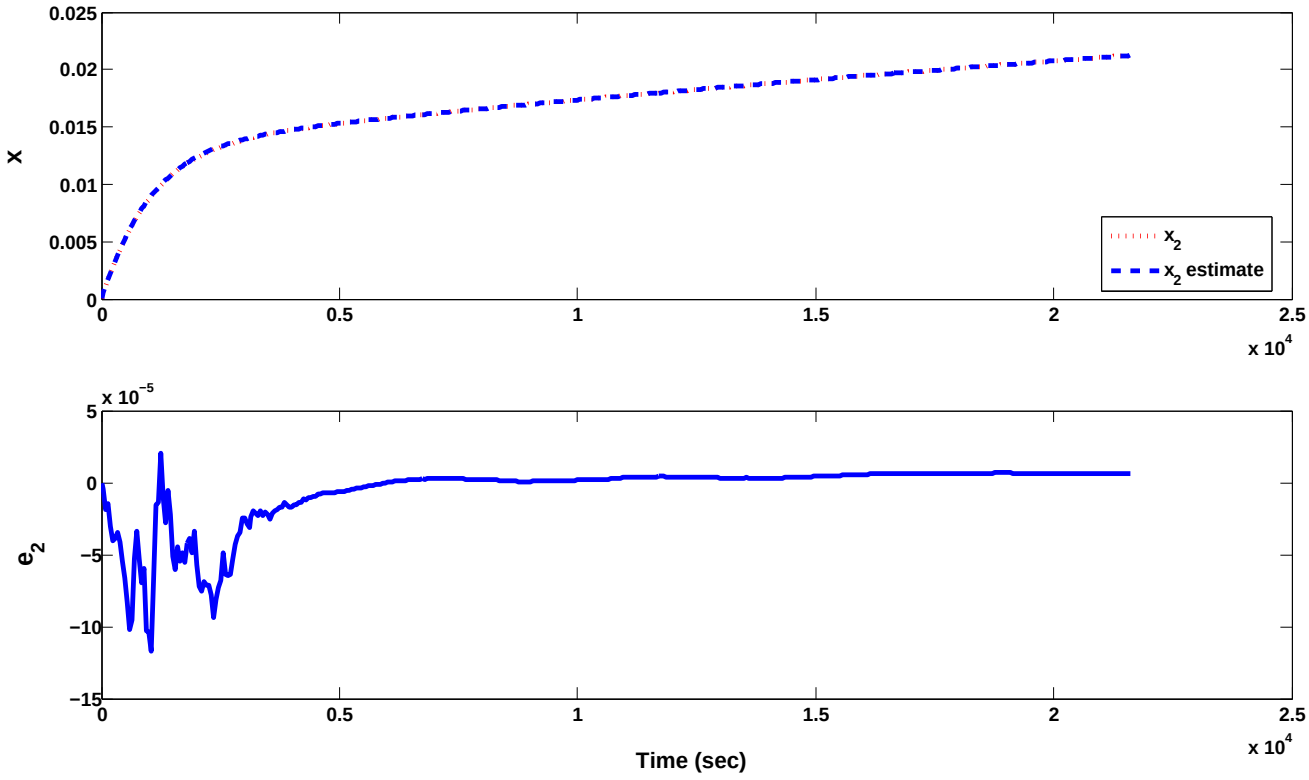

Figure 4.3: Open-loop trajectory for true state x_2, x_2 estimate from hybrid EKF and prediction error e_2 with measurement noise covariance $\mathrm{R} = 0.01^2\mathbf{I}_{4x4}$. $e_2 = x_2 - \hat{x}_2$

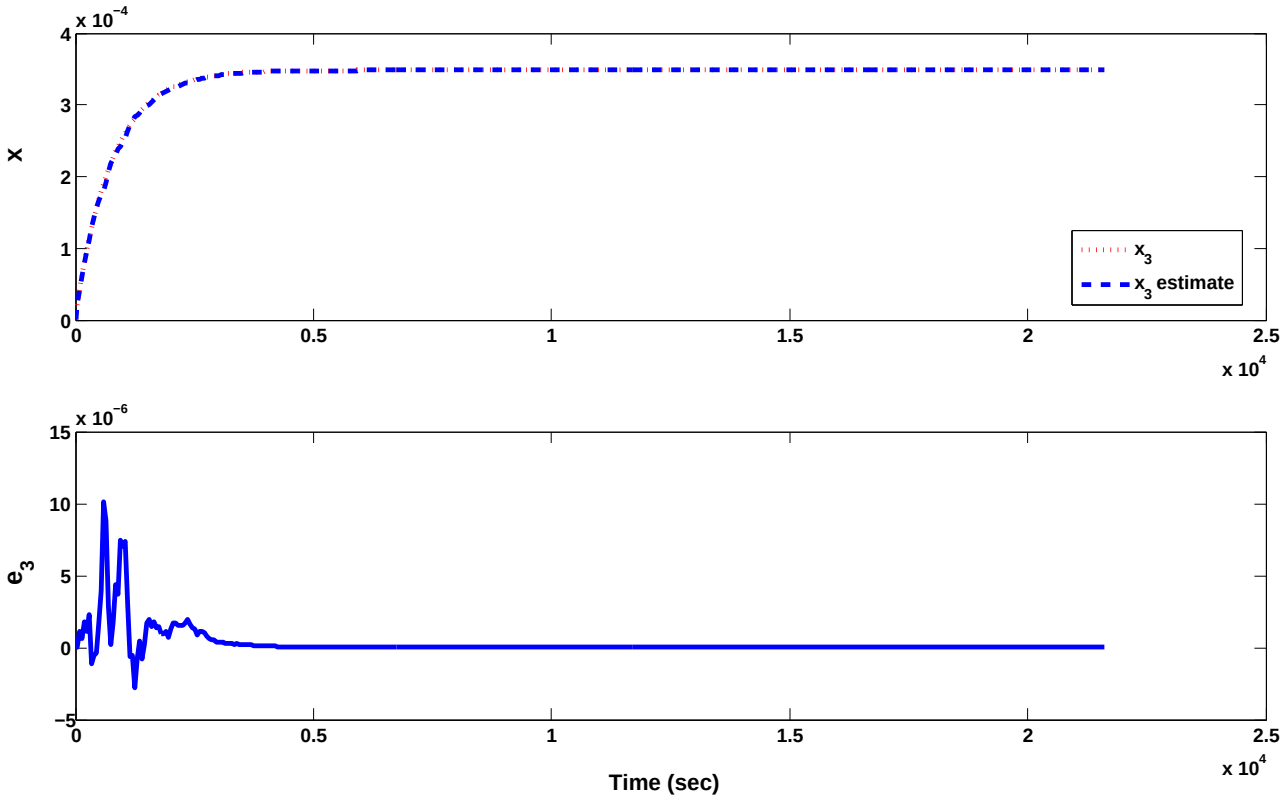

Figure 4.4: Open-loop trajectory for true state x_3, x_3 estimate from hybrid EKF and prediction error e_3 with measurement noise covariance $\mathrm{R} = 0.01^2\mathbf{I}_{4x4}$. $e_3 = x_3 - \hat{x}_3$

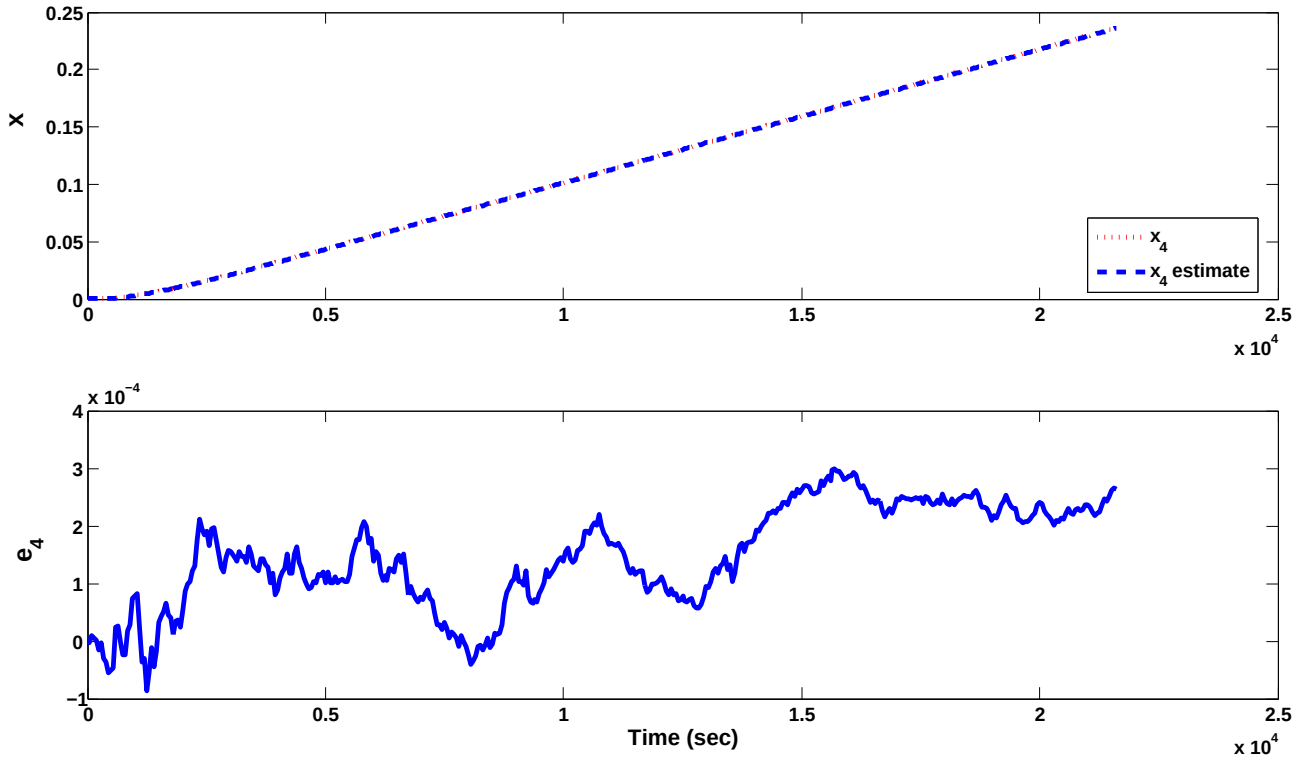

Figure 4.5: Open-loop trajectory for true state x_4, x_4 estimate from hybrid EKF and prediction error e_4 with measurement noise covariance $\mathrm{R} = 0.01^2\mathbf{I}_{4x4}$. $e_4 = x_4 - \hat{x}_4$

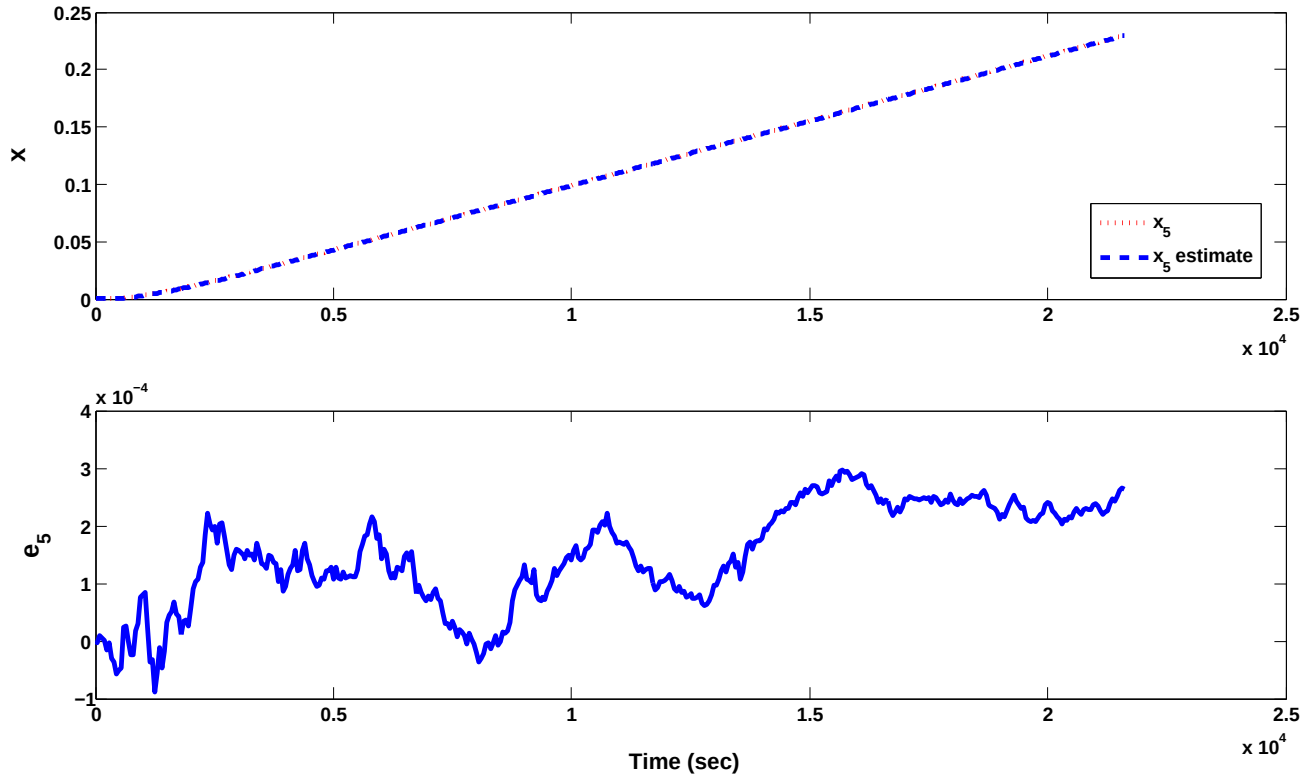

Figure 4.6: Open-loop trajectory for true state x_5, x_5 estimate from hybrid EKF and prediction error e_5 with measurement noise covariance $\mathrm{R} = 0.01^2\mathbf{I}_{4x4}$. $e_5 = x_5 - \hat{x}_5$

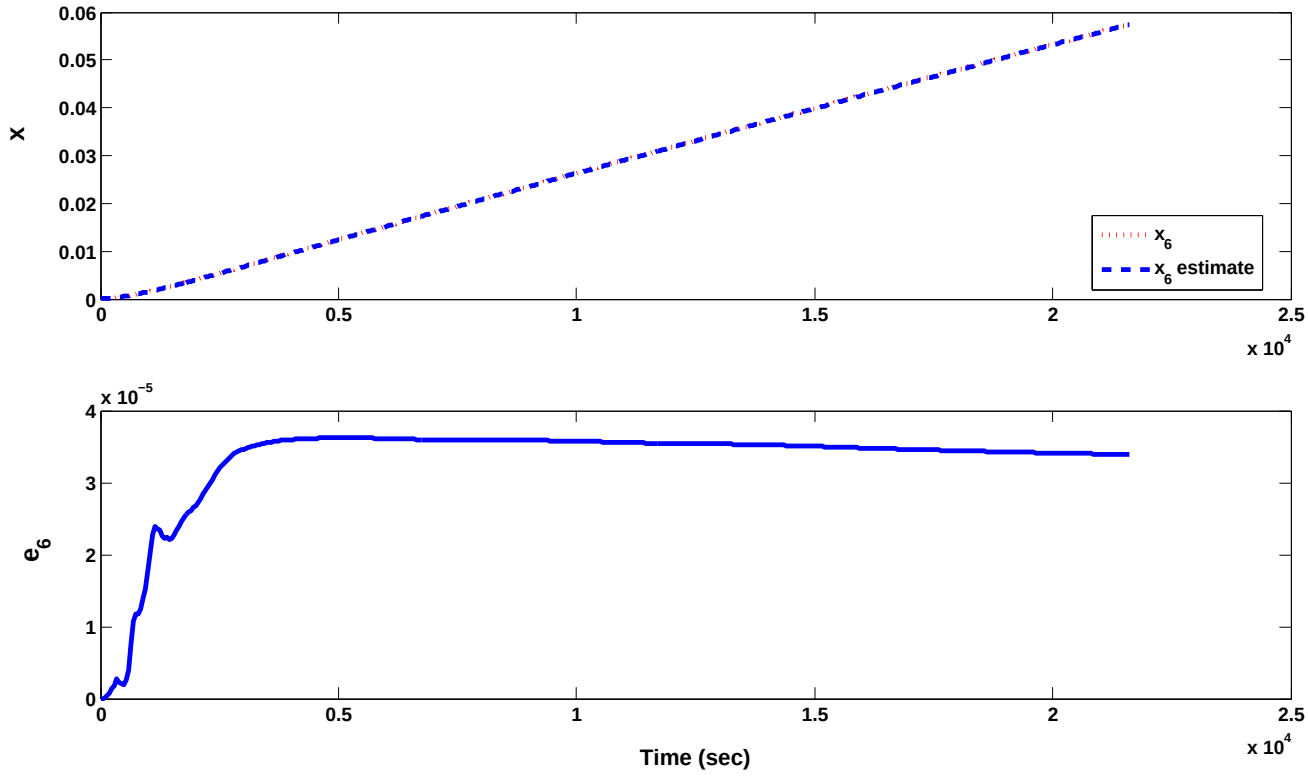

Figure 4.7: Open-loop trajectory for true state x_6, x_6 estimate calculated from output of x_1 through x_5 estimate of hybrid EKF and prediction error e_6 with measurement noise covariance $\mathrm{R} = 0.01^2\mathbf{I}_{4x4}$. $e_6 = x_6 - \hat{x}_6$

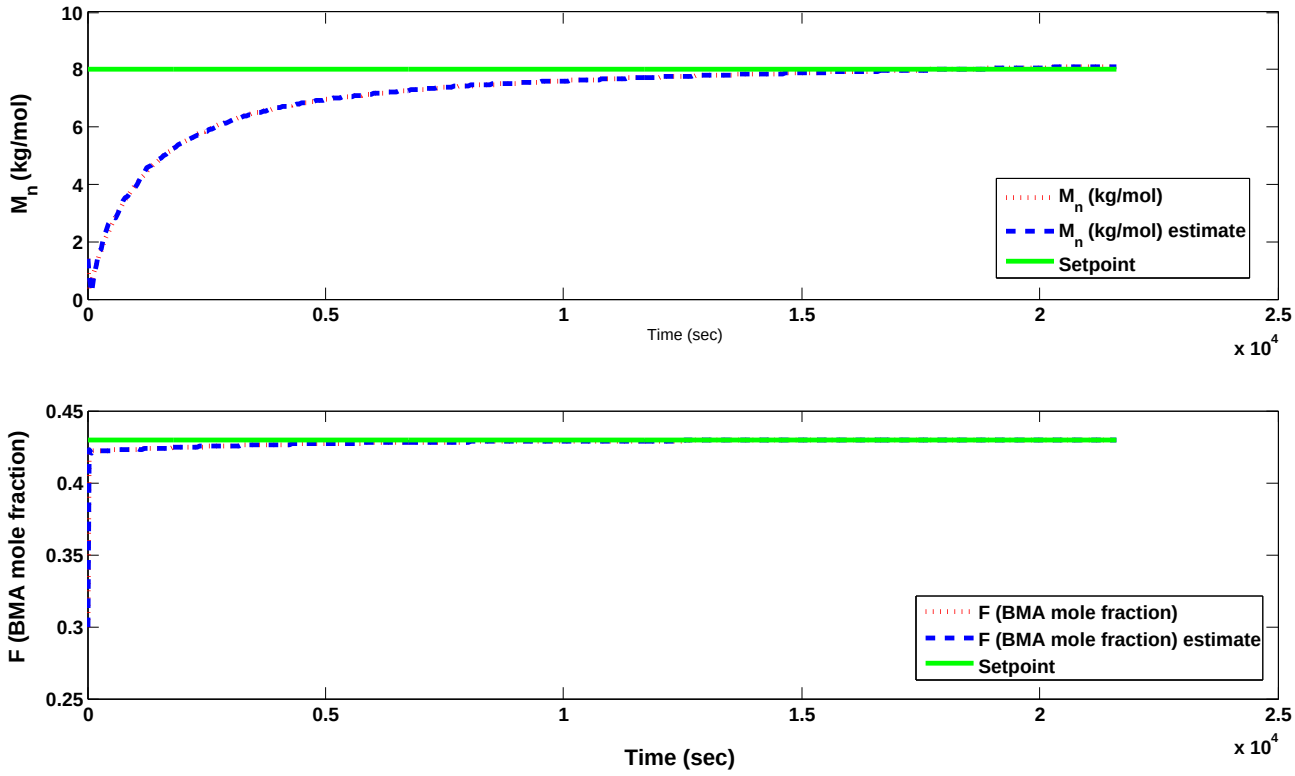

Figure 4.8: Open-loop trajectory for true M_n, true F, M_n and F estimates based on hybrid EKF estimation of x_1 through x_5 and calculated x_6 estimate with measurement noise covariance R = $0.01^2\mathbf{I}_{4x4}$

the process until new measurements are received from the batch. Essentially, the gradient information was used to calculate the next control move and the parameters were incremented in the direction of the gradient.

Simulation Results

The simulation results for Case 2 showing the hybrid EKF implementation with the real-time optimization technique are compared with results without the hybrid EKF state estimates as shown in Figures 4.9, 4.10, 4.11, and 4.12. These optimization results start with the initial trajectory matching the experimental conditions in Table 3.4. Again, the simulation was carried out for the same conditions as that without the hybrid EKF in Chapter 3 to provide an unbiased comparison.

Figure 4.9 represents the outputs of the system, $M_n(kg/mol)$, F, mass of polymer generated, and total mass of reactor content. The corresponding input profiles, u_1, u_2, u_3, are shown in Figure 4.10. The state trajectories, x_1, x_2, x_3, are presented in Figure 4.11; and trajectories for x_4, x_5, x_6 are shown in Figure 4.12.

A comparison of M_n and F for Case 1, 2, and 3 are displayed in Figures 4.13 and 4.14, respectively. For all three cases the profiles showed improvement in the reaction time. Case 3 produced the most reduction in batch time, followed by Case 1, then Case 2 with times of 11300 sec, 13600 sec and 13900 sec, respectively.

These results are better than those presented in Chapter 3 for the case of the optimization without state estimation. In fact, the proposed hybrid EKF with real-time optimization reduces the final batch time further by 1100 sec compared to using only the dynamic optimization scheme. This improvement is due to the fact that the optimization is not at the true optimum and the incorporation of the hybrid EKF

finds a better path for the optimization. From view of the simulation profiles, the hybrid EKF with real-time optimization tracks the true state estimates effectively.

4.3.1 Robustness Analysis for Filter Implementation with Optimization

To evaluate the robustness of the system with the newly reconstructed states, the system was perturbed to introduce model mismatch with respect to change in parameters used to calculate the sensitivities of the proposed dynamic optimization schemes. Given that the model parameters are not perfect, disturbances were introduced to the system by varying the values of the parameters. Four different scenarios were tested for Case 2:

1. **Varying reactivity ratio,** r_A: The reactivity ratio is known to affect polymerization rate and hence also influences polymer composition. The further the reactivity ratio is from unity, the more difficult it is to control copolymer composition. In fact, the extent of composition drift increases with increasing r_A/r_B [50]. For this reason, a wide range of reactivity ratios was chosen from $50\%r_A$ to $150\%r_A$, to evaluate how the optimization scheme would handle the perturbation. The results are displayed in Figures 4.16 and 4.17. Discussions for all the test results are at the end of this section and the final batch time is presented in Table 4.1.

2. **Varying propagation rate coefficient,** $k_{p_{AA}}$: The propagation rate coefficient is also know to have an effect on the polymerization rate, thus the polymer composition. Simulations were done for $80\%k_{p_{AA}}$ and $120\%k_{p_{AA}}$ and the results

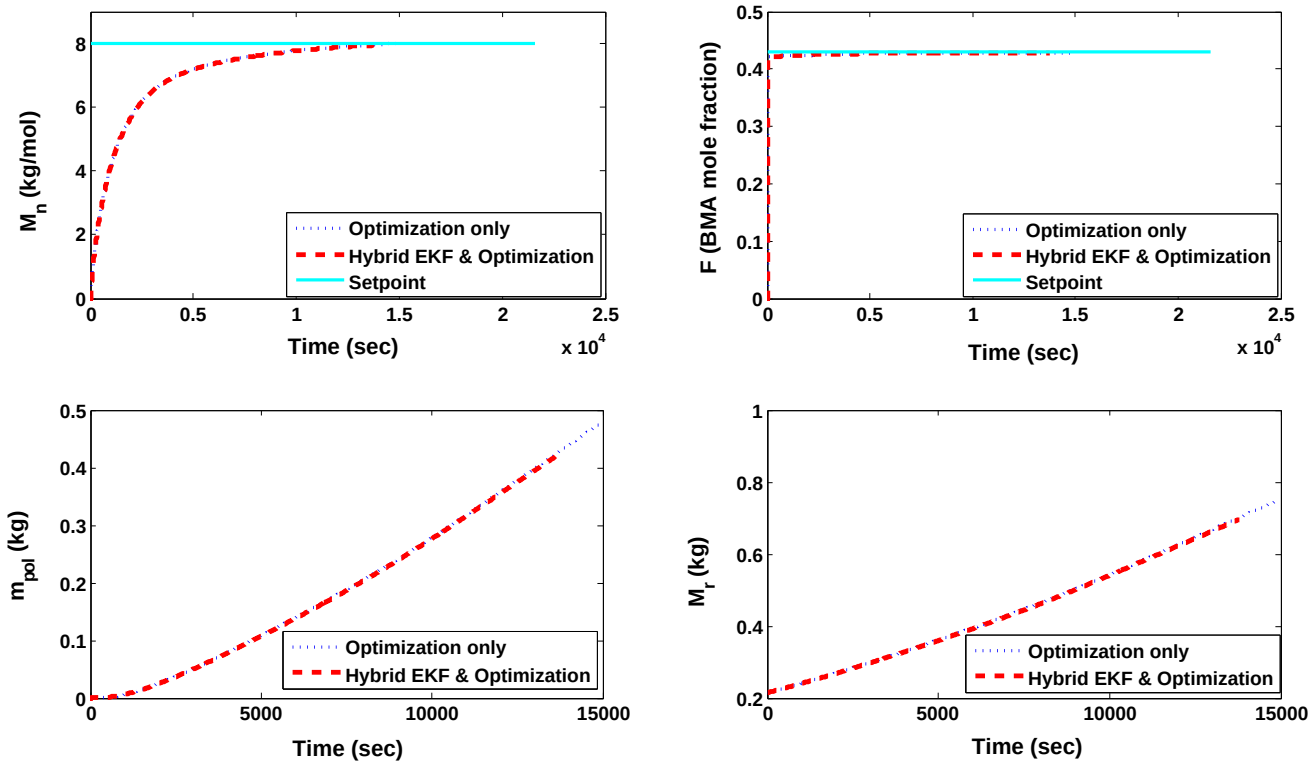

Figure 4.9: Profiles for M_n (kg/mol), F (BMA mole fraction), mass of polymer generated (kg) and total mass of reactor content (kg) with Case 2 dynamic optimization and optimization with hybrid EKF state estimates for $u_i(t) \in [0, 0.03], i = 1, 2, 3, x_1(t) = x_2(t) \in [0, 0.03], x_3(t) \in [0, 5.0 \times 10^{-3}], k = 5 \times 10^{-3}$

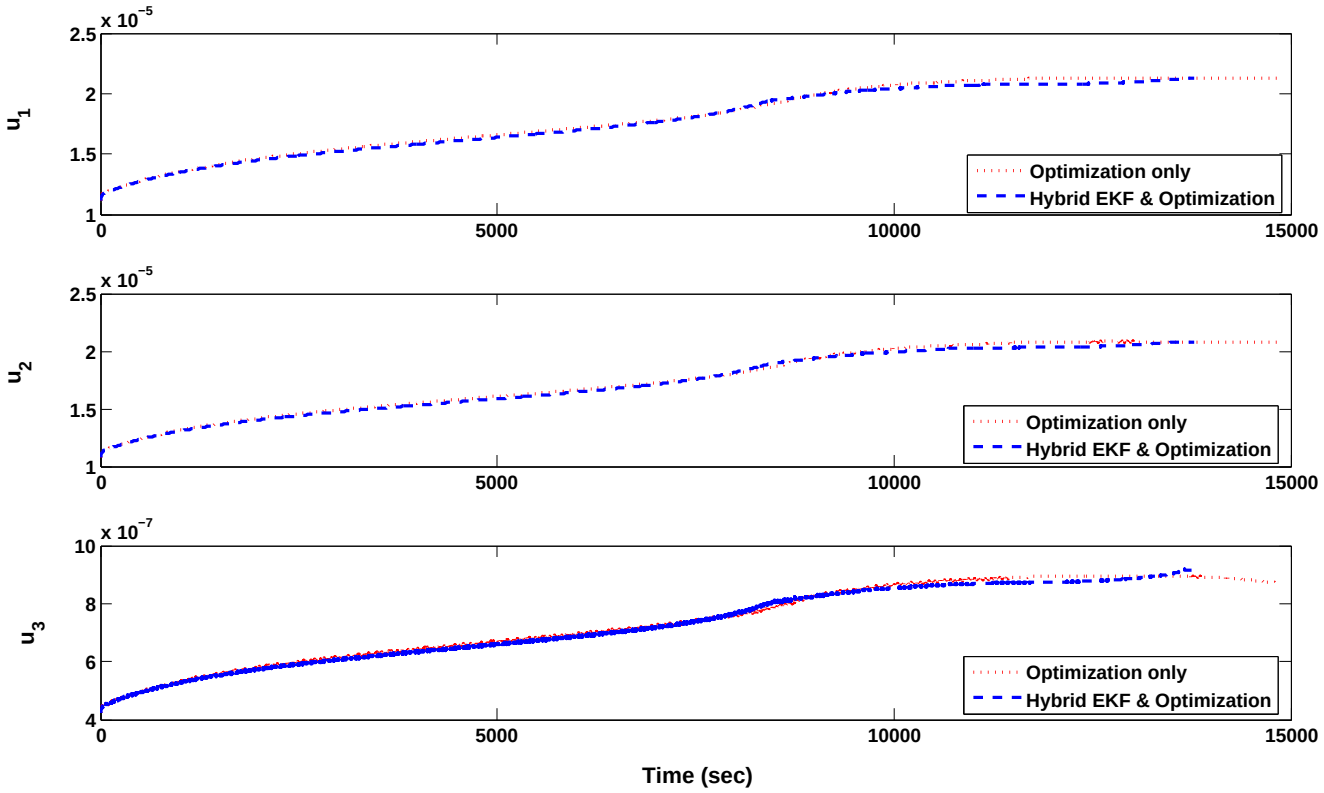

Figure 4.10: Profiles for u_1, u_2, u_3 with Case 2 dynamic optimization and optimization with hybrid EKF state estimates for $u_i(t) \in [0, 0.03], i = 1, 2, 3, x_1(t) = x_2(t) \in [0, 0.03], x_3(t) \in [0, 5.0 \times 10^{-3}], k = 5 \times 10^{-3}$

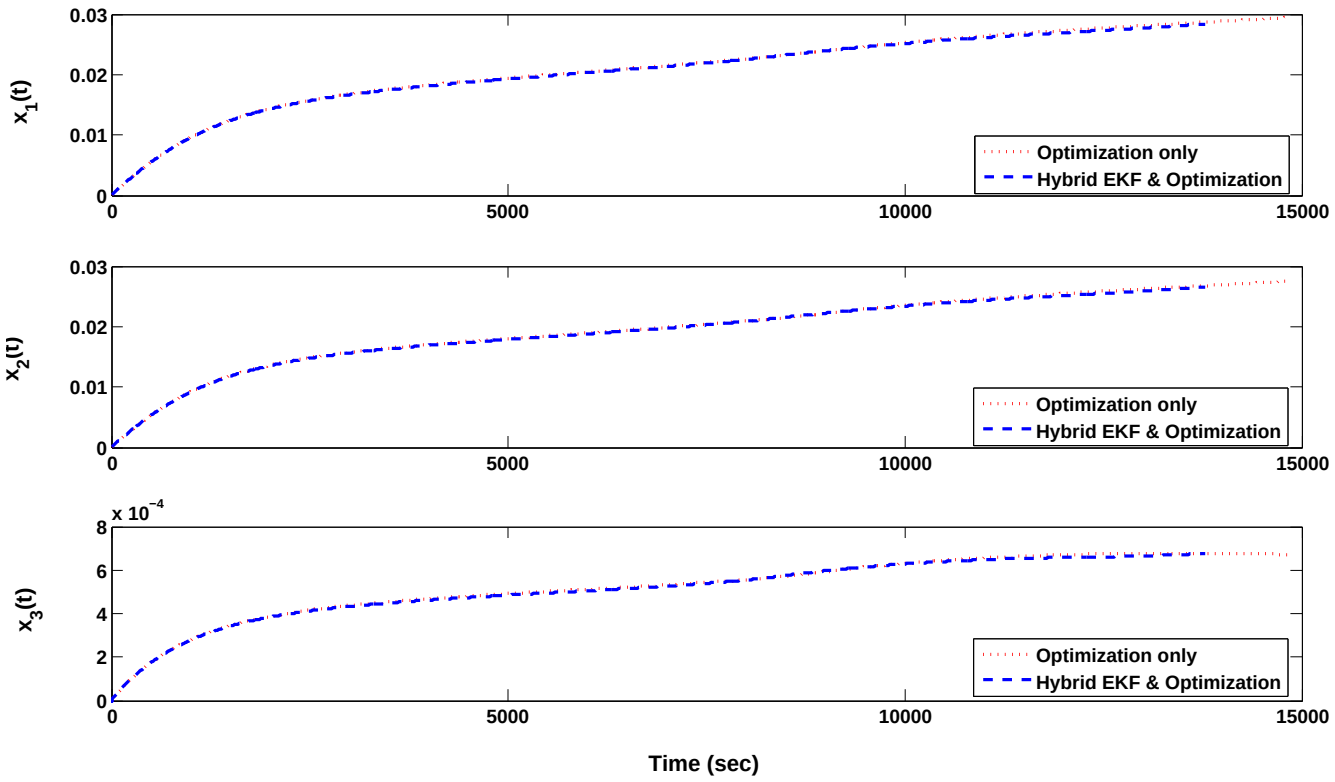

Figure 4.11: Profiles for x_1, x_2, x_3 with Case 2 dynamic optimization and optimization with hybrid EKF state estimates for $u_i(t) \in [0, 0.03], i = 1, 2, 3, x_1(t) = x_2(t) \in [0, 0.03], x_3(t) \in [0, 5.0 \times 10^{-3}], k = 5 \times 10^{-3}$

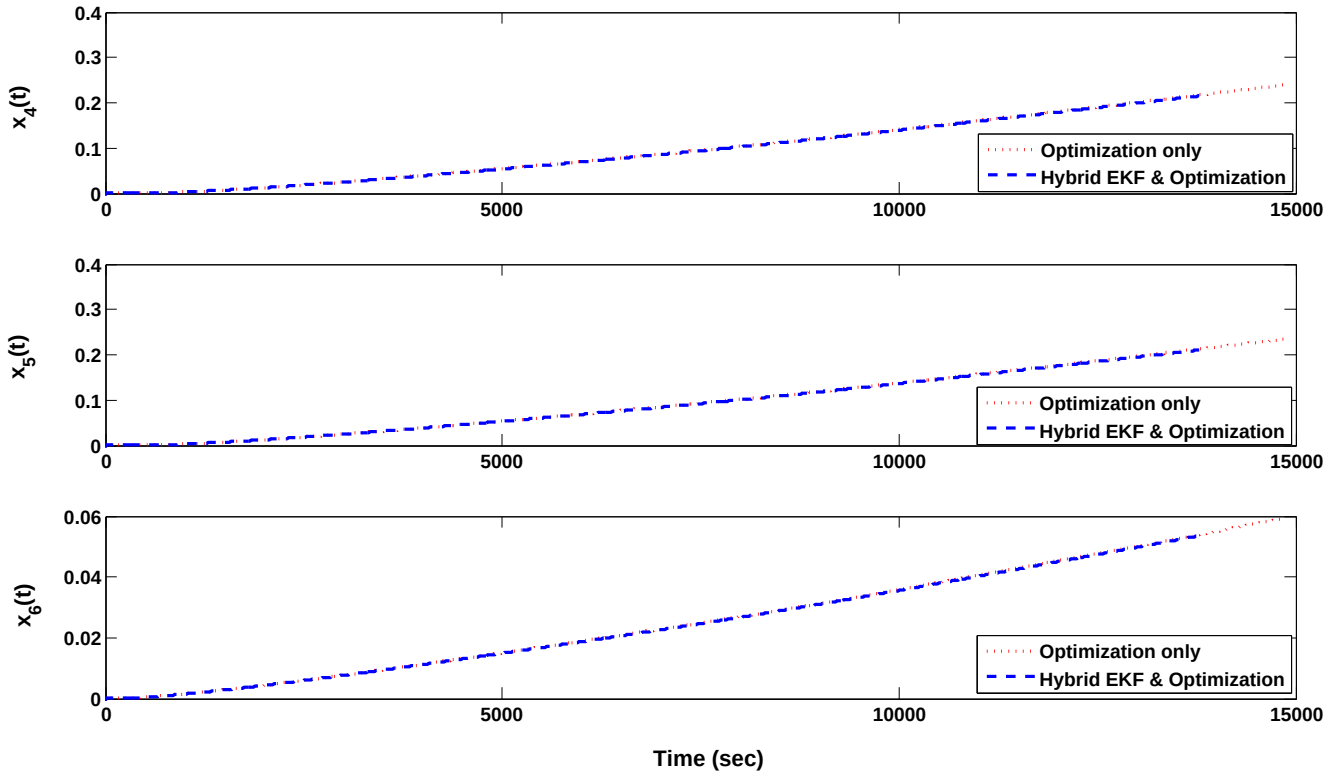

Figure 4.12: Profiles for x_4, x_5, x_6 with Case 2 dynamic optimization and optimization with hybrid EKF state estimates for $u_i(t) \in [0, 0.03], i = 1, 2, 3, x_1(t) = x_2(t) \in [0, 0.03], x_3(t) \in [0, 5.0 \times 10^{-3}], k = 5 \times 10^{-3}$

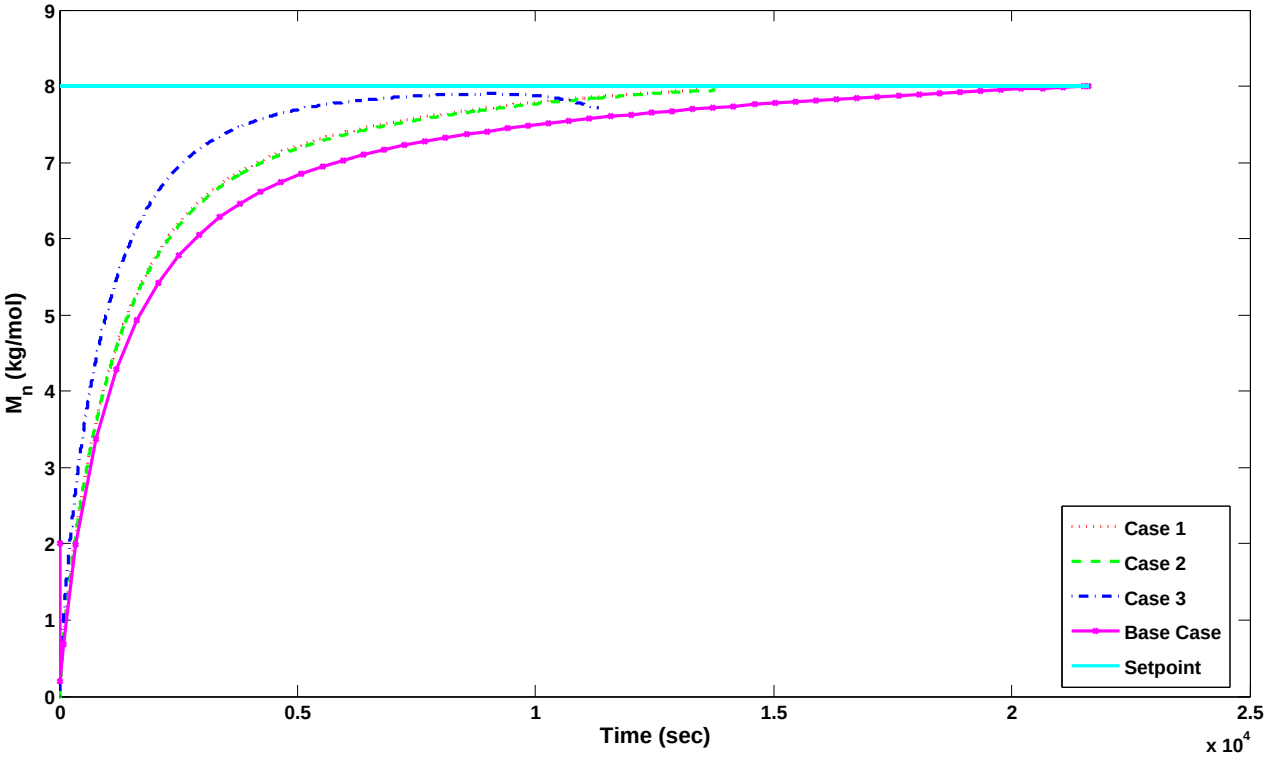

Figure 4.13: M_n from state estimates of hybrid EKF incorporated with real-time optimization for Case 1, 2 and 3 with $u_i(t) \in [0, 0.03], i = 1, 2, 3, x_1(t) = x_2(t) \in [0, 0.03], x_3(t) \in [0, 5.0 \times 10^{-3}], k = 5 \times 10^{-3}$; base case model represents experiment setup with constant input

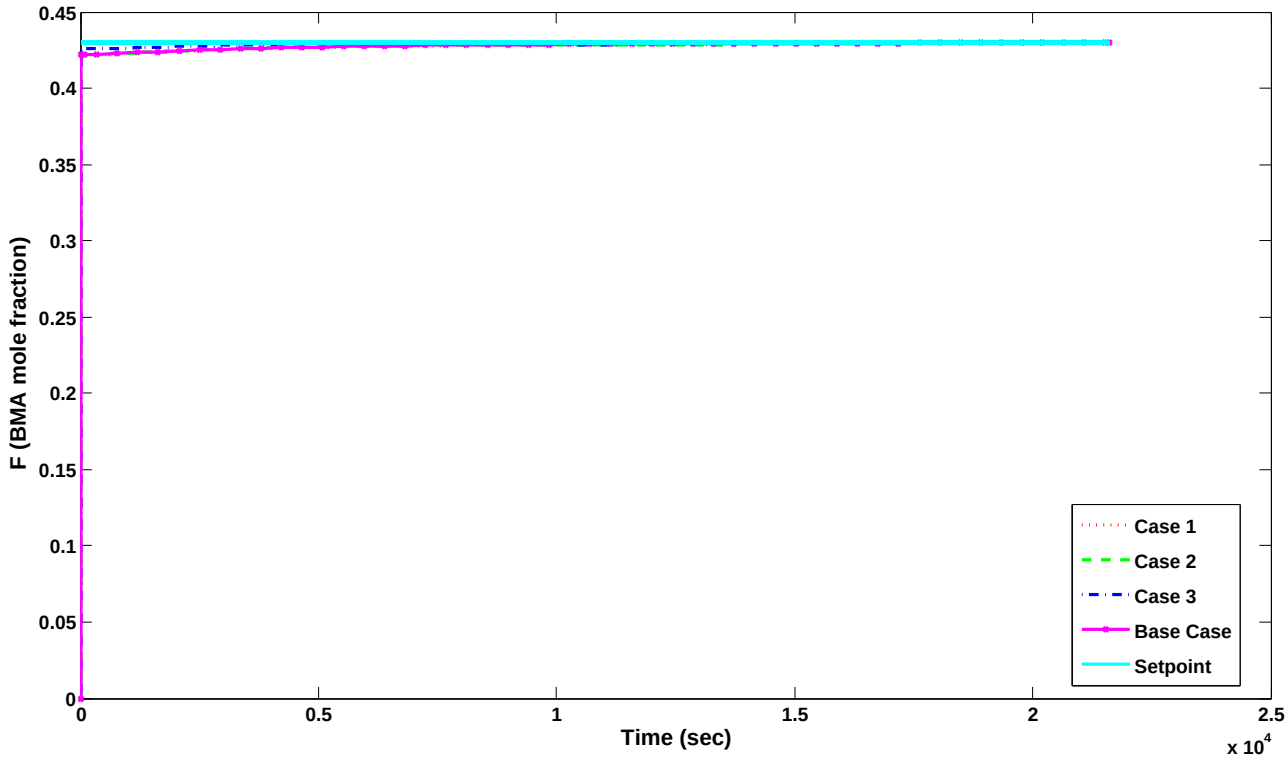

Figure 4.14: F from state estimates of hybrid EKF incorporated with real-time optimization for Case 1, 2 and 3 with $u_i(t) \in [0, 0.03], i = 1, 2, 3, x_1(t) = x_2(t) \in [0, 0.03], x_3(t) \in [0, 5.0 \times 10^{-3}], k = 5 \times 10^{-3}$; base case model represents experiment setup with constant input

were compared to the true $k_{p_{AA}}$ value in Figures 4.20 and 4.21.

3. **Varying transfer to solvent ratio,** C_A^{sol}: The transfer to solvent ratio does not have a great impact on molecular weight or copolymer composition, despite the relatively large change in the parameter values as illustrated in Figures 4.24 and 4.25 for $80\%C_A^{sol}$ and $160\%C_A^{sol}$.

4. **Varying initiator efficiency,** f: The fraction of radicals produced from initiator decomposition that effectively initiates polymerization, f, was varied. The initiator efficiency has an effect on the rate of production of new polymer chains which is needed to compute the molecular weight. Most initiators have values of f between 0.3 and 0.8 [51]. Values were chosen for f at 0.35 and at 0.75. The simulation results are shown in Figures 4.28 and 4.29.

Table 4.1: Results from perturbing the system by varying model parameters for hybrid EKF state estimates implemented with real-time optimization scheme. The % reduction in batch time is compared to the nominal value from the experimental results

Varied model parameters	**Final batch time t_f(sec)**	**% reduction in batch time**	**Cost function (10^5)**
Case 2 - True parameters	13800	36	7.8300
$50\%r_A$	13400	38	8.6800
$150\%r_A$	12000	44	7.4100
$80\%k_{p_{AA}}$	12800	41	7.6100
$120\%k_{p_{AA}}$	13600	37	7.9900
$80\%C_A^{sol}$	13800	36	8.0000
$160\%C_A^{sol}$	13600	37	7.3900
$f = 0.35$	9730	55	13.100
$f = 0.75$	12900	40	8.0300

Simulation Results

Effect of Varying r_A

As shown in Figures 4.16 and 4.17, the reactivity ratio affects molecular weight and copolymer composition. The further the reactivity ratio is from unity, the more difficult it is to control the copolymer composition. This effect is seen for $50\%r_A$ in Figure 4.17. F exceeds its target slightly and the optimization scheme handles the deviation effectively but at the cost of a reduction in molecular weight as shown in Figure 4.16. The higher reactivity ratio ($150\%r_A$) produced a 44% reduction in the final batch time, while $50\%r_A$ had 38% reduction compared to Case 2 at 36% which was simulated with true parameter values. However, Case 2 without system perturbation through varying parameter approached the setpoint faster than the $50\%r_A$ case. This result is justified by the cost function (3.14) value for $50\%r_A$ as shown in Table 4.1. As discussed in Chapter 3, the objective of the on-line optimization is to minimize the cost function so the lowest possible value of the cost function is desired. Corresponding inputs (u_1 - u_3) and state profiles (x_1 - x_3) are shown in Figures 4.18 and 4.19, respectively.

In terms of the actual process and knowledge about the kinetics of the system, Figure 4.15 demonstrates how the system responds to changing reactivity ratios. The system under study operates at a copolymer composition of 42% (represented with the line across Figure 4.15) and functions to maintain this copolymer composition by controlling the ratio of the two monomers BMA and STY at $f_m = 0.44$, as shown by the arrow at $F_p = 0.42$. However, when a wrong reactivity ratio is used, $r_A = 0.21(50\%r_A)$, the system still tries to match the copolymer composition of BMA at 42%. Therefore, the optimization scheme has to adjust the ratio of monomers in

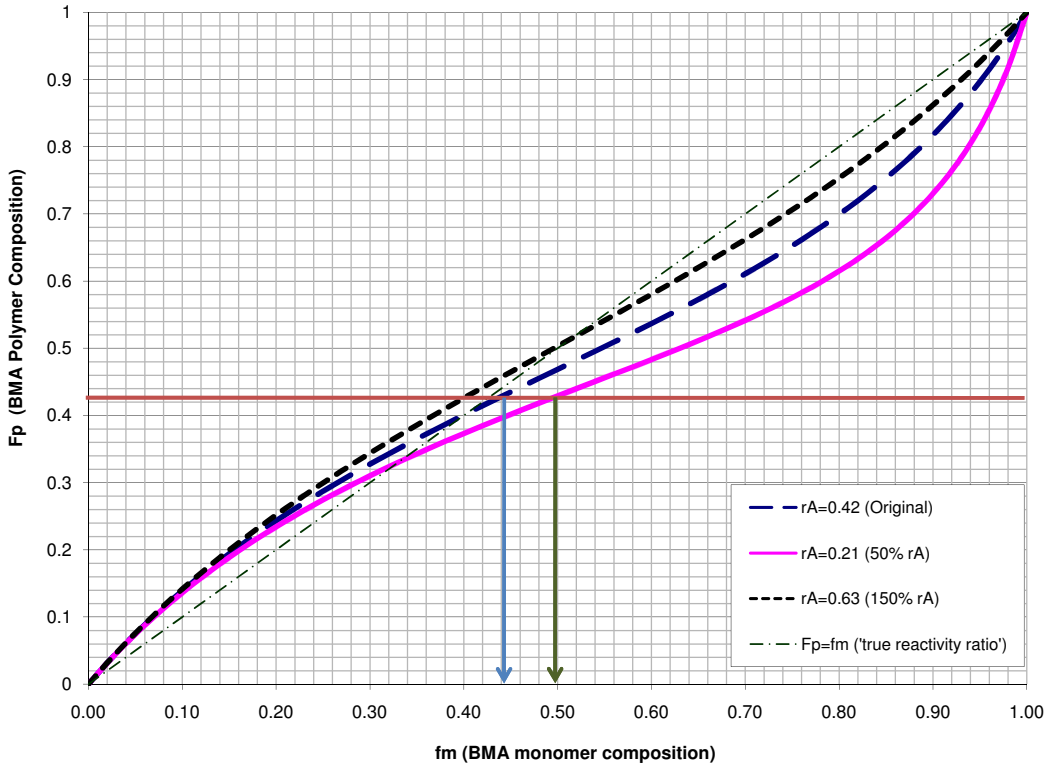

Figure 4.15: BMA copolymer composition assuming terminal model kinetics for BMA. fm is presented in molar basis and can be converted to mass fraction by fm $= \frac{x_1}{x_1+x_2}$

the reactor to 0.50 (as shown in the arrow at $r_A = 0.21(50\% r_A)$) by changing the relative flow rate of BMA and STY through the manipulation of u_1, u_2 and u_3 to maintain M_n on target.

Effect of Varying $k_{p_{AA}}$

Figures 4.20 and 4.21 show that the propagation rate coefficient influences molecular weight and copolymer composition only slightly. As the propagation rate constant increases, the rate of polymer chain growth increases. This is shown for a change of $120\% k_{p_{AA}}$ and the opposite effect is displayed for $80\% k_{p_{AA}}$. The corresponding state and input profiles are displayed in Figures 4.23 and 4.22

The propagation rate coefficients $k_{p_{AA}}$ and $k_{p_{AB}}$ are linked through the reactivity ratio (see Table 3.2). Therefore, changing $k_{p_{AA}}$ will affect $k_{p_{AB}}$. Increasing $k_{p_{AA}}$ will increase the reaction rate and the reaction rate affects the relative rate of consumption of the two monomers BMA and STY as shown in (3.1a) and (3.1b), which also affects the value of $M_n(kg/mol)$ and F.

Effect of Varying C_A^{sol}

Simulation results in Figures 4.24 and 4.25 show that the optimization mechanism is efficient in responding to model mismatch of using the wrong C_A^{sol} as it directs the profiles to their respective setpoints. The equivalent input profile is shown in Figure 4.26. Unlike the case of varying r_A and $k_{p_{AA}}$, C_A^{sol} does not affect x_1 or x_2 (see Figure 4.27) but it influences the molecular weight $M_n(kg/mol)$.

Even though the molecular weight for the process is predicted, the real-time optimization with hybrid EKF estimates showed adequate control of the process for

varied transfer to solvent ratio over a wide range from $80\%C_A^{sol}$ to $160\%C_A^{sol}$. The expected behavior for varying chain transfer to solvent is that increasing C_A^{sol} should decrease M_n causing the system to respond by decreasing u_3. However, the opposite behavior is found which is justified since x_6 is predicted without any experimental measure. Therefore, there should be no difference in profiles as shown in the final batch times which were approximately the same for both transfer to solvent variations that matched the original Case 2 value with true parameters.

Effect of Varying f

The profiles for initiator efficiencies at 0.35 and at 0.75 is illustrated in Figure 4.29. Initiator efficiency f affects rate of radical generation from initiation through the term in (3.8) and, hence, the rate of generation of new polymer chains. Therefore, increasing f initiates more chains in the system leading to an increase in the reaction rate. This effect is shown by having a very high initiator efficiency at 0.75 which should lead to more chains and hence a decrease in molecular weight; instead it translated to an overshoot in M_n beyond the setpoint as seen in Figure 4.28. However, the optimization scheme brought back the molecular weight to the setpoint towards the end of the batch.

Changing f has a great impact on how much initiator is fed to the system as shown in the u_3 profile in Figure 4.30 and x_3 profile in Figure 4.31. At the beginning of the batch, the system feeds less initiator for $f = 0.75$. Intuition would suggest that for every mole of initiator fed, more chains are generated which leads to an increase in the reaction rate and also to an increase in the number of chains in the system. To counteract this increase, less initiator is therefore needed.

As the batch progresses, $M_n(kg/mol)$ starts to increase rapidly and the system responds to counteract the increase by a gradual raise in the feed rate of x_3 (the effect can be seen in the plateau of $M_n(kg/mol)$). Towards the end of the batch, however, the system feeds large amounts of initiator (see Figure 4.30) to force $M_n(kg/mol)$ back to its setpoint.

For $f = 0.35$, the system feeds more initiator at the start of the batch. This is expected since more moles of initiator are necessary to generate chains. The raise in x_3 increases the rate of initiation as shown in (3.8) and this affects the rate of chain generation (3.7). As a result, x_6 (Figure 4.32) increases. The system responds to these changes early in the batch by keeping the molecular weight for $f = 0.35$ relatively low as shown in Figure 4.28.

It is worth noting that the result for $f = 0.35$ showed the greatest reduction in reaction time at 55% from the nominal value. However, it had the greatest cost function value as shown in Table 4.1. Part of the objective of the on-line optimization is to reach the target for molecular weight as the cost function is minimized. Therefore, the fact that $f = 0.35$ results in the greatest cost function value is justified by the results shown in Figure 4.28, since it produced the lowest molecular weight profile compared to all the other cases.

4.4 Summary

This chapter presented the structure of the state estimation technique that was incorporated into the BMA/ STY copolymerization on-line optimization system. The background for the hybrid extended Kalman filter was discussed and comparisons were made to compare the filter application to the real-time optimization scheme of

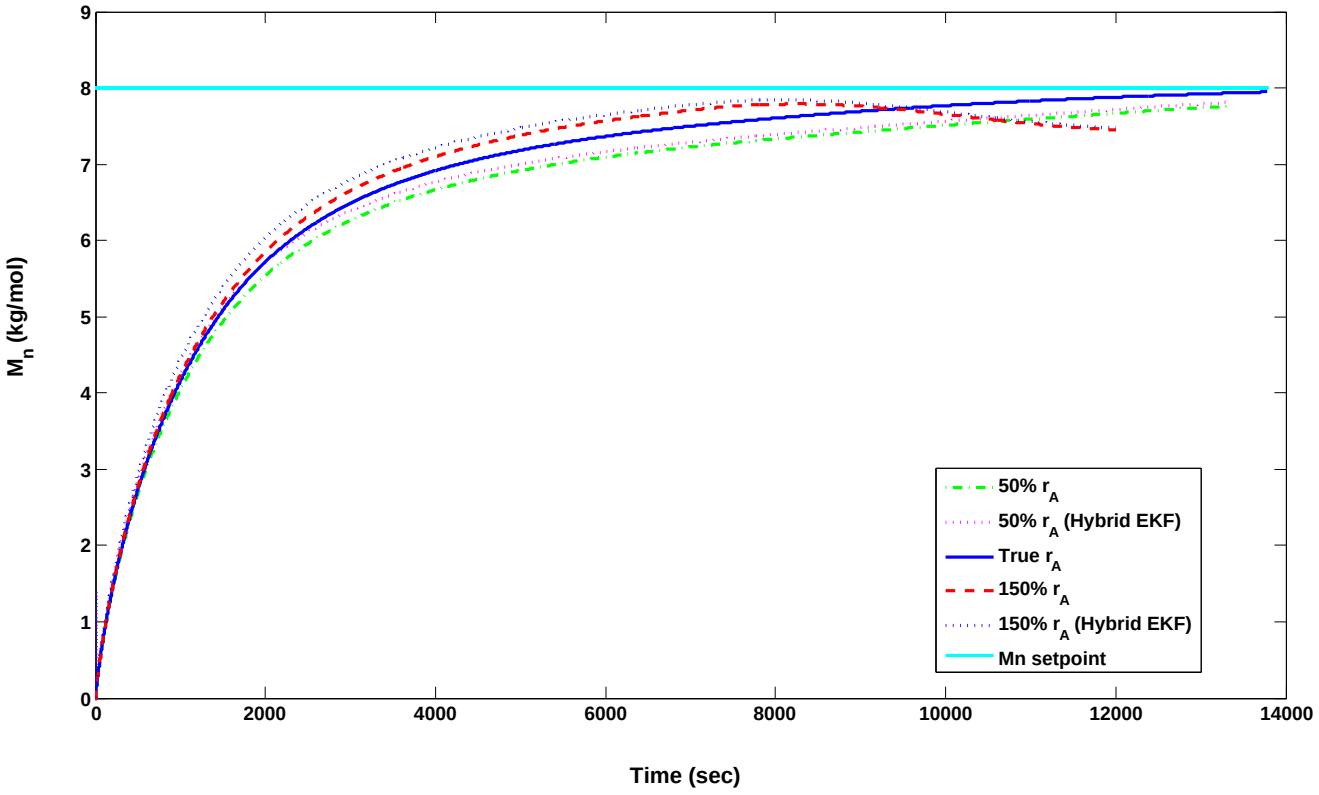

Figure 4.16: M_n from state estimates of hybrid EKF incorporated with real-time optimization for Case 2 for $50\%r_A$ and $150\%r_A$, with $u_i(t) \in [0, 0.03], i = 1, 2, 3, x_1(t) = x_2(t) \in [0, 0.03], x_3(t) \in [0, 5.0 \times 10^{-3}], k = k = 5 \times 10^{-3}$. (Hybrid EKF) denotes the profile from the observer and all others are from the true process

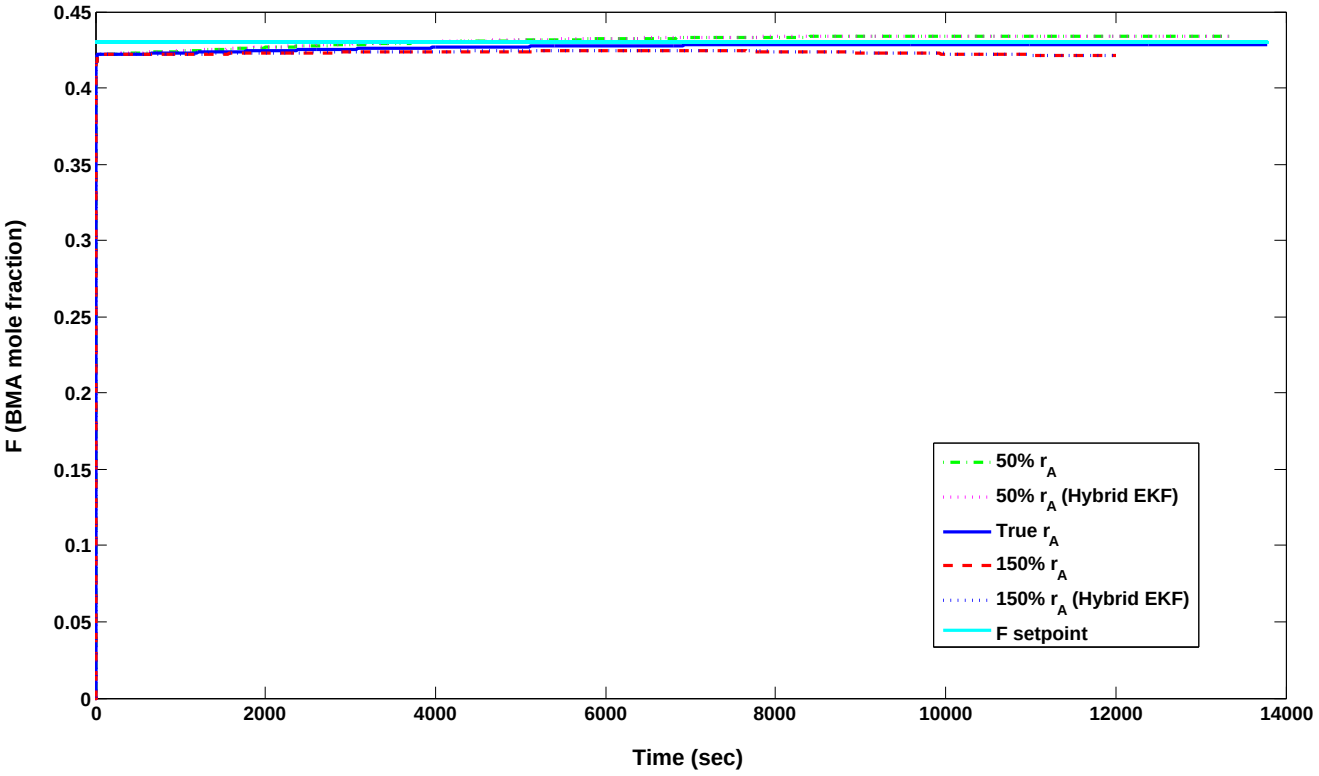

Figure 4.17: F from state estimates of hybrid EKF incorporated with real-time optimization for Case 2 for $50\%r_A$ and $150\%r_A$, with $u_i(t) \in [0, 0.03], i = 1, 2, 3, x_1(t) = x_2(t) \in [0, 0.03], x_3(t) \in [0, 5.0 \times 10^{-3}], k = 5 \times 10^{-3}$. (Hybrid EKF) denotes the profile from the observer and all others are from the true process

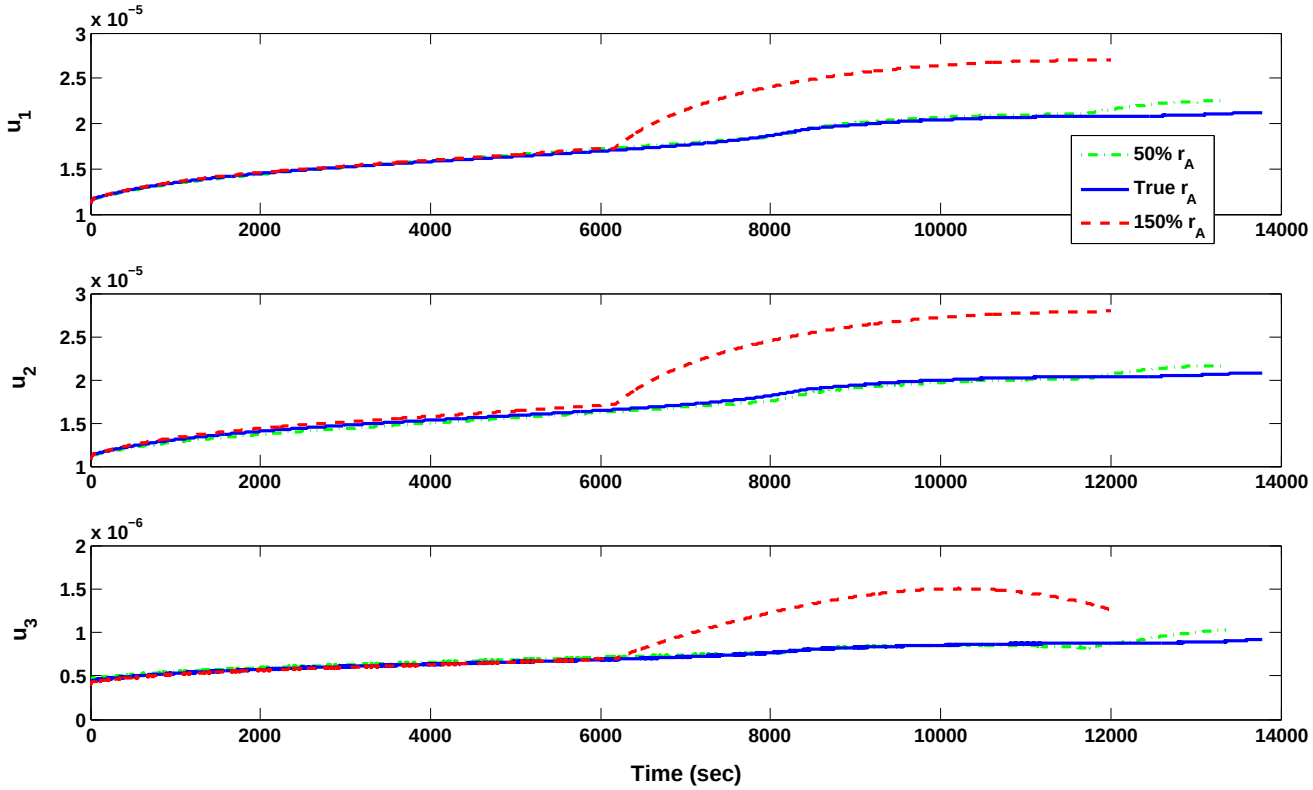

Figure 4.18: u_1, u_2, u_3 from state estimates of hybrid EKF incorporated with real-time optimization for Case 2 for $50\%r_A$ and $150\%r_A$, with $u_i(t) \in [0, 0.03], i = 1, 2, 3, x_1(t) = x_2(t) \in [0, 0.03], x_3(t) \in [0, 5.0 \times 10^{-3}], k = 5 \times 10^{-3}$

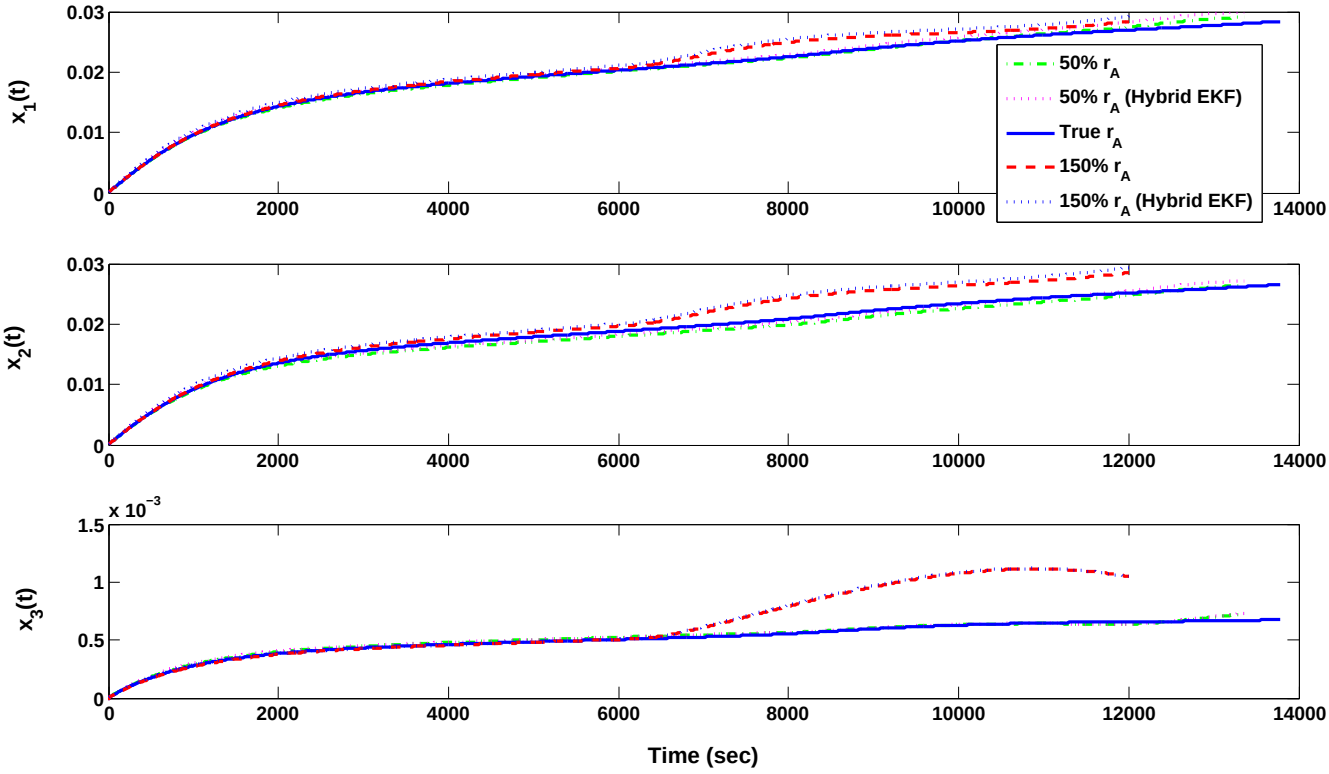

Figure 4.19: x_1, x_2, x_3 from state estimates of hybrid EKF incorporated with real-time optimization for Case 2 for $50\% r_A$ and $150\% r_A$, with $u_i(t) \in [0, 0.03], i = 1, 2, 3, x_1(t) = x_2(t) \in [0, 0.03], x_3(t) \in [0, 5.0 \times 10^{-3}], k = 5 \times 10^{-3}$. (Hybrid EKF) denotes the profile from the observer and all others are from the true process

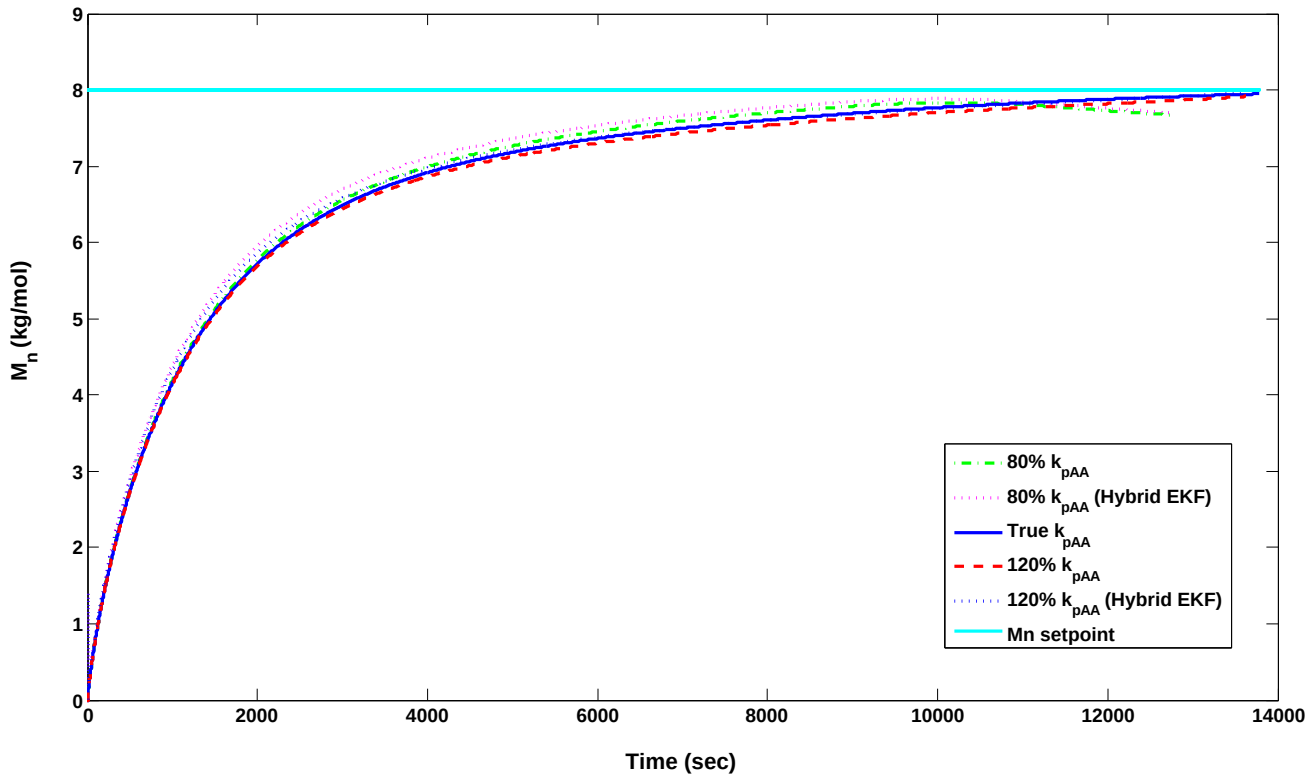

Figure 4.20: M_n from state estimates of hybrid EKF incorporated with real-time optimization for Case 2 for $80\%k_{p_{AA}}$ and $120\%k_{p_{AA}}$, with $u_i(t) \in [0, 0.03], i = 1, 2, 3, x_1(t) = x_2(t) \in [0, 0.03], x_3(t) \in [0, 5.0 \times 10^{-3}], k = k = 5 \times 10^{-3}$. (Hybrid EKF) denotes the profile from the observer and all others are from the true process

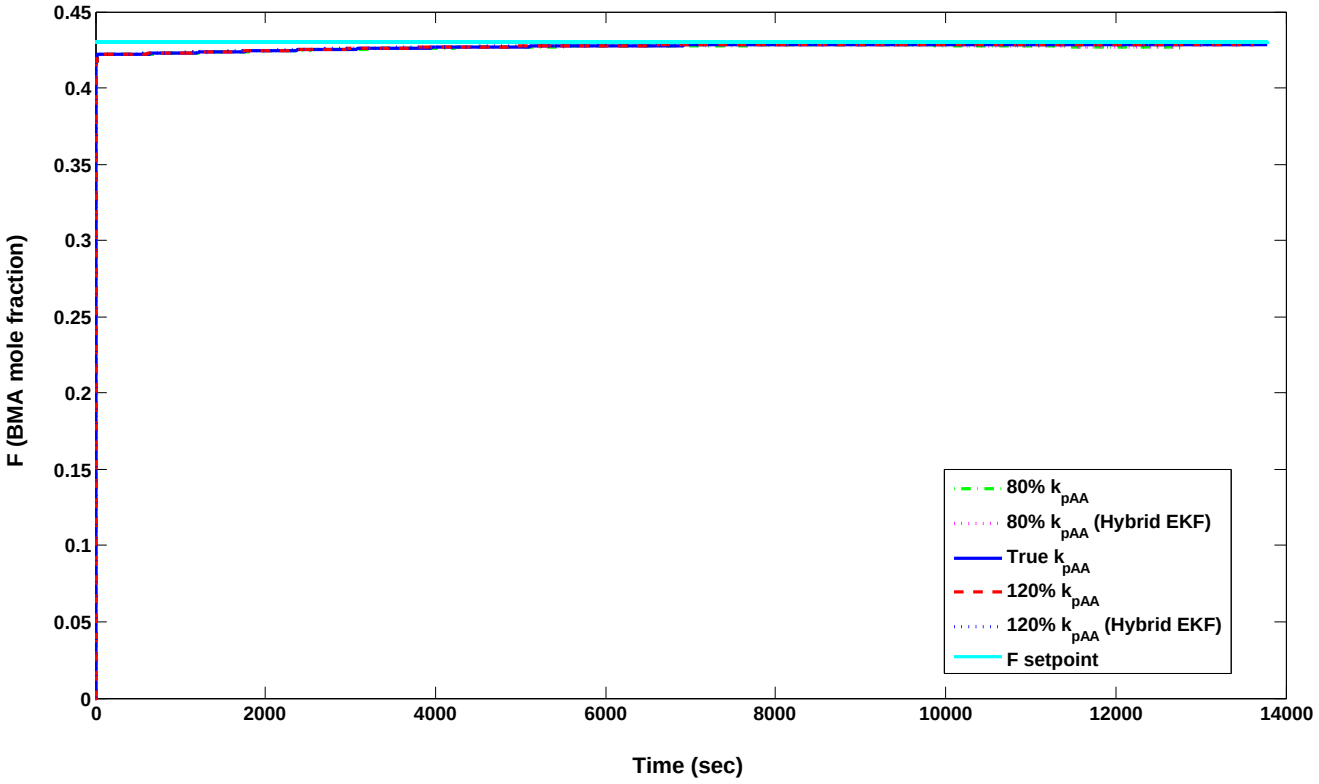

Figure 4.21: F from state estimates of hybrid EKF incorporated with real-time optimization for Case 2 for $80\%k_{p_{AA}}$ and $120\%k_{p_{AA}}$, with $u_i(t) \in [0, 0.03], i = 1, 2, 3, x_1(t) = x_2(t) \in [0, 0.03], x_3(t) \in [0, 5.0 \times 10^{-3}], k = 5 \times 10^{-3}$. (Hybrid EKF) denotes the profile from the observer and all others are from the true process

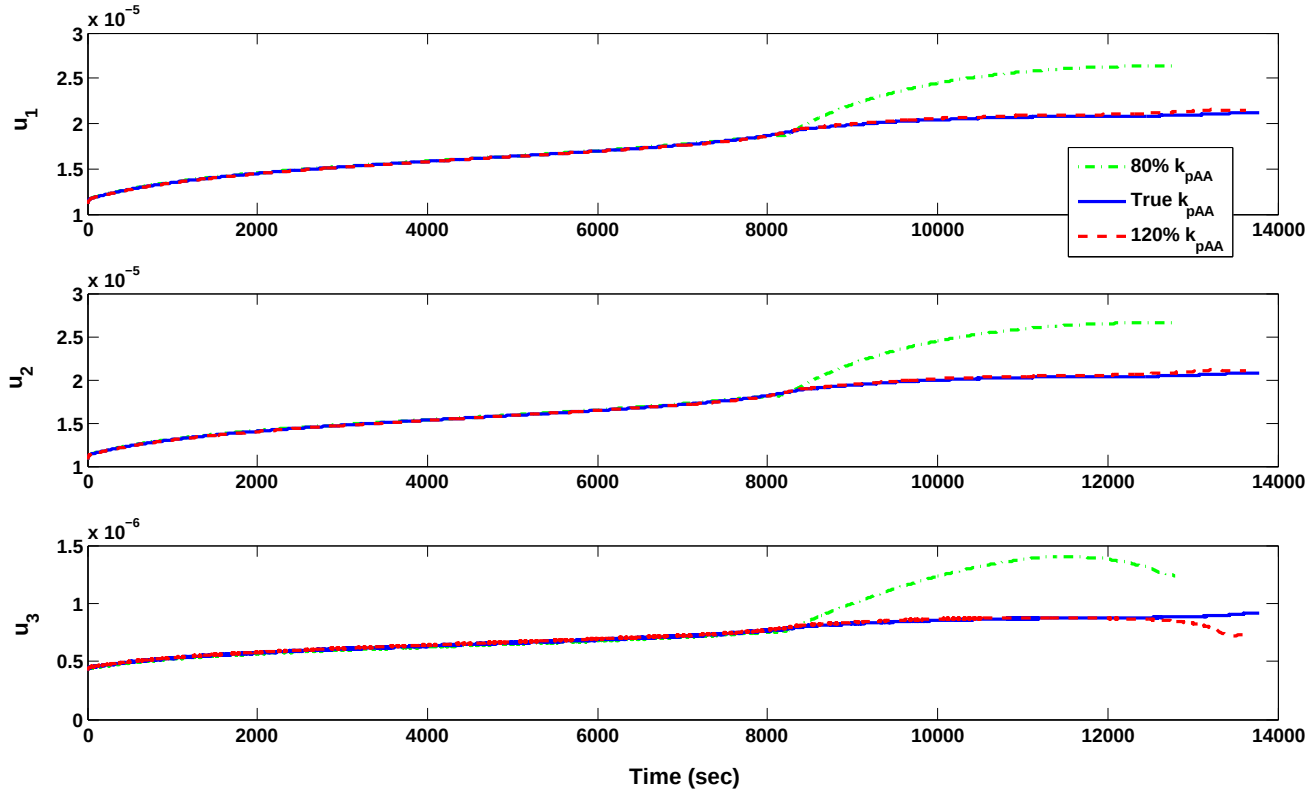

Figure 4.22: u_1, u_2, u_3 from state estimates of hybrid EKF incorporated with real-time optimization for Case 2 for $80\%k_{p_{AA}}$ and $120\%k_{p_{AA}}$, with $u_i(t) \in [0, 0.03], i = 1, 2, 3, x_1(t) = x_2(t) \in [0, 0.03], x_3(t) \in [0, 5.0 \times 10^{-3}], k = 5 \times 10^{-3}$

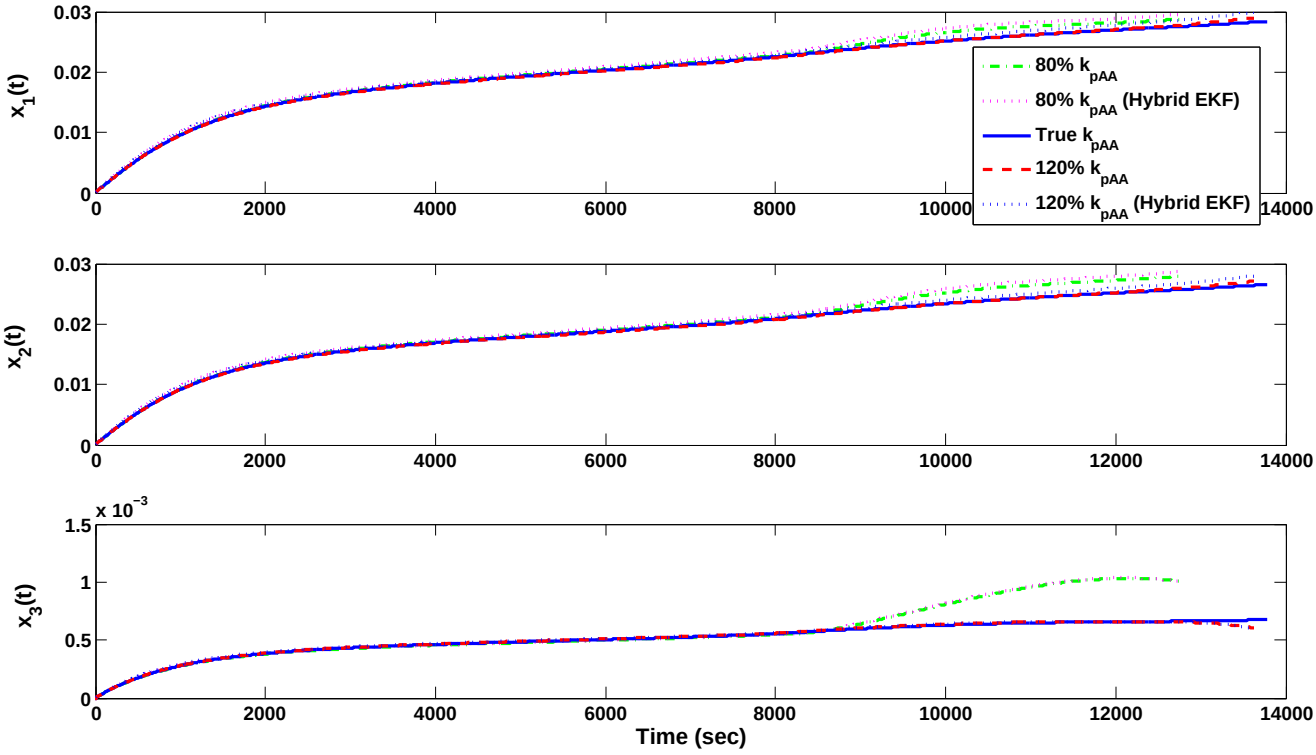

Figure 4.23: x_1, x_2, x_3 from state estimates of hybrid EKF incorporated with real-time optimization for Case 2 for $80\%k_{p_{AA}}$ and $120\%k_{p_{AA}}$, with $u_i(t) \in [0, 0.03], i = 1, 2, 3, x_1(t) = x_2(t) \in [0, 0.03], x_3(t) \in [0, 5.0 \times 10^{-3}], k = 5 \times 10^{-3}$.(Hybrid EKF) denotes the profile from the observer and all others are from the true process

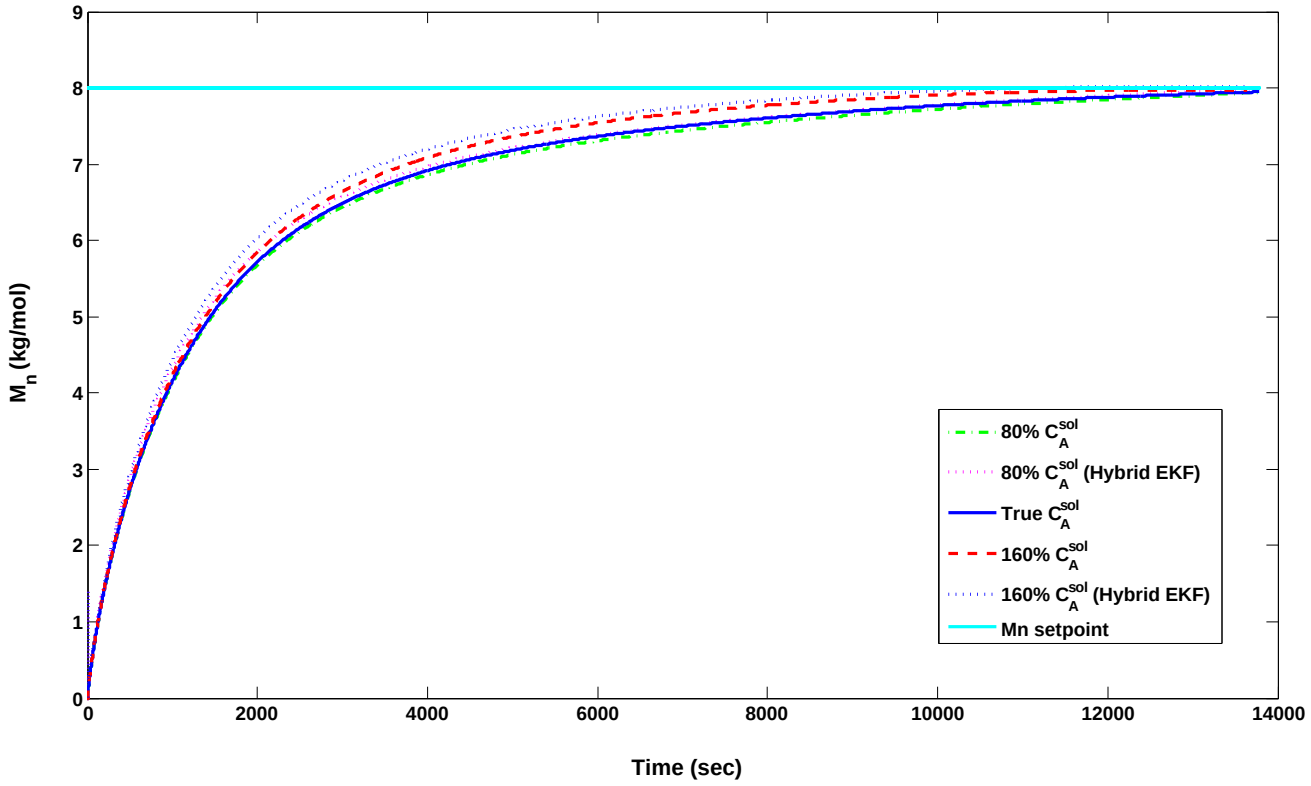

Figure 4.24: M_n from state estimates of hybrid EKF incorporated with real-time optimization for Case 2 for $80\%C_A^{sol}$ and $160\%C_A^{sol}$, with $u_i(t) \in [0, 0.03], i = 1, 2, 3, x_1(t) = x_2(t) \in [0, 0.03], x_3(t) \in [0, 5.0 \times 10^{-3}], k = 5 \times 10^{-3}$. (Hybrid EKF) denotes the profile from the observer and all others are from the true process

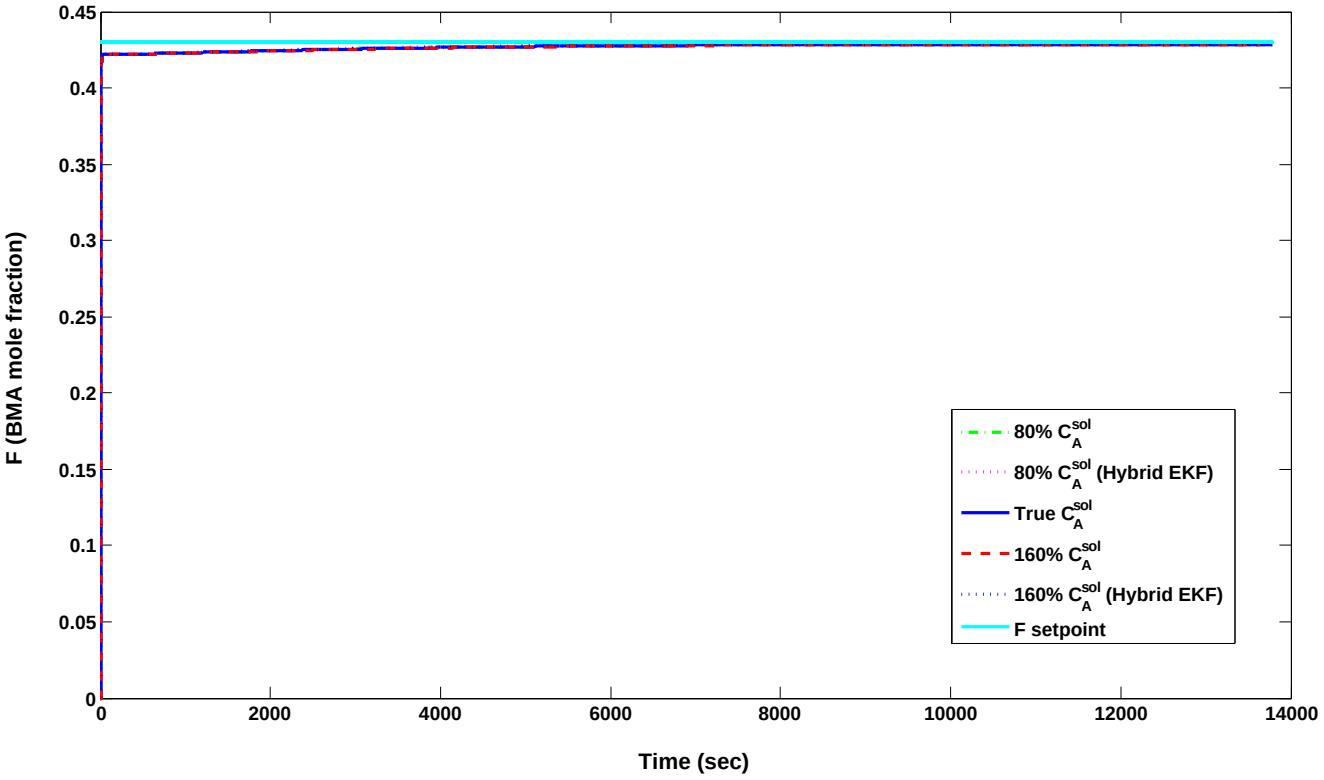

Figure 4.25: F from state estimates of hybrid EKF incorporated with real-time optimization for Case 2 for $80\%C_A^{sol}$ and $160\%C_A^{sol}$, with $u_i(t) \in [0, 0.03], i = 1, 2, 3, x_1(t) = x_2(t) \in [0, 0.03], x_3(t) \in [0, 5.0 \times 10^{-3}], k = 5 \times 10^{-3}$. (Hybrid EKF) denotes the profile from the observer and all others are from the true process

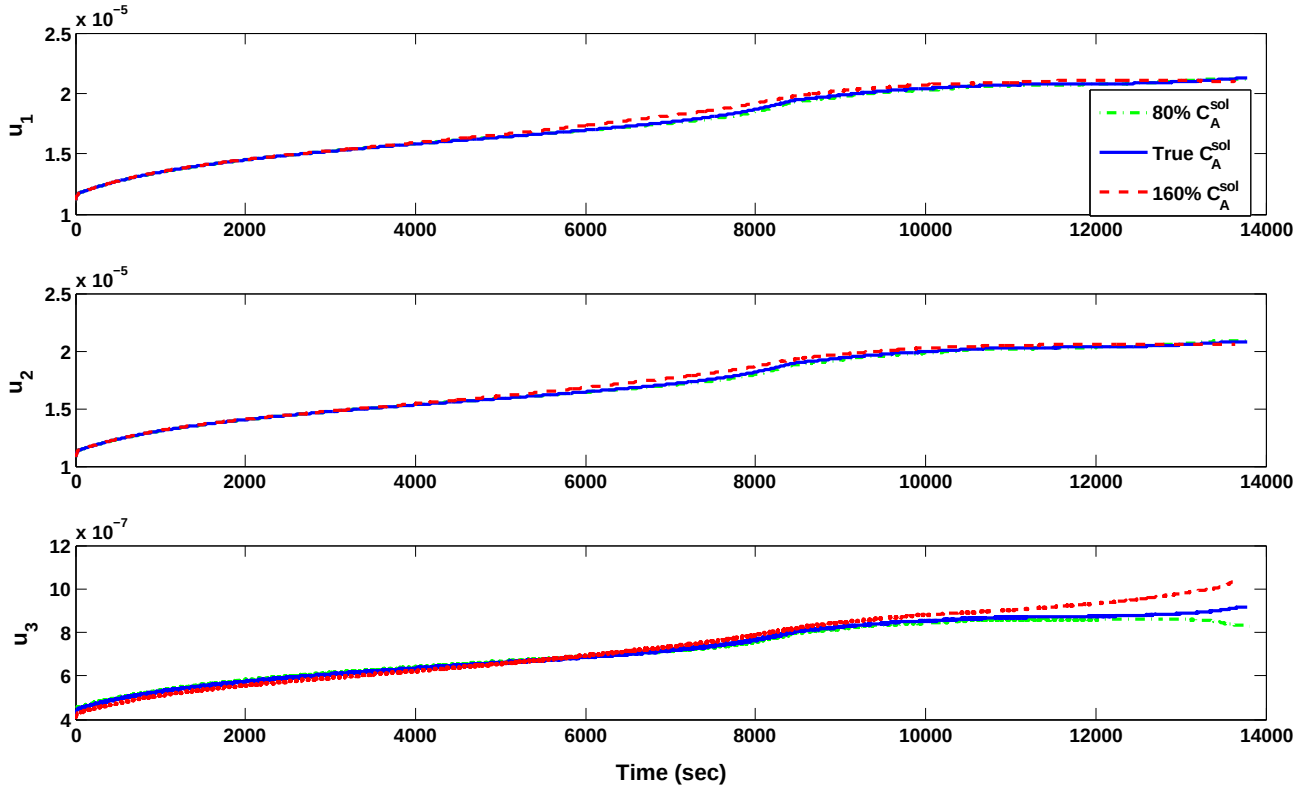

Figure 4.26: u_1, u_2, u_3 from state estimates of hybrid EKF incorporated with real-time optimization for Case 2 for $80\%C_A^{sol}$ and $160\%C_A^{sol}$, with $u_i(t) \in [0, 0.03], i = 1, 2, 3, x_1(t) = x_2(t) \in [0, 0.03], x_3(t) \in [0, 5.0 \times 10^{-3}], k = 5 \times 10^{-3}$

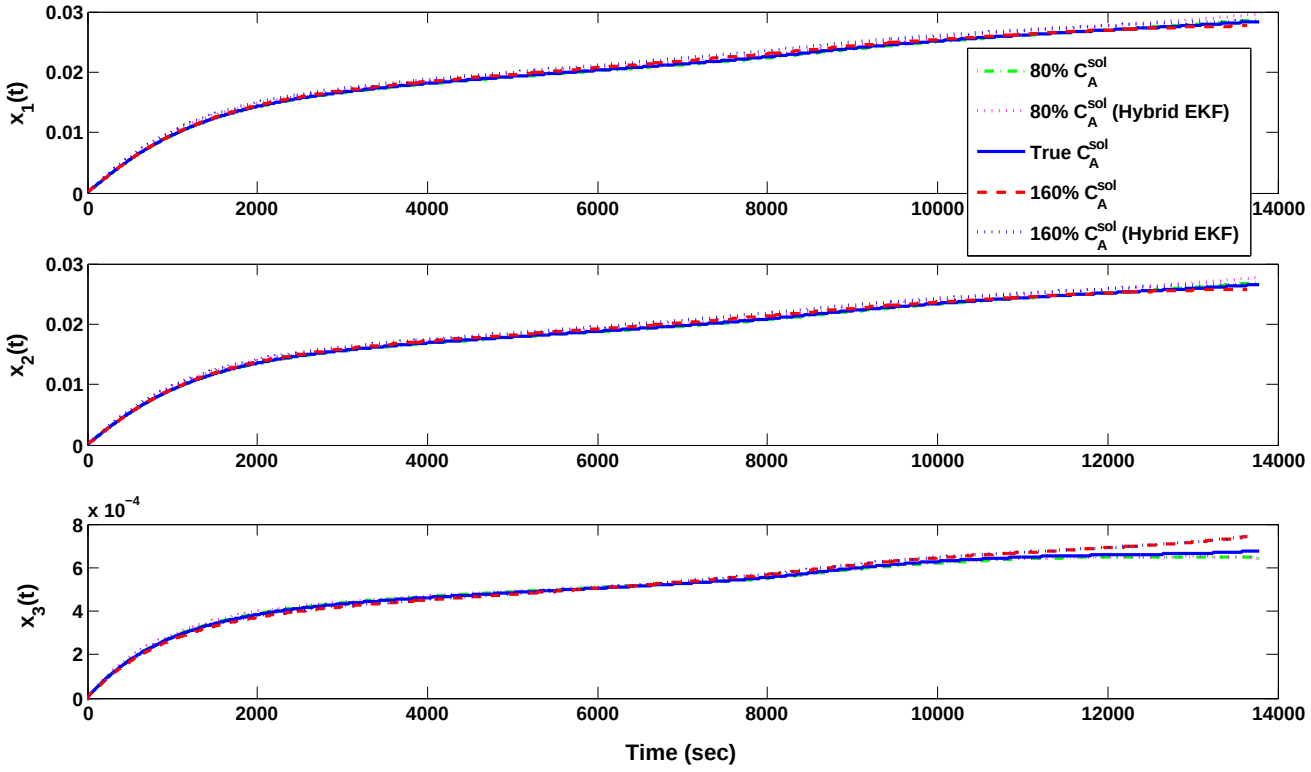

Figure 4.27: x_1, x_2, x_3 from state estimates of hybrid EKF incorporated with real-time optimization for Case 2 for $80\%C_A^{sol}$ and $160\%C_A^{sol}$, with $u_i(t) \in [0, 0.03], i = 1, 2, 3, x_1(t) = x_2(t) \in [0, 0.03], x_3(t) \in [0, 5.0 \times 10^{-3}], k = 5 \times 10^{-3}$. (Hybrid EKF) denotes the profile from the observer and all others are from the true process

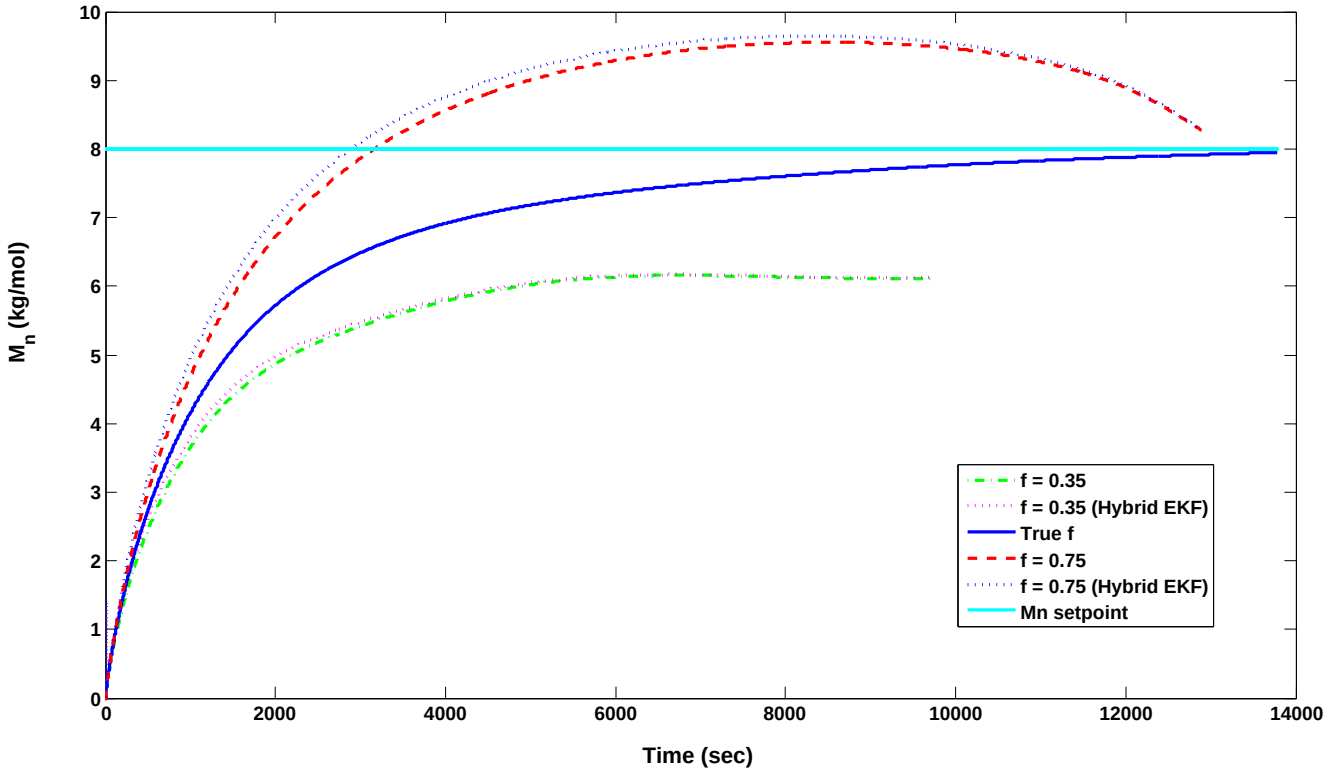

Figure 4.28: M_n from state estimates of hybrid EKF incorporated with real-time optimization for Case 2 for $f = 0.35$ and $f = 0.75$, with $u_i(t) \in [0, 0.03], i = 1, 2, 3, x_1(t) = x_2(t) \in [0, 0.03], x_3(t) \in [0, 5.0 \times 10^{-3}], k = 5 \times 10^{-3}$. (Hybrid EKF) denotes the profile from the observer and all others are from the true process

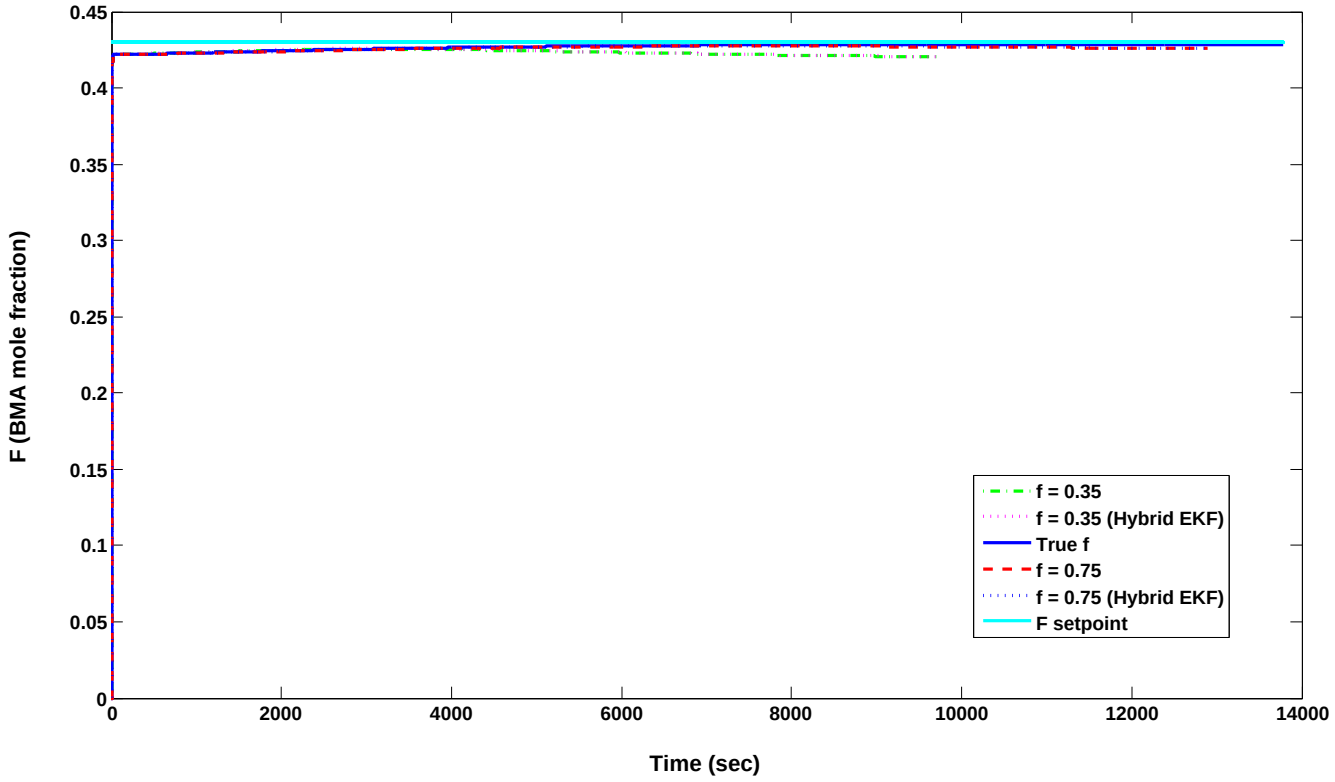

Figure 4.29: F from state estimates of hybrid EKF incorporated with real-time optimization for Case 2 for $f = 0.35$ and $f = 0.75$, with $u_i(t) \in [0, 0.03], i = 1, 2, 3, x_1(t) = x_2(t) \in [0, 0.03], x_3(t) \in [0, 5.0 \times 10^{-3}], k = 5 \times 10^{-3}$. (Hybrid EKF) denotes the profile from the observer and all others are from the true process

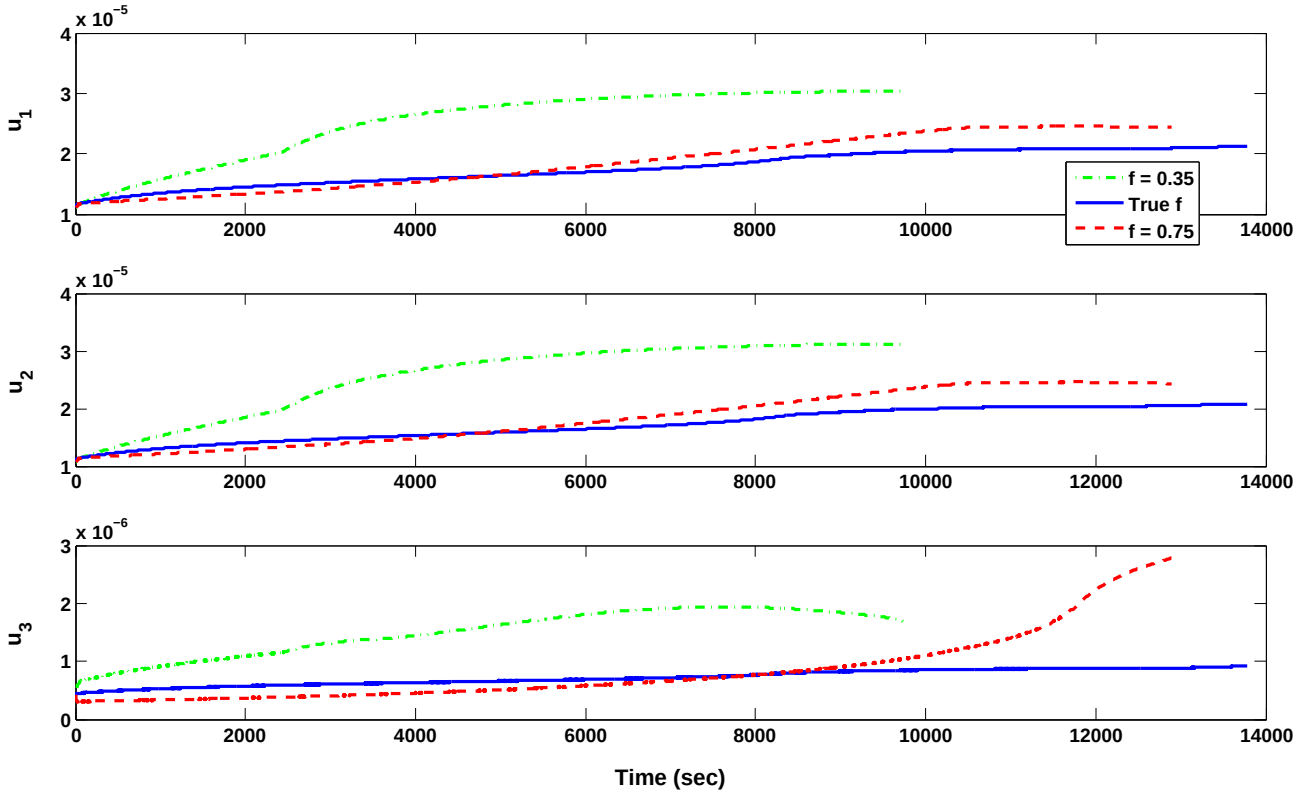

Figure 4.30: u_1, u_2, u_3 from state estimates of hybrid EKF incorporated with real-time optimization for Case 2 for $f = 0.35$ and $f = 0.75$, with $u_i(t) \in [0, 0.03], i = 1, 2, 3, x_1(t) = x_2(t) \in [0, 0.03], x_3(t) \in [0, 5.0 \times 10^{-3}], k = 5 \times 10^{-3}$

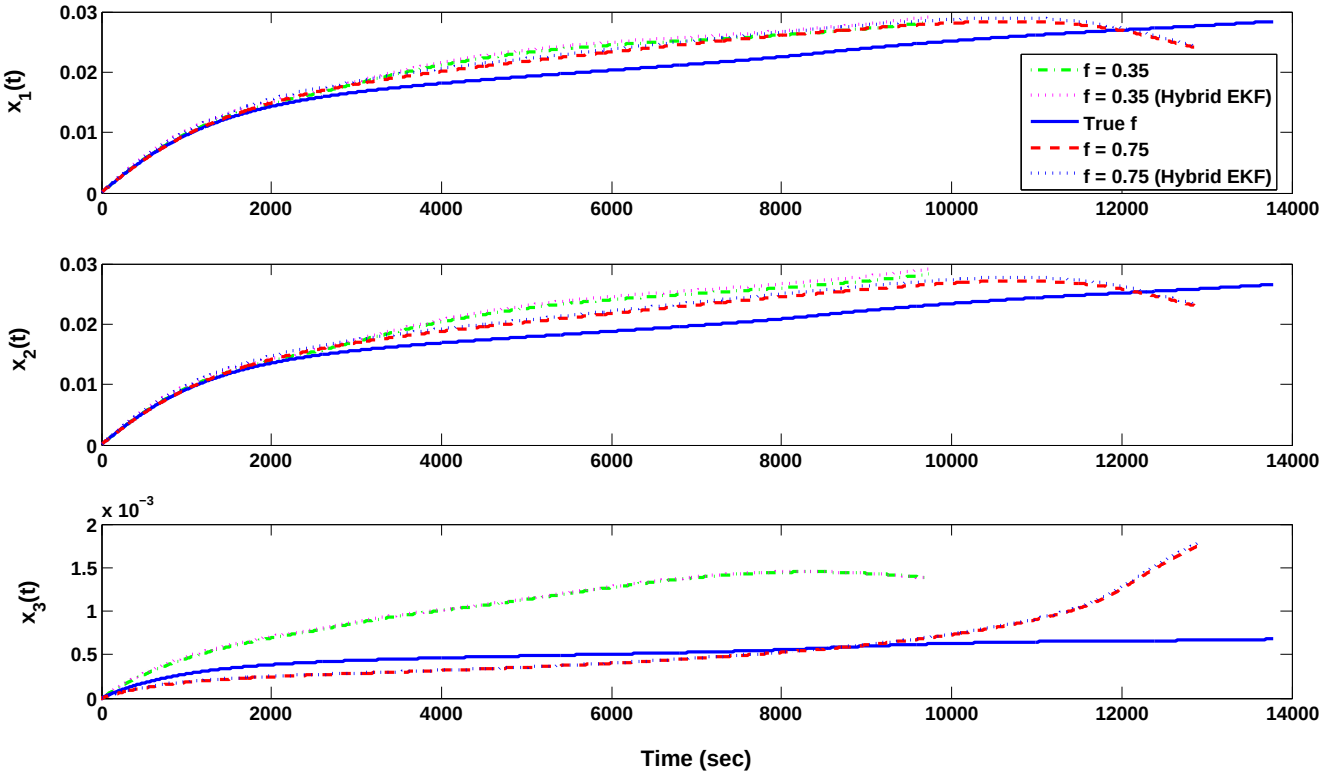

Figure 4.31: x_1, x_2, x_3 from state estimates of hybrid EKF incorporated with real-time optimization for Case 2 for $f = 0.35$ and $f = 0.75$, with $u_i(t) \in [0, 0.03], i = 1, 2, 3, x_1(t) = x_2(t) \in [0, 0.03], x_3(t) \in [0, 5.0 \times 10^{-3}], k = 5 \times 10^{-3}$. (Hybrid EKF) denotes the profile from the observer and all others are from the true process

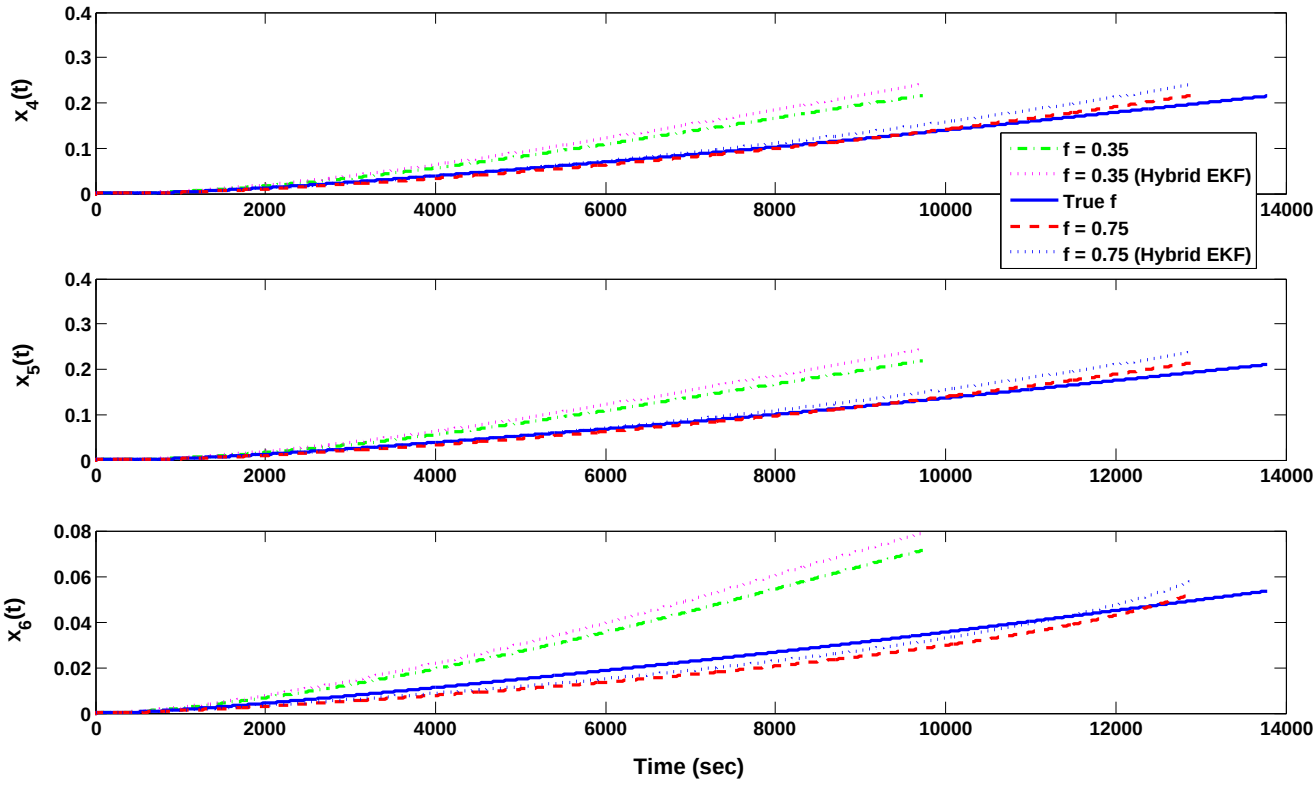

Figure 4.32: x_4, x_5, x_6 from state estimates of hybrid EKF incorporated with real-time optimization for Case 2 for $f = 0.35$ and $f = 0.75$, with $u_i(t) \in [0, 0.03], i = 1, 2, 3, x_1(t) = x_2(t) \in [0, 0.03], x_3(t) \in [0, 5.0 \times 10^{-3}], k = 5 \times 10^{-3}$. (Hybrid EKF) denotes the profile from the observer and all others are from the true process

the actual process in an open-loop and closed-loop form and also with model mismatch.

For the open-loop comparison, the hybrid EKF estimates were found to closely match the true states of the system (Figures 4.2 to 4.7). In addition, the estimated molecular weight and copolymer composition from the filter tracked the actual ones of the process (Figures 4.8). Overall, the error from the state estimates were all below 4×10^{-4}.

For the closed-loop comparison, the observer implemented performed effectively. All of the constraints on the system were satisfied as the limitations placed on the input, states, total mass of reactor content, and final mass of polymer produced were not exceeded. Furthermore, the estimated molecular weight and copolymer composition reached their target. All in all, the observer was successful in reconstructing the system states (Figures 4.11 and 4.12); tracking the inputs (Figure 4.10); estimating the desired polymer properties (Figure 4.9); and it even minimized the final batch time further by 1100 sec from the results with only the dynamic optimization in Chapter 3.

The robustness analysis of the process with the hybrid EKF estimates and on-line optimization subject to model mismatch introduced by incorporating incorrect parameters showed that the system was able to perform adequately for most of the perturbations. Of all the tests conducted, the process achieved the best control for varying the chain transfer to solvent constant 80% above and below the true value (Figures 4.24 to 4.27). Appropriate adjustments were made to the flow rate of monomers and input profiles to reach the target for molecular weight and copolymer composition for $\pm$ 50% r_A (Figures 4.16 to 4.19) as well as for 80%$k_{p_{AA}}$ and 120%$k_{p_{AA}}$

(Figures 4.20 to 4.23). The same adequate process control was shown for all the cases with initiator efficiency f at 0.35 and most of the cases of f at 0.75, except for molecular weight tracking (Figures 4.28 to 4.31).

Overall, none of the constraints on the states and inputs were violated for all of the cases by using incorrect parameters. Therefore, the system is considered to be sufficiently robust, except for very high efficiency factors (f at 0.75) where it exceeded the target for the molecular weight.

Chapter 5

Conclusions and Future Work

State estimation is crucial for most processes in the chemical industry as system states are not always available for measurement or may not be measurable. There is great incentive to improve observer design to obtain effective and applicable methods. In this research project, the on-line optimization routine was improved upon and sensitivity analysis of the system was performed. In addition, a hybrid extended Kalman filter was developed for a butyl methacrylate and styrene semi-batch free-radical copolymerization process subject to on-line optimization control algorithm.

The entire thesis is summarized in Section 5.1 and recommendations for future work are presented in Section 5.2

5.1 Summary of Thesis

In Chapter 2, the importance of state estimation was addressed. Analysis of Kalman filtering techniques for linear and nonlinear systems were presented. It was found that the process and measurement noise structures were important for tuning the

Kalman filter to achieve desired performance. The literature review of application of Kalman filtering to polymerization systems showcased the difficulties in on-line monitoring, such as the need for extensive calibration of equipment and the inability to measure certain polymer properties. However, state estimation coupled with on-line optimization is shown to overcome many of these challenges and obstacles. The literature review discussed cases of successful observer implementation with real-time optimization. The on-line optimization techniques presented in the review were different from the work in this thesis. For this research, the existing observer was directly incorporated in the on-line optimization scheme as opposed to coupling the state estimator with a control scheme for tracking purposes. The present optimization scheme is easier to implement and uses feedback measurements to update the remaining profile of the batch.

The background of the polymerization process studied and details of the real-time optimization scheme are discussed in Chapter 3. The technique incorporated is on-line optimization, a feedback control mechanism that uses process information to continually change the control action. The cost function was formulated to meet the system constraints as batch time is minimized, while maintaining the molecular weight and copolymer compositions at their target. The improvements made to the real-time optimization routine are also presented.

The system was found to be robust to various tuning parameters. From the sensitivity analysis in Chapter 3, it was discovered that the most suitable way to reduce the batch time for the process was to increase the number of time intervals for optimization which resulted in a prolonged simulation time.

The significance of observer design and implementation with on-line optimization

are highlighted in Chapter 4. The hybrid EKF as an observer was shown to reconstruct the states of the process effectively as it tracked the true states of the system. In addition, all the constraints for the state, input, total reactor content and final mass of polymer were satisfied. The targets for molecular weight and copolymer composition were also reached. In light of model mismatch with incorrect parameters, the system with observer and real-time optimization was found to be robust, especially for great variations in chain transfer to solvent ratio. The observer connected with the on-line optimization scheme performed effectively for most of the cases studied. The best results were obtained for variations in model parameters for reactivity ratio, propagation rate coefficient, and low initiator efficiency. However, the setpoint for molecular weight was exceeded for very high initiator efficiency. This result was expected as the process bases its response on the estimation of molecular weight and has no knowledge of the true value. Therefore, without availability of a sensor to measure molecular weight on-line, the optimization software is not capable of perfectly controlling molecular weight in the presence of model mismatch.

As shown in Chapter 4, the proposed observer coupled with the real-time optimization was successful in controlling copolymer composition and molecular weight for the process without model mismatch. With model mismatch, the process performed efficiently for all the cases except for varied initiator efficiency factor. It was noted that on-line optimization scheme was highly sensitive to the efficiency factor.

5.2 Recommended Future Research

The first and foremost recommendation for this project is to include on-line estimation of initiator efficiency in the observer design. To do this, the initiator efficiency should

be considered as an extra state of the system, without having any dynamics. Process noise at high frequency should be added for this additional state to excite the system. Once the states of the system are successfully reconstructed by the hybrid EKF, the hybrid EKF should be implemented with the on-line optimization routine. With real-time estimation of initiator efficiency, the on-line optimization scheme should control the molecular weight more effectively.

Another interesting extension of this work would be to replace the process model of the process with an actual process. For the proposed project, measurement information would be obtained from on-line infra-red (IR) spectroscopy. These measurements of butyl methacrylate and styrene combined together would be inputs to the hybrid EKF developed in Chapter 4. The observer would then reconstruct the states of the system, given the measurement and process information. The on-line optimization routine presented in Chapter 3 coupled with the observer would then be used to control the copolymer composition and molecular weight, while reducing the reaction time.

Other areas of study include implementing a different observer to compare the system performance and incorporating a more complex kinetics of the process that considers styrene thermal initiation, methacrylate depropagation and penultimate chain growth kinetics. Predici software could be used to develop a more complex kinetics of the process which would replace the existing process model.

Bibliography

[1] A. Cherfi G. Fervotte and C. Novat. Robust on-line measurement of conversion and molecular weight using nir spectroscopy during solution polymerization. *Journal of Applied Polymer Science*, 85(12):2510–2520, 2002.

[2] M. Soroush. Nonlinear state-observer design with application to reactors. *Chemical Engineering Science*, 52(3):387–404, 1997.

[3] S.I. Biagiola and J.L. Figueroa. A high gain nonlinear observer: Application to the control of an unstable nonlinear process. *Computers and Chemical Engineering*, 28(9):1881–1898, 2004.

[4] M. C. Gragy W. J. Simonsick and R. A. Hutchinson. Studies of Higher Temperature Polymerization of n-Butyl Methacrylate and n-Butyl Acrylate. *Macromolecular Symposia*, 182(1):149–168, 2002.

[5] D. H. Li and R. A. Hutchinson. High-temperature semibatch free radical copolymerization of butyl methacrylate and stryene. *Macromolecular Symposium*, 243: 24–34, 2006.

[6] W. Harmon Ray. *Advanced Process Control (Chemical Engineering)*. McGraw-Hill, 1980.

[7] D. Simon. *Optimal State Estimation: Kalman, H Infinity, and Nonlinear Approaches*. Wiley-Interscience, first edition, 2006.

[8] R. E. Kalman. A new approach to linear filtering and prediction problems. *Journal of Basic Engineering*, 82:35–45, 1960.

[9] A. Gelb J. F. Kasper Jr. R. A. Nash Jr. C. F. Price and A. A. Sutherland Jr. *Applied Optimal Estimation*. The MIT Press, 1974.

[10] A. V. Balakrishnan. *Kalman Filtering Theory (Series in Communication and Control Systems)*. Optimization Software, Inc., second edition, 1987.

[11] C. K. Chui and G. Chen. *Kalman Filtering with Real-Time Applications*. Springer-Verlag, 1987.

[12] A. E. Bryson and Y-C Ho. *Applied Optimal Control: Optimization, Estimation and Control*. Hemisphere Pub. Corp., 1975.

[13] J. C. Spall. *Introduction to Stochastic Search and Optimization: Estimation, Simulation, and Control*. Wiley-Interscience, first edition, 2003.

[14] K. C. Miller and D. L. Leskiw. *An Introduction to Kalman Filtering With Applications*. Robert E. Krieger Publishing Company, 1987.

[15] H. Wu and G. Chen. Suboptimal Kalman filtering for linear systems with non-gaussian noise. In Guanrong Chen, editor, *Approximate Kalman Filtering (Approximations and Decompositions, Vol 2)*. World Scientific Publishing, 1993.

[16] C. A. Sandink. Screening diagnostics for parameter selection in extended Kalman filter implementations. Master's thesis, Queens University, 1999.

[17] R. K. Mehra. Approaches to adaptive filtering. *IEEE Transactions on Automatic Control*, 17(5):693–698, 1972.

[18] P. R. Belanger. Estimation of Noise Covariance Matrices for a Linear Time-Varying Stochastic-Process. *Automatica*, 10(3):267–275, 1974.

[19] B. J. Odelson M. R. Rajamani and J. B. Rawlings. A new autocovariance least-squares method for estimating noise covariances. *Automatica*, 42(2):303–308, 2006.

[20] R. M. Rajamani and J. B. Rawlings. Estimation of the disturbance structure from data using semidefinite programming and optimal weighting. *Automatica*, 45(1):142–148, 2009.

[21] S. S. Na and H. K. Rhee. Polymonial ARMA model identification for a continuous styrene polymerization reactor using on-line measurments of polymer properties. *Journal of Applied Polymer Science*, 76:1889–1901, 2000.

[22] A. Cherfi and G. Fevotte. On-line conversion monitoring of the solution polymerization of methyl methacrylate using near-infrared spectroscopy. *Macromolecular Chemistry and Physics*, 203(9):1189–1193, 2002.

[23] W. Vautz W. Mauntz S. Engell and J. I. Baumbach. Monitoring of emulsion polymerisation processes using ion mobility spectrometry - a pilot study. *Macromolecular Reaction Engineering*, 3(2-3):85–90, 2009.

[24] T. Kreft and W. F. Reed. Predictive control and verification of conversion kinetics and polymer molecular weight in semi-batch free radical homopolymer reactions. *European Polymer Journal*, 45(8):2288 – 2303, 2009.

[25] J. R. R. Richards and J. P. C Congalidis. Measurement and control of polymerization reactors. *Computers and Chemical Engineering*, 30:1447–1463, 2006.

[26] J. H. Jo and S. G. Bankoff. Digital monitoring and estimation of polymerization reactors. *AIChE Journal*, 22(2):361–369, 1976.

[27] M. J. Park S. M Hur H. K. and Rhee. Online Estimation and Control of Polymer Quality in a Copolymerization Reactor. *AIChE Journal*, 48(5):1013–1021, 2002.

[28] R. J Fitzgerald. Divergence of the Kalman filter. In Harold W. Sorenson, editor, *Kalman Filtering: Theory and Application*. IEEE Press, 1985.

[29] F. H. Schlee C. J. Standish and N. F. Toda. Divergence in the Kalman filter. In Harold W. Sorenson, editor, *Kalman Filtering: Theory and Application*. IEEE Press, 1985.

[30] D. Semino M. Morretta and C. Scali. Parameter estimation in extended Kalman filters for quality control in polymerization reactors. *Computers and Chemical Engineering*, 20(Suppl. B):S913–S918, 1996.

[31] D. J. Kozub and J. F. MacGregor. State estimation for semibatch polymerization reactors. *Chemical Engineering Science*, 47(5):1047–1062, 1992.

[32] V. Liotta C. Georgakis and M. S. El-Aasser. Real-time estimation and control of particle size in semi-batch emulsion polymerization. In *Proceedings of the American Control Conference*, pages 1172–1176, 1997.

[33] R. Berber, K. Yetik, and A. Calimli. Nonlinear model predictive control with state estimation in batch polymerization. In *Proceedings of the American Control Conference*, pages 3778–3782, 1998.

[34] J. Valappil and C. Georgakis. Nonlinear model predictive control of end-use properties in batch reactors. *AIChE Journal*, 48(9):2006–2021, 2002.

[35] S. Kramer R. Gesthuisen and S. Engell. Re-optimization based control of copolymer quality in semi-continuous emulsion polymerization. In *Proceedings of the American Control Conference*, volume 5, pages 3870–3875, 2002.

[36] S. Kramer and R. Gesthuisen. Semi-batch emulsion copolymerization: A general model for a copolymer formed from n monomeric units. In *Conference Proceedings of ESCAPE11. CAPEC*, 2001.

[37] R. Gesthuisen S. Kramer and S. Engell. State estimation for semicontinuous emulsion copolymerization using calorimetric data. In *Proceedings of the American Control Conference*, pages 362–367, 2001.

[38] J.E. Cuthrell and L.T. Biegler. On the optimization of differential algebraic process systems. *AIChE Journal*, 33(8):1257–1270, 1987.

[39] J. E. Cuthrell and L. T. Biegler. Simultaneous-Optimization and Solution Methods for Batch Reactor Control Profiles. *Computers and Chemical Engineering*, 13(1-2):49–62, 1989.

[40] F. S. Rantow M. Soroush and M. C. Grady. Reduced-order model for monitoring spectroscopic and chromatographic polymer properties. *Journal of Chemometrics*, 21(12):612–620, 2007.

[41] O. Abel A. Helbig W. Marquardt H. Zwick T. Daszkowski. Productivity optimization of an industrial semi-batch polymerization reactor under safety constraints. *Journal of Process Control*, 10(4):351–362, 2000.

[42] N. Peters. Real-time dynamic optimization of non-linear batch systems. Master's thesis, Queens University, 2005.

[43] C. Kravaris V. Sotiropoulos C. Georgiou N. Kazantzis, M. Q. Xiao, and A. J. Krener. Nonlinear observer design for state and disturbance estimation. *Systems and Control Letters*, 56(11-12):730 – 735, 2007.

[44] C. M. Astorga N. Othman S. Othman H. Hammouri and T. F. McKenna. Nonlinear continuous-discrete observers: application to emulsion polymerization reactors. *Control Engineering Practice*, 10(1):3 – 13, 2002.

[45] T. Chen J. Morris E. Martin. Particle filters for state and parameter estimation in batch processes. *Journal of Process Control*, 15(6):665 – 673, 2005.

[46] Luis F. T. Perea. Development of optimization-based control strategies for a starved-feed semibatch copolymerization reactor. Master's thesis, Queens University, 2007.

[47] W. Wang and R. A. Hutchinson. Recent advances in the study of high-temperature free radical acrylic solution copolymerization. *Macromolecular Reaction Engineering*, 2(3):199–214, 2008.

[48] L.F.T. Perea O. E. Okorafo R. A. Hutchinson and M. Guay. Development of on-line optimization-based control strategies for a starved-feed semibatch copolymerization reactor. *Control Engineering Practice*, 17, 2009.

[49] J. R. Leis and M. A. Kramer. Odessa - an ordinary differential-equation solver with explicit simulataneaous sensitivity analysis. *ACM Transactions on Mathematical Software*, 14(1):61–67, 1988.

[50] T. Fujisawa and A. Penlidis. Copolymer composition control policies: Characteristics and applications. *Journal of Macromolecular Science*, 45(2):115–132, 2008.

[51] G. G. Odian. *Principles of Polymerization*. Wiley-Interscience, fourth edition, 2004.